



Università di Foggia

**UNIVERSITÀ  
DI FOGGIA**



HR EXCELLENCE IN RESEARCH

Department of Medical and Surgical Sciences  
PhD Course in Translational Medicine and  
Management of Health System  
XXXV Cycle

In Vitro Delivery of *Brassica oleracea L.* (Broccoli)-  
Derived Nanovesicles (BDNVs) to Lung Epithelial Cell  
Lines as Potential approach for the treatment of Chronic  
Respiratory Diseases

**Tutor**

Prof. Sante Di Gioia

**PhD Student**

Md Niamat Hossain

**Co-Tutor**

Prof. Massimo Conese

**Supervisor**

Prof. Teresa Antonia Santantonio

---

A.A. 2019/2020

<b>ABSTRACT</b> .....	<b>p.3-4</b>
<b>Abbreviation</b> .....	<b>p.5</b>
<b>Introduction</b> .....	<b>p.6-7</b>
<b>Aim of the Study</b> .....	<b>p.8</b>
<b>Materials and Methods</b>	
Chemicals.....	<b>p.9</b>
Isolation and Purification of BDNVs.....	<b>p.9-10</b>
Transmission Electron Microscopy (TEM) and Size Determination.....	<b>p.11</b>
Cryo-Transmission Electron Microscopy (Cryo-TEM) .....	<b>p.11</b>
Nanoparticle Tracking Analysis (NTA) .....	<b>p.11</b>
Measurement of Zeta Potential.....	<b>p.11-12</b>
Determination of Protein Concentration and SDS-PAGE.....	<b>p.12</b>
Determination of Protein Concentration.....	<b>p.12</b>
Cell Culture.....	<b>p.12-13</b>
Viability assay (MTT assay) .....	<b>p.13-14</b>
BDNVs Labelling and Uptake.....	<b>p.14-15</b>
Uptake Mechanism .....	<b>p.16</b>
Determination of Anti-oxidant Activity.....	<b>p.16-17</b>
Extraction of Glucosinolates (GSLs) and sample preparation.....	<b>p.17-18</b>
Determination of Sulforaphane (SFN) content.....	<b>p.18-19</b>
Identification of Bioactive Natural Compounds present in BDNVs.....	<b>p.20-21</b>
Global Natural Product Social Molecular Networking (GNPS) Library searching.....	<b>p.21</b>
Filter Compatibility Study (Terminal Sterilization) .....	<b>p.21</b>
Lyophilization and Reconstitution of BDNVs.....	<b>p.22</b>
Long-Term Stability Study.....	<b>p.22</b>
Trans-Epithelial Electrical Resistance (TEER) .....	<b>p.22-23</b>
RNA extraction and Quantitative reverse transcription polymerase chain reaction (RT-qPCR) .....	<b>p.23-24</b>
Cytokine Cytometric Bead Array (CBA) .....	<b>p.25</b>
<b>Results</b>	
Isolation and physico-chemical characterization of BDNVs.....	<b>p.26-28</b>
Isolation and physico-chemical characterization of BDNVs isolated at DDEL, HIPS....	<b>p.28-31</b>
Determination of Protein Concentration.....	<b>p.32-33</b>

Viability Assay (MTT assay) .....	p.33-35
Cell uptake of BDNVs.....	p.36-41
Uptake Mechanism.....	p.42-43
Anti-oxidant activity of BDNVs.....	p.44
Extraction and identification of GSLs in BDNVs.....	p.45
Determination of SFN content.....	p.46-48
Identification of Bioactive Natural Compounds with GNPS.....	p.49-51
Filter Compatibility Study (Terminal Sterilization) .....	p.52-53
Long-Term Stability Study.....	p.54-55
Trans-Epithelial Electrical Resistance (TEER) .....	p.56-57
Cytokine Gene Expression.....	p.58
Cytokine Cytometric Bead Array (CBA) .....	p.59-60
Comparison of Isolation of BDNVs from Two different countries (Italy and Germany).....	p.61-62
<b>Discussion.....</b>	<b>p.63-66</b>
<b>Conclusion.....</b>	<b>p.67</b>
<b>Bibliography.....</b>	<b>p.68-76</b>

## ABSTRACT

In this *in vitro* study, we test our hypothesis that Broccoli-derived nanovesicles (BDNVs), combining the anti-oxidant properties of their components and the advantages of their structure, can influence the metabolic activity of different cancer cell lines. BDNVs were isolated from homogenized fresh broccoli (*Brassica oleracea* L.) using a sucrose gradient ultracentrifugation method and were characterized in terms of physical properties, such as particle size, morphology, and surface charge by transmission electron microscopy (TEM), Cryo transmission electron microscopy (Cryo-TEM), Nanoparticle Tracking Analysis (NTA) and laser doppler electrophoresis (LDE). Glucosinolates (GSLs) content was assessed by RPLC–ESI–MS analysis and Sulforaphane (SFN) content was assessed by LC-MS/MS. Four therapeutically potent molecule were identified by Global Natural Product Social Molecular Networking (GNPS) library searching. Four different human cancer cell lines (colorectal adenocarcinoma Caco-2, lung adenocarcinoma NCI-H441, A549 and neuroblastoma SHSY5Y) as well as two non cancer cell lines (differentiated THP-1, diff.THP-1 and immortalized human alveolar type I-like cell, hAELVi) were evaluated for metabolic activity by the MTT assay. Cellular uptake of BDNVs by cancer cell lines (Caco-2, NCI-H441 and SHSY5Y) was evaluated by fluorescence as well as confocal microscopy whereas cellular uptake by non-cancer cell lines (diff. THP-1, hAELVi) was evaluated by confocal microscopy. Anti-oxidant activity was evaluated by a fluorimetric assay detecting intracellular reactive oxygen species (ROS) considering Caco-2, NCI-H441 and SHSY5Y cells. Anti-inflammatory activity was evaluated as a means of cytokine gene expression (TNF, IL-6, IL-8 and IL-10) by RT-qPCR as well as a means of measurement of cytokine release (TNF, IL-6 and IL-10) by Cytokine Cytometric Bead Array (CBA) method. Suitability of the freeze-drying method for the storage of BDNVs was also analyzed and long term stability study was assessed for this condition along with conventional -80°C and 4°C storage conditions. Co-culture model of hAELVi and diff.THP-1 was used for assessing the epithelial tightness and barrier integrity after treated with BDNVs. Three bands were obtained with average size measured by TEM based size distribution analysis of 52 nm (Band 1), 70 nm (Band 2), & 82 nm (Band 3) as well as by NTA based size distribution analysis of 170 nm (B 1), 173 nm (B 2), & 179 nm (B 3) and by Cryo-TEM size distribution analysis of 100 nm (B 1), 101 nm (B 2), & 113 nm (B 3). Glucobrassicin, glucoraphanin and neoglucobrassicin were found mostly concentrated in Band 1. Sulforaphane was also found mostly concentrated in Band 1. BDNVs affected the metabolic activity of different cancer cell lines in a dose dependent manner compared with untreated cells. Overall, Band 2 and 3 were more toxic than Band 1 irrespective of the cell lines. The metabolic activity of non cancer cell lines (diff. THP-1, hAELVi) were less affected as compared to cancer

cell lines. BDNVs were taken up by cells in a dose- and time-dependent manner. Pre-incubation of cells with BDNVs resulted in a significant decrease in ROS production in Caco-2 and NCI-H441 stimulated with hydrogen peroxide and SHSY5Y treated with 6-hydroxydopamine, with all three Bands. BDNVs were also able to reduce the pro inflammatory cytokine gene expression (TNF) as well as pro inflammatory cytokine release (TNF and IL-6). Long term stability study revealed that freeze drying or lyophilization can be a suitable alternative storage condition for the storage of BDNVs. Trans-Epithelial Electrical Resistance (TEER) value measurement revealed that BDNVs treatment had no negative effect on the barrier integrity of co-culture model (hAELVi and diff. THP-1 cells). Our findings open to the possibility to find a novel “green” approach for the treatment of chronic diseases including cancer, focused on using vesicles from broccoli, although a more in-depth characterization of bioactive molecules is warranted.

## **Abbreviation**

**COPD** Chronic obstructive pulmonary disease

**IPF** Idiopathic pulmonary fibrosis

**CF** Cystic fibrosis

**PDNVs** Plant-derived nanovesicles

**SFN** Sulforaphane

**GSLs** Glucosinolates

**BDNVs** Broccoli Derived Nanovesicles

**RT-qPCR** reverse transcription quantitative real-time PCR

**CBA** Cytometric Bead Array

**TEM** Transmission Electron Microscopy

**Cryo-TEM** Cryo-Transmission Electron Microscopy

**NTA** Nanoparticle Tracking Analysis

**LDE** laser doppler electrophoresis

**MTT** Methyl-thiazol-tetrazolium

**DMSO** dimethyl sulfoxide

**DAPI** 4-,6-diamidino-2-phenylindole

**6-OHDA** 6-hydroxydopamine

**D<sub>2</sub>CFDA** Dichlorodihydrofluorescein diacetate

**LC-MS/MS** Liquid Chromatography Tandem Mass Spectrometry

**GNPS** Global Natural Products Social Molecular Networking

**HRESI** high-resolution electrospray ionization

**TEER** Trans-Epithelial Electrical Resistance

## **Introduction**

Chronic respiratory diseases, such as allergic asthma, chronic obstructive pulmonary disease (COPD), idiopathic pulmonary fibrosis (IPF), and cystic fibrosis (CF) represent a significant cause of morbidity and mortality in the Western world and a significant social burden to be afforded. They currently represent the fourth leading cause of death in the western world. In particular, allergic asthma is increasing in its prevalence<sup>1</sup>, and mortality for COPD increased in the last 30-40 years<sup>2</sup>. Another chronic lung disease, whose incidence is increasing due to the progress in diagnostics and therapeutics is CF<sup>3</sup>. The total cost of respiratory diseases in Europe is more than €100 billion per year.

In general, the interaction of host genetic factors with the environment generates the pathologic triad in chronic respiratory diseases: persistent inflammation, protease–antiprotease imbalance, and oxidative stress. Oxidative stress is generated mainly by resident epithelial cells and macrophages, as well as by infiltrating inflammatory cells, which are represented by polymorphonuclear cells (eosinophils and neutrophils)<sup>4,5,6</sup>.

In these clinical conditions, the mucus shifts from a protective role to one that contributes to the respiratory disease. Excessive production of airway mucus, termed mucus hypersecretion, and changes in the biophysical properties of the mucus can impair mucociliary clearance, with associated accumulation of mucus in the lungs<sup>7</sup>. Initiating factors, including allergen exposure (in asthma), cigarette smoking (in COPD), defects in the cystic fibrosis transmembrane conductance regulator (CFTR) in CF, and bacterial infection (COPD and CF), set up a vicious cycle of inflammation, oxidative stress and mucus overproduction.

Recently, plant-derived nanovesicles (PDNVs) have gained immense attention as potential therapeutic candidates because of having the advantages like low immunogenicity<sup>8</sup>, good tissue specific targeting<sup>9</sup>, ability to pass through the blood-brain barrier without crossing the placental barrier<sup>10</sup> and possibility of large scale production<sup>11,12</sup>. Considering these wide scale advantages, it can be expected as next generation therapeutic drug delivery system for the treatment of a wide range of diseases. PDNVs are generally round shape or cup shaped having lipids, proteins, nucleic acids, and secondary metabolites inside and surrounded by a lipid bilayer with membrane proteins, channels, ligands, and receptors (Figure 1). PDNVs can enter into the mammalian cells and thus participate in the plant–animal cross-kingdom gene regulation<sup>13</sup>.

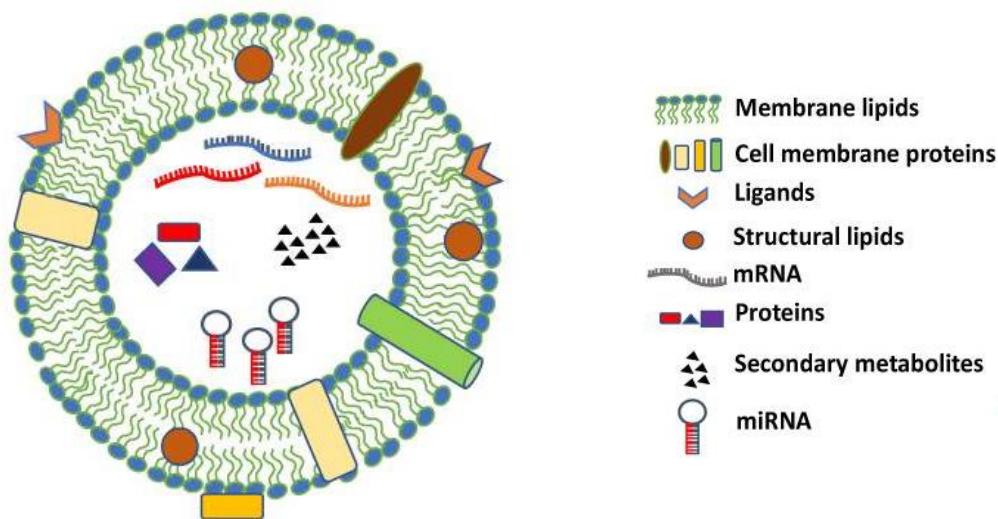


**Figure 1:** Representation of PDNVs along with their Composition. Modified from 14.

A small molecule named Sulforaphane (SFN) derived from cruciferous vegetables like Broccoli can activate multiple antioxidant and detoxifying genes which can inhibit the inflammatory pathways related to chronic respiratory diseases<sup>15</sup>. SFN can play a crucial role for maintaining Nrf2 activity which is responsible for the production of antioxidant proteins<sup>16</sup>. Glucosinolates (GSLs) are secondary plant metabolites also enriched in cruciferous vegetables. GSLs, along with their products, possess diverse biological activities, including antimicrobial, antioxidant, and anticancer actions<sup>17,18</sup>. So, the presence of such secondary metabolites in the nanovesicles can enhance their therapeutic applicability.

At the moment an anti-inflammatory therapy based on the administration of plant-derived nanovesicles (such as Broccoli-Derived Nanovesicles, BDNVs) into the lungs, has not been implemented. Thus, this project is extremely original and may be seen as the first step to bring novel anti-oxidant agents into the clinics since BDNVs are not prepared synthetically in pharmaceutical laboratories. Thus, the aim of this project is to find a novel therapy combining the antioxidant properties of some Broccoli components, such as SFN, with the advantages of nanovesicles obtained directly from the plant.



## **Aim of the Study**

This project proposes to convey natural antioxidants to respiratory as well as non respiratory epithelial like cancer cells by two levels of complexity. The complexity includes the isolation of BDNVs having the antioxidant inside with functionality as well as determination of the antioxidant activity by standard quantitative method. So my first year activities were related to obtain such nanovesicles from the Cruciferous vegetable Broccoli as well as their physicochemical characterization and evaluation of their effect on cellular viability of cancer cell lines; NCI-H441 which is lung epithelial type adenocarcinoma cell line, CaCO2 which is colorectal epithelial type adenocarcinoma cells and SHSY5Y which is epithelial like neuroblastoma cells.

My second year activities were focused on the evaluation of these nanovesicles as concerning their cellular uptake and anti-oxidant activities considering NCI-H441, CaCO2 and SHSY5Y cancer cell lines. Alongside GSLs were extracted from different bands of BDNVs.

My third year activities were mostly conducted at the Department of Drug Delivery (DDEL) in Helmholtz Institute for Pharmaceutical Research Saarland (HIPS), Germany as part of my abroad training period. In that period, new batch of BDNVs were isolated and characterized. The anti-inflammatory properties were evaluated considering reverse transcription quantitative real-time PCR (RT-qPCR) and Cytometric Bead Array (CBA) method. Their effect on cellular viability was evaluated considering A549 which is lung epithelial type adenocarcinoma cell line, diff. THP-1 which is Human monocytic cell line used as an *in vitro* model of human alveolar macrophages and hAELVi cell line which is Human alveolar epithelial lentivirus immortalized cell line used as Alveolar epithelial type I cell. Labeling and cellular uptake efficiency were evaluated considering A549 and hAELVi cell lines. The endocytosis mechanism was studied considering diff. THP-1 cell line.

## **Materials and Methods**

### **Chemicals**

LC–MS grade acetonitrile (Cat# 1.00029), water (Cat# 270733), and methanol (Cat# 34860), used for Reversed Phase Liquid Chromatography- Electrospray Ionization-Mass Spectrometry (RPLC-ESI–MS) separations and/or for glucosinolate extraction, and LC–MS grade formic acid, used as mobile phase additive, were purchased from Merck (Milan, Italy). Standard glucocamelinin (Cat# PHL85744), used as internal standard for glucosinolate quantification, was purchased from Merck (Milan, Italy). HPLC grade methanol (Cat# BDH20864.050), and formic acid (Cat# 8222541001) used for Liquid Chromatography with tandem mass spectrometry (LC-MS-MS) method for Sulforaphane identification, and HPLC grade acetonitrile (Cat# 20060.320), formic acid (Cat# 8222541001), used as mobile phase additive. Standard Sulforaphane (Cat#10496), used for Sulforaphane content identification.

### **Isolation and Purification of BDNVs**

BDNVs were isolated from the flower heads juice. All methods were carried out in accordance with relevant institutional, national, and international guidelines and legislation guidelines complying with with the Convention on Biological Diversity (<https://www.cbd.int/convention/>) and the Convention on the Trade in Endangered Species of Wild Fauna and Flora (<https://cites.org/eng>). Broccoli (580.0 g), obtained from a local grocery store, was carefully washed three times with distilled water to remove dust, soil, and pesticides and then finally washed with 1 × phosphate buffered saline (PBS), produced from DPBS 10 × (Corning, Cat# 20-031-CV). After the final washing, the broccoli was blended under maximum power for 10 min (2 min on, 2 min pause) in a juicer mixer (Ariete Juicer Mixer; Centrika Slow Juicer metal 177/1, Cat# 00C017710AR) to obtain juice. The collected juice (about 280–300 mL) was always maintained at 4 °C (using an ice bucket) and passed through a sterile cotton-gauze which is clamped to the lower edge of a bucket, so as to exclude rough residues. Then the juice was sequentially centrifuged (Thermo Scientific Biofuge Stratos Benchtop Centrifuge, rotor# 3334) at 1000×g for 10 min, 3000×g for 20 min and 10,000×g for 40 min at 4 °C to remove cell debris, fibers, various aggregates and intracellular organelles. The supernatant was then ultracentrifuged (Beckman Optima L-90 K) at 146,000×g for 60 min at 4 °C using a Type SW 32 Ti Beckman rotor and the pellet was suspended in 1 × PBS.

For purification of BDNVs, the suspension was transferred to a discontinuous sucrose gradient (IBI Scientific, Cat# IB37160) (8%, 30%, 45% and 60% [g/v]) and ultracentrifuged at

146,000×g for an additional 60 min at 4 °C using a Type SW 32 Ti Beckman rotor. The bands between 8/30%, 30/45%, and 45/60% layers, which correspond to Band 1, Band 2 and Band 3, respectively, were recovered, ultracentrifuged for 60 min in PBS 1 × and pellets were collected and resuspended in 10% mannitol (Sigma-Aldrich, Cat# 15719) in 1 × PBS. The suspensions were then stored at – 80 °C until use (Figure 2).

BDNVs were also isolated during my research activities carried out at DDEL,HIPS according to the method already described above.

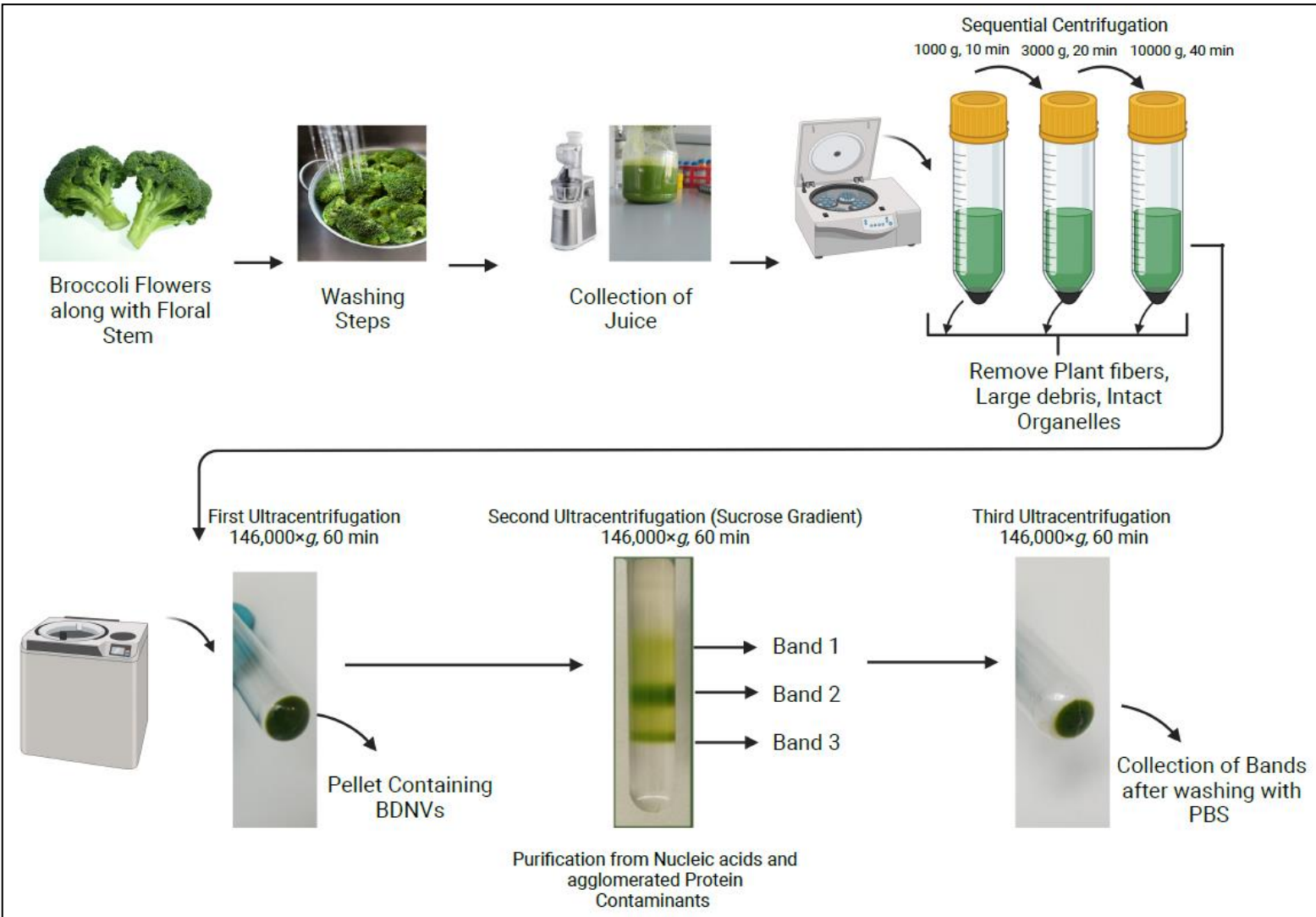


**Figure 2:** Isolation Process of BDNVs.

### **Transmission Electron Microscopy (TEM) and Size Determination**

The TEM analysis was done by a method previously described with modification<sup>19</sup> for the observation of BDNVs. In brief, samples were prepared by dropping the BDV aqueous suspension (2  $\mu$ L) on a 400-mesh amorphous carbon-coated Cu grid (Agar Scientific Ltd, Stansted, UK, Cat# S160-4) and letting the solvent evaporate. Sample on the grid was left to dry overnight and finally stored in a vacuum chamber until analysis. The samples were stable under the electron beam and did not degrade within the typical observation times. No staining was used in these experiments. Micrographs were recorded using a Jeol JEM-1011 microscope working at an accelerating voltage of 100 kV and acquired by an Olympus Quemesa Camera (11 Mpx). Size statistical analysis (BDV average size and size distribution) of each sample (Band 1, Band 2 and Band 3) was performed on 200 nanostructures by means of a freeware Image J analysis program (National Institutes of Health, USA).

### **Cryo-Transmission Electron Microscopy (Cryo-TEM)**

Cryo-TEM analysis was done for the BDNVs isolated at DDEL, HIPS. For Cryo-TEM, 3  $\mu$ l of the sample solution was placed on a holey carbon film (Plano, Wetzlar, Germany, type S147-4), blotted for 2 s and plunge frozen at  $-165^{\circ}\text{C}$  using under cooled liquid ethane and a Gatan (Pleasanton, CA, United States) CP3 plunge freezer. The vitreous film was transferred under liquid nitrogen to a Gatan model 914 cryo-TEM sample holder and examined by TEM bright field imaging using a JEOL JEM-2100 LaB6 TEM at  $-170^{\circ}\text{C}$ . A Gatan Orius SC1000 CCD camera captured images with a dwell time of 2s.

### **Nanoparticle Tracking Analysis (NTA)**

NTA was used to confirm the size distribution and concentration of the BDNVs isolated at DDEL, HIPS using a LM14C instrument (Malvern Panalytical Ltd, UK). The samples were diluted 1:10000 with PBS1X to obtain less than 100 particles per frame with 1 $\times$ PBS, and 1 mL of the diluted sample was loaded into the laser chamber using a syringe. Then, 3  $\times$  30 seconds measurements were performed and analyzed by the built in software of the instrument (NanoSight NTA software 3.4 Build 3.4.4).

### **Measurement of Zeta Potential**

BDNVs Zeta potential was measured by laser doppler electrophoresis (LDE) using a Zeta sizer Nano ZS and in diffusion barrier mode with water<sup>20</sup>.

The same above mentioned method was used to determine the Zeta potential value of the BDNVs isolated at DDEL, BDNVs.

### **Determination of Protein Concentration and SDS-PAGE**

The protein concentration of the samples was determined using a Coomassie Plus (Bradford) assay kit (Thermo Scientific, Cat# 23238). An aliquot (25 µl) of each band sample was lysed with 10 µl of Radioimmunoprecipitation assay (RIPA) lysis buffer (EMD Millipore Corporation, Cat# 20–188). After centrifugation at 12,000 rpm for 10 min at 4 °C, the supernatant was considered for the determination of protein concentration as per manufacturer's instruction. Proteins were electrophoresed on 10% SDS–polyacrylamide gels and stained with Coomassie blue. Bovine serum albumin was used as standard. Bio-Rad Precision plus protein standards (Cat# 161-0374) was used as marker. Integrated intensity for each lane was evaluated by the ImageJ software.

### **Determination of Protein Concentration**

The protein concentration of the BDNVs isolated at DDEL, HIPS was determined using a Bradford reagent assay kit (Sigma-Aldrich, Cat# B6916). The samples were diluted 1:3 with 10% Mannitol in PBS 1x and 50 µl of the diluted sample was lysed with 50 µl of Radioimmunoprecipitation assay (RIPA) lysis bufer (0.5 M Tris.HCl, pH 7.4 [Tris.HCl Carl Roth Cat#9090.2, Trizma-Base Sigma-Aldrich Cat#T1503]; 1% Deoxycholic acid Sigma-Aldrich Cat#30970 ; 10 mM EDTA Carl Roth Cat#8043.1; 0.15 M NaCl Sigma Aldrich Cat#7647-14-5; Triton X 100 0.09% Sigma Aldrich Cat#T9287) or diluted further with 50 µl of 10% Mannitol in PBS 1x. After centrifugation at 12,000 rpm for 10 min at 4 °C, the supernatant was considered for the determination of protein concentration as per manufacturer’s instruction.

### **Cell Culture**

Caco2 cells (ATCC, Manassas, VA, USA) were grown in DMEM with 4.5 g/L glucose, L-glutamate and sodium pyruvate supplemented with 10% Fetal Bovine Serum (FBS, Corning, Cat# 35-010-CV), 1% penicillin and streptomycin, 25 µg/mL amphotericin B, and 2 mM L-Glutamine.

NCI-H441 cells (ATCC) were grown in RPMI-1640 (Corning, Cat# 10-040-CV) with L-glutamine, supplemented with 10% FBS, 1% penicillin and streptomycin (EuroClone, Cat# ECB3001D), 25 µg/mL amphotericin B (Corning, Cat# 30-003-CF), and 2 mM L-glutamine (EuroClone, Cat# ECB3000D).

SHSY5Y cells (kindly provided by Dr. Maria Lasalvia, University of Foggia) were grown in Dulbecco's Modified Eagle's Medium Nutrient Mixture F-12 Ham (Sigma-Aldrich, Cat# D8062), 20% FBS, 1% non-essential amino acids, 2 mM L-glutamine, 1% penicillin and streptomycin, and 25 µg/mL amphotericin B.

A549 cells were purchased from DSMZ (No. ACC 107, Leibniz Institute) and cultured in RPMI-1640 medium (1X) (Gibco™Life Technologies Europe B.V., 21875-034) supplemented with 10% Fetal Calf Serum (FCS; Cat. No. 10270106, Life Technologies, USA).

THP-1 cells were purchased from DSMZ (No. ACC 16, Leibniz Institute) and cultured in RPMI-1640 medium (1X) (Gibco™Life Technologies Europe B.V., 21875-034) supplemented with 10% Fetal Calf Serum (FCS; Cat. No. 10270106, Life Technologies, USA).

To differentiate THP-1 monocytes into macrophage-like cells, the cells are incubated for 48h with 7.5 ng/mL of phorbol 12-myristate 13-acetate (PMA; Sigma-Aldrich Cat. No. PA585)<sup>21</sup>. Then, differentiated THP-1 cells were detached from the T75 flask with 3 mL of AccutaseR (Cat. No. A6964, Sigma-Aldrich, Germany) for 30 mins, at 37°C, counted and seeded according to the experiment protocol.

The establishment and characterization of the hAELVi cell line has been detailed by Kuehn *et al.*, 2016.<sup>22</sup> In short, hAELVi cells (passages 10-20) were maintained on T25 flasks coated with 2 mL of a coating solution (ddH<sub>2</sub>O + 1% collagen (Product No. C4243, Sigma-Aldrich) + 1% fibronectin (Cat. No. 356008, Corning). These ATI-like cells grow in a complex small airway epithelial cell growth medium (SAGM™; Lonza Cat. No. CC-3118) supplemented with 1% FCS + 1% penicillin/streptomycin (P/S; Cat.No. 356008, 10000 U/mL, Gibco, USA).

### **Viability assay (MTT assay)**

Cell viability was assessed with Methyl-thiazol-tetrazolium (MTT, Sigma-Aldrich, Cat# MKBL6157V) assay as detailed previously<sup>23</sup>. For the assessment, Caco-2, NCI-H441, or SHSY5Y cells were seeded in quadruplicate at a density of  $2 \times 10^4$  or  $1 \times 10^4$  in a 96-well plate respectively and exposed to escalating doses of BDVs (from 5 to 5000 µg/mL) for 24 h. After which the BDNVs-containing medium was removed and cells were thoroughly rinsed once with  $1 \times$  PBS. Cells were then incubated with 100 µL of MTT solution (0.5 mg/mL) at 37 °C for 4 h until a purple precipitate was visible. Thereafter, the media were discarded and 100 µl dimethyl

sulfoxide (DMSO, Corning, Cat# 25-950-CQC) was added to each well prior to spectrophotometric measurements at 595 nm. Means and standard deviations were generated from three independent experiments and reported as the percentage of viability versus control (untreated cells). Triton X-100 (10% v/v solution, BioUltra, Cat# 93443) treated cells were used as positive control. Untreated cells were used as a negative control.

Cellular viability was also assessed considering A549, diff.THP-1, and hAELVi cells during my research activities carried out at DDEL, HIPS. For the assessment, A549, diff.THP-1, or hAELVi cells were seeded in quadruplicate at a density of  $1 \times 10^4$ ,  $8 \times 10^4$  or  $3.3 \times 10^4$  in a 96-well plate (Greiner-bio-one CELLSTAR®, 3470-Clear) respectively and exposed to escalating doses of BDNVs (from 5 to 5000  $\mu\text{g}/\text{mL}$ ) for 24 h. After which the BDNVs-containing medium was removed and cells were thoroughly rinsed once with  $1 \times \text{PBS}$ . Cells were then incubated with 100  $\mu\text{L}$  of MTT solution (0.5 mg/mL) at 37 °C for 4 h until a purple precipitate was visible. Thereafter, the media were discarded and 100  $\mu\text{L}$  dimethyl sulfoxide (DMSO, Thermo Scientific, Cat#67-68-5) was added to each well prior to spectrophotometric (Infinite M200 PRO TECAN, Cat# 1308007421) measurements at 550 nm. Means and standard deviations were generated from two independent experiments and reported as the percentage of viability versus control (untreated cells). Triton X-100 (10% v/v solution, Sigma Aldrich, Cat#9036-19-5) treated cells were used as positive control. Untreated cells were used as a negative control.

### **BDNVs Labelling and Uptake**

To verify that BDNVs can be taken up by human cells, BDNVs were stained with PKH26 red dye (Sigma-Aldrich, Cat# MIDI26) followed by incubation with cells. BDNVs were isolated as described above and labeled with PKH26 for 5 min at room temperature as previously described with minor modifications<sup>24</sup>. Labelling was stopped by adding 10% Bovine Serum Albumin (BSA, BioReagent, Cat# a8806). All unlabeled dye was washed away by ultracentrifugation at  $100,000 \times g$  for 70 min, and labelled BDNVs pellets were re-suspended in  $1 \times \text{PBS}$ .

NCI-H441, Caco-2 and SHSY5Y cells were seeded in 8-chamber glass tissue culture slides (Sarstedt, Nümbrecht, Germany, Cat# 94.6170.802) and incubated overnight in growth medium. Then the cells were treated with 5  $\mu\text{g}/\text{mL}$  and 22  $\mu\text{g}/\text{mL}$  of PKH26-labelled BDNVs for 2 or 24 h at 37°C. Negative controls for background fluorescence were cells incubated with medium only for 2 or 24 h. After co-culture, uptake was stopped by washing and the cells were fixed with fix solution in  $1 \times \text{PBS}$  for 5 min at room temperature. After washing twice with  $1 \times \text{PBS}$ , finally the

cells were coverslip-mounted with mounting medium containing 4-,6-diamidino-2-phenylindole (DAPI, H-1200; Vector Laboratories, Burlingame, CA, USA, Cat# H-1200-10) for nuclear staining and analysed by fluorescence microscopy. Images were acquired on the Nikon Eclipse Ni Fluorescence Microscopy system. Acquisition, storage and analysis of data were performed with NIS Elements imaging software (Nikon Europe B.V.).

For confocal microscopy, images were acquired on the Leica TCS SP8 confocal laser scanning microscopy system. Acquisition, storage and analysis of data were performed with LasX software (Leica Microsystems GmbH, Wetzlar, Germany).

BDNVs were also labelled according to the method described above during my research activities at DDEL, HIPS.

For the uptake study, diff. THP-1 and hAELVi cells were seeded in 8-chamber glass tissue culture slides (Thermo Fisher Scientific, Cat# 155409) and incubated overnight in growth medium. Then the cells were treated with 5 µg/mL and 22 µg/mL of PKH26-labelled BDNVs for 6h at 37 °C. In case of diff. THP-1, after 2 h of application of labelled BDNVs, the cells were stimulated with LPS (0.1 µg/ml) like the cytokine assay experiment and continued to incubate further for an additional 4 h. Negative controls for background fluorescence were cells incubated with medium only for 6 h. After co-culture, uptake was stopped by washing and the cells were fixed with 3% paraformaldehyde for 30 min at room temperature. Nuclei were stained with 4',6-Diamidin-2-phenylindol (DAPI, 1 µg/mL ) (Sigma-Aldrich, Cat#32670-5MG-F) for 15 min.

For confocal microscopy, images were acquired on the Leica TCS SP8 confocal laser scanning microscopy system. Acquisition, storage and analysis of data were performed with LasX software (Leica Microsystems GmbH, Wetzlar, Germany). A confocal laser-scanning microscope (CLSM Leica TCS SP8, Leica Microsystems, Germany) was used to visualize cells. Images were taken with a 25× water immersion objective (1024 × 1024 resolution) and processed using LAS X software (LAS X 1.8.013370, Leica Microsystems, Germany).



## **Uptake Mechanism**

Uptake mechanism of the BDNVs by the cellular systems of diff. THP-1 was also studied at DDEL, HIPS.

Cells were cultured like the cell uptake mechanisms. After 24 h of seeding, cells were washed with PBS and then different inhibitors were added separately, chlorpromazine (10 µg/mL) (Sigma-Aldrich, Cat#C8138), cytochalasin D (1 mg/mL) (Sigma-Aldrich, Cat#C2618), filipin III (1 µg/mL) (Sigma-Aldrich, Cat#F 4767), and methyl-β-cyclodextrin lovastatin (10 mmol /L 1 µg/mL) (Abcam, Cat#ab120614) in respective media<sup>25,26</sup>.

After 1 h of incubation at 37° C with inhibitors, labelled BDNVs were applied (22 µg/ml) and incubated for another 2 h at 37° C in the presence of inhibitors. After 2 h coincubation, diff. THP-1 cells were stimulated with LPS (0.1 µg/ml) and continued to grow for additional 4 h in the presence of inhibitors and BDNVs.

Afterward, cells were washed and fixed with 3% paraformaldehyde for 30 min at room temperature. Nuclei were stained with 4',6-Diamidin-2-phenylindol (DAPI, 1 µg/mL) (Sigma-Aldrich, Cat#32670-5MG-F) for 15 min.

For confocal microscopy, images were acquired on the Leica TCS SP8 confocal laser scanning microscopy system. Acquisition, storage and analysis of data were performed with LasX software (Leica Microsystems GmbH, Wetzlar, Germany). A confocal laser-scanning microscope (CLSM Leica TCS SP8, Leica Microsystems, Germany) was used to visualize cells. Images were taken with a 25× water immersion objective (1024 × 1024 resolution) and processed using LAS X software (LAS X 1.8.013370, Leica Microsystems, Germany).

## **Determination of Anti-oxidant Activity**

To evaluate the efficiency of anti-oxidant activity, Caco-2, NCI-H441 and SHSY5Y cells were pretreated with BDNVs (5 and 22 µg/mL) for 24 h. Then, in order to induce oxidative stress, Caco-2 and NCI-H441 cells were treated with 100 µM hydrogen peroxide (H<sub>2</sub>O<sub>2</sub>, Sigma-Aldrich, Cat# H1009) for 24 h<sup>27,28</sup> and SHSY5Y cells were treated with 100 µM 6-hydroxydopamine (6-OHDA, Sigma-Aldrich, Cat# H4381) for 24 h<sup>29</sup>. Reactive oxygen species (ROS) production was evaluated by fluorimetry by using the 2',7'-Dichlorodihydrofluorescein diacetate (D<sub>2</sub>CFDA, Sigma-Aldrich, Cat# D6883), as previously described<sup>30</sup>. The dose and timing of H<sub>2</sub>O<sub>2</sub> and 6-

OHDA incubation with cells were chosen based on preliminary experiments that evaluated significant ROS production in the absence of overt reduced viability. Briefly, Caco-2, NCI-H441 and SHSY5Y cells were washed and then incubated with 10  $\mu\text{M}$  D<sub>2</sub>CFDA for 90 min at 37°C and the fluorescent signal of DCF obtained from the conversion of D<sub>2</sub>CFDA by intracellular ROS produced was measured at excitation/emission wavelengths of 485/530 nm using a Fluorescent Plate Reader (FilterMax F5 Multi-Mode Microplate Reader (Molecular Devices, Beckman Coulter, CA, USA). The results were expressed as mean fluorescence intensity (MFI). The assay was performed two times in quadruplicates.

### **Extraction of Glucosinolates (GSLs) and sample preparation**

Aliquots of the PBS suspensions obtained from pellets recovered from Bands 1, 2 and 3 were mixed with methanol to obtain a final methanol/water 70:30 (v/v) solvent composition, corresponding to the one previously employed by Cataldi et al.<sup>31</sup> for the extraction of GSLs from vegetal matrices. The resulting suspensions were sonicated for 20 min at 40°C and then centrifuged at 12000 rpm; afterwards, the supernatant was recovered and stored at +4°C for 24 h. Since mannitol crystals precipitated upon prolonged low temperature storage, a new centrifugation at 12000 rpm was effected. The resulting supernatant was first pre-concentrated by a factor 2 through partial solvent evaporation, then it was stored at -20°C until RPLC-ESI-MS analysis was performed.

Just before the analysis, the methanol/water extracts referred to Bands 1, 2 and 3 were fortified with glucocamelinin (final concentration 5.76  $\mu\text{mol/L}$ ), that was adopted as internal standard to estimate the concentration of glucosinolates extracted from BDNVs, under the assumption that electrospray ionization yields for different glucosinolates (and, consequently, the MS response vs concentration dependence) are comparable.

### **RPLC-ESI-MS instrumentation and operating conditions**

RPLC-ESI(-)-MS analyses were performed using an LC-MS platform including an Ultimate 3000 HPLC quaternary chromatographic system interfaced to a Q-Exactive high resolution quadrupole-Orbitrap mass spectrometer (Thermo Fisher, West Palm Beach, CA, USA), that was used for Fourier-transform MS (FTMS) and for Higher-energy Collisionally-induced Dissociation tandem MS acquisitions (HCD-FTMS/MS).

RPLC separations of BDNV extracts were performed using a C18 Ascentis Express column (15 cm length, 2.1 mm internal diameter) packed with core-shell 2.6  $\mu\text{m}$  particles (Supelco, Bellefonte, PA, USA) and operated at a 0.2 mL/min flow; 5  $\mu\text{L}$  sample volumes were injected. The following multi-step binary elution gradient, based on an water as phase A and acetonitrile as phase B, both containing 0.1% (v/v) formic acid, was adopted for lipid separation: 0-2 min) isocratic at 1% B; 2-3 min) linear increase of B from 1% to 2%; 3 -5 min) isocratic at 2% B; 5-10 min) linear increase of B from 2% to 10%; 10-20 min) linear increase of B from 10% to 30%; 20-30 min) linear increase of B from 30% to 80%; 30-40 min) isocratic at 80% B; 40-50 min) linear decrease of B from 80% to 1%; 50-60 min) reconditioning at 1% B.

The Heated ElectroSpray Ionization (HESI) interface (Thermo Fisher, West Palm Beach, CA, USA) mounted on the Q-Exactive spectrometer was adopted to ionize analytes eluted from the chromatographic column and transfer the resulting ions into the mass spectrometer.

The parameters of the HESI interface and of the ion optics of the Q-Exactive spectrometer were set as follows: sheath gas (nitrogen) flow rate) 40 a.u.; auxiliary gas (nitrogen) flow rate) 15 a.u.; spray voltage) -3 kV; capillary temperature) 320°C; S-lens RF level 60. The spectrometer was operated in negative polarity at its maximum resolving power (140000 at  $m/z$  200) and high-resolution spectra were acquired in a 300-700  $m/z$  interval. HCD-FTMS/MS acquisitions were performed systematically on all ions generated into the HESI source by using the All-Ion Fragmentation (AIF) acquisition mode, enabling the retrieval of fragmentation (HCD-MS/MS) spectra of eluted compounds with an untargeted approach. AIF scans were acquired at a 70000 resolving power in a 50-700  $m/z$  interval, using a normalized collisional energy (NCE) of 35 units. During FTMS measurements the Orbitrap fill time was set to 100 ms and the Automatic Gain Control (AGC) level was set as  $1 \times 10^6$ . Before analyses the spectrometer was calibrated by infusing, at a 5  $\mu\text{L}/\text{min}$  flow rate, calibration solutions provided by the instrument manufacturer for positive or negative polarity acquisitions. As a result, a mass accuracy always better than 5 ppm was achieved.

### **Determination of Sulforaphane (SFN) content**

A modified and sensitive LC-MS/MS method was used for the identification as well as quantification of Sulforaphane if present in the isolated BDNVs at DDEL, HIPS<sup>32</sup>.

### Preparation of Samples

An aliquot (10  $\mu$ l) of each band sample was transferred to Eppendorf tubes with 1 ml Methanol, (M) or 1 ml mixture of RIPA lysis Buffer + Methanol (10  $\mu$ l RIPA lysis Buffer+ 990  $\mu$ l Methanol), (R) or 1 ml of 0.1% formic acid in Methanol, (MF). Samples were quickly sonicated for 30 min. Then passed through 0.2  $\mu$ m membrane filter and collected into LC–MS vials. The samples were placed into LC–MS compartment (4°C) and analyzed without delay.

### Preparation of Standard Stock solutions

Sulforaphane standard (Cayman Chemical Company, Cat#10496) stock solution was prepared at a concentration of 0.5 mg/ml with Methanol. Then 1 ml of this stock was diluted in 10 ml with Methanol to have a concentration of 50  $\mu$ g/ml. Sequentially 20  $\mu$ g/ml and 10  $\mu$ g/ml solutions were prepared in Methanol. The 10  $\mu$ g/ml solution was used to prepare the standard solutions for the calibration curve.

### Preparation of Standard solutions

The concentrations of working solutions were varied in the range of 1–1000 ng/mL. All of the subsequent dilutions for working standards were prepared by using Methanol. Separate standard calibration graphs were constructed by plotting the area underneath the chromatograms versus concentrations of the standards.

### Liquid Chromatography Tandem Mass Spectrometry(LC-MS/MS)

LC-MS/MS measurements were performed using TSQ Quantum Access MAX Triple Quadrupole Mass Spectrometer (Thermo Fisher Scientific) coupled with UHPLC system *Dionex UltiMate 3000-Series* (Thermo Fisher Scientific). Electrospray ionization in positive mode and selected reaction monitoring (SRM) with a spray voltage of 3.5 kV, a sheath gas pressure of 45 arb, an auxiliary gas pressure of 10 arb, and a capillary temperature of 250°C were selected. Scan time and scan width were 0.2 s and 0.7 amu respectively.

Chromatographic separation was performed using a Accucore RP-MS column (150 mm length, 2.1 mm internal diameter) (Thermo Fisher Scientific) and operated at a 0.3 mL/min flow; 3  $\mu$ L sample volumes were injected. The following multi-step binary elution gradient, based on Acetonitrile as phase A and Water as phase B, both containing 0.1% (v/v) formic acid, was adopted: 0–3.5 min) linear decrease of B from 90 to 1%; 3.5–4.5 min) isocratic at 1% B; 4.5–4.6 min) linear increase of B from 1% to 90%; 4.6–8.0 min) reconditioning at 90% B.

## Identification of Bioactive Natural Compounds present in BDNVs

MS/MS spectra of BDNVs analysis done at DDEL, HIPS was sent to Global Natural Products Social Molecular Networking (GNPS) for the dereplication to identify known potent biologically active compounds if present in the BDNVs (B1, B2 and B3).

### Sample Preparation for UHPLC-MS/MS

An aliquot (10  $\mu$ l) of each band sample was transferred to Eppendorf tubes with 1 ml of Methanol. Samples were quickly sonicated for 30 min. Then passed through 0.2  $\mu$ m membrane filter and collected into LC-MS vials. The samples were placed into LC-MS compartment (4°C) and analyzed without delay.

### LC-MS/MS

UHPLC-hrMS analysis was performed on a Dionex UltiMate 3000 rapid separation liquid chromatography (RSLC) system (Thermo Fisher Scientific, Waltham, MA, USA) coupled to a Bruker maXis 4G ultra-high-resolution quadrupole time-of-flight (UHR-qTOF) MS equipped with a high-resolution electrospray ionization (HRESI) source (Bruker Daltonics, Billerica, MA, USA). The separation of 5  $\mu$ L sample was achieved with a linear 5–95% gradient of acetonitrile with 0.1% formic acid in ddH<sub>2</sub>O with 0.1% formic acid on an ACQUITY BEH C18 column (100 mm  $\times$  2.1 mm, 1.7  $\mu$ m d<sub>p</sub>) (Waters, Eschborn, Germany) equipped with a Waters VanGuard BEH C18 1.7  $\mu$ m guard column at a flow rate of 0.6 mL/min and 45 °C for 18 min with detection by a diode array detector at 200–600 nm. The LC flow was split into 75  $\mu$ L/min before entering the mass spectrometer. Mass spectrograms were acquired in centroid mode ranging from 150–2500  $m/z$  in positive MS mode. Source parameters were set to 500 V end-plate offset; 4000 V capillary voltage; 1 bar nebulizer gas pressure; 5 L/min dry gas flow; and 200 °C dry gas temperature. Ion transfer and quadrupole parameters were set to 350 V<sub>PP</sub> funnel RF; 400 V<sub>PP</sub> multipole RF; 5 eV ion energy; and 120  $m/z$  low-mass cut-off. Collision cell was set to 5.0 eV and pre-pulse storage was set to 5  $\mu$ s. Automatic tandem MS data acquisition was conducted by selecting two precursors per cycle with smart exclusion after five spectra and performing CID and MS/MS spectra acquisition time ramping. CID energy was ramped from 35 eV for 500  $m/z$  to 45 eV for 1000  $m/z$  and 60 eV for 2000  $m/z$ . MS full-scan acquisition rate was set to 2 Hz and MS/MS spectra acquisition rate was ramped from 1 to 4 Hz for precursor ion intensities of 10 kcts to 100 kcts. Calibration was conducted automatically before every HPLC-MS run by the injection of sodium formate and calibration on the respective clusters formed in the ESI source. All MS analyses were acquired in the presence of the lock masses C<sub>12</sub>H<sub>19</sub>F<sub>12</sub>N<sub>3</sub>O<sub>6</sub>P<sub>3</sub>, C<sub>18</sub>H<sub>19</sub>F<sub>24</sub>N<sub>3</sub>O<sub>6</sub>P<sub>3</sub> and

$C_{24}H_{19}F_{36}N_3O_6P_3$ , which generate the  $[M + H]^+$  ions of 622.0289, 922.0098 and 1221.9906. The HPLC-MS system was operated by HyStar 5.1 (Bruker Daltonics, Billerica, MA, USA), and LC chromatograms as well as UV spectra and mass spectrograms were analyzed with DataAnalysis 5.3 (Bruker Daltonics, Billerica, MA, USA). The resulting tandem MS chromatograms were exported as MZML file using Data Analysis 5.3 (Bruker Daltonics, Billerica, MA, USA) and submitted to the GNPS online workflow<sup>33</sup>. In the GNPS networking pipeline MS/MS spectra were window filtered by choosing only the top six peaks in the  $\pm 50$  Da window throughout the spectrum. The data was clustered with MS-Cluster with a parent mass tolerance of 0.05 Da and a MS/MS fragment ion tolerance of 0.1 Da to create consensus spectra. A spectral network was created where edges were filtered to have a cosine score above 0.7 and more than 6 matched peaks. Further edges between two nodes were kept in the network if and only if each of the nodes appeared in each other's respective top 10 most similar nodes. The spectra in the network were then searched against GNPS' spectral libraries. The library spectra were filtered in the same manner as the input data. All matches kept between network spectra and library spectra were required to have a score above 0.7 and at least 6 matched peaks.

### **Global Natural Product Social Molecular Networking (GNPS) Library searching**

The output of the GNPS was used to identify the bioactive compounds present in different bands of BDNVs.

### **Filter Compatibility Study (Terminal Sterilization)**

Sterile filtration is a kind of terminal sterilization process which is suitable to sterilize thermosensitive and chemical-sensitive nanosystems like BDNVs. Additionally it does not produce any adverse effects on nanoparticles as well as it does not generate toxic impurities<sup>34</sup>. The sterility testing was performed on the isolated BDNVs at DDEL, HIPS. Typically, the samples diluted 1:10000 with PBS were passed through 0.2  $\mu\text{m}$  membrane filter (Sartorius Cat#16534-K) and 0.45  $\mu\text{m}$  membrane filter (Sartorius Cat#17846-ACK). The particle size distribution and concentration before and after filtration were examined to determine if significant quantities of BDNVs had been retained by the membrane or not.

### **Lyophilization and Reconstitution of BDNVs**

Samples (BDNVs suspension prepared immediately after isolation in 10% Mannitol in PBS 1X at DDEL, HIPS) were frozen at  $-80^{\circ}\text{C}$  for 12 h and were lyophilized using a bench-top manifold freeze dryer (ALPHA 2-4 LSC, Martin Christ) for 24 h at the vacuum pressure less than 0.3 mbar and condenser temperature below  $-80^{\circ}\text{C}$ . Final drying was performed after manual main drying for an additional 1 h at the vacuum pressure less than 0.010 mbar and condenser temperature below  $-80^{\circ}\text{C}$ . Lyophilized BDNVs were reconstituted to their original volume with PBS1X for size and concentration measurement by NTA and Zeta potential value by Zeta sizer followed by gentle swirling for a few seconds before use.

### **Long-Term Stability Study**

The shelf life and storage condition of the BDNVs were assessed with different storage durations at 0, 1, 2, 4, and 8 weeks and different conditions at  $4^{\circ}\text{C}$ ,  $-80^{\circ}\text{C}$ , and Lyophilized BDNVs at DDEL, HIPS. Then, the physical properties, including size, concentration and zeta potential, of the BDNVs were examined.

### **Trans-Epithelial Electrical Resistance (TEER)**

A co-culture model with epithelial cells and other cell types could narrow the gap between 2D cell monolayers and in vivo models and can mimic biological barriers models that reconstitute cellular crosstalk as well as cell-cell and cell-matrix interactions<sup>35,36</sup>. Offering higher accessibility and reproducibility than primary cells, a three-dimensional model of epithelial Alveolar Type I (ATI) like cells (hAELVi) co-cultured with surrogates for alveolar macrophages (diff. THP-1) occurs to be a relevant model for assessing epithelial tightness and barrier integrity. In Transwell inserts, hAELVi cells formed a monolayer which corresponds to the thin epithelial layer observed in alveoli<sup>22</sup>. This observation was confirmed by TEER measurements which is a largely approved measure for epithelial tightness and barrier integrity<sup>37</sup>. Transwell supports (Cat. No. 3470; growth area 0,33 cm<sup>2</sup>; Corning®, New York, NY, USA) were used to set up the co-culture model for the experiment at DDEL, HIPS. TEER value was measured to evaluate the barrier integrity of the hAELVi monolayer until 10 days. The reading which was taken at 10<sup>th</sup> Day was considered as the reading of before treatment.

At 10<sup>th</sup> day, diff-THP 1 cells were applied on top of hAELVi and continued to grow for 24h. After 24h (Day 11), diff.TH P-1 cells were inflamed by LPS 0.1  $\mu\text{g}/\text{ml}$  to represent activated macrophage. After 2h of inflammation, the co culture system was treated with two concentrations

of BDNVs 5 µg/ml and 22 µg/ml and continued to grow for 24 h. After 24h (Day 12), TEER values were measured to observe the barrier integrity of that complex situation. The reading which was taken at 12<sup>th</sup> Day was considered as the reading of after treatment.

TEER measurement is performed with an epithelial voltohmmeter (EVOM 3, Ser. No. 188110, World Precision Instruments, Sarasota, USA), calibrated at 1000 W, and a chopstick electrode (Item No. STX2- PLUS, World Precision Instruments). The following formula was used to calculate surface-corrected TEER values:

$$\text{TEER } (\Omega \cdot \text{Cm}^2) = [\text{Raw Value } (\Omega) - \text{Blank } (\Omega)] * \text{Surface area } (\text{Cm}^2)$$

“raw value” corresponds to the EVOM output.

### **RNA extraction and Quantitative reverse transcription polymerase chain reaction (RT-qPCR)**

To investigate the anti-inflammatory effects, mRNA expression of pro-inflammatory cytokines TNF, IL-6, IL-8 and anti-inflammatory cytokine IL-10 was measured by RT-qPCR at DDEL, HIPS.

For the assessment, diff.THP-1 cells were seeded at a density of  $8 \times 10^4$  in a 96-well plate (Greiner-bio-one CELLSTAR ®, 3470-Clear). After 24 h, cells were first pretreated with three concentrations of BDNVs (5 µg/mL, 22 µg/mL and 45 µg/mL). After 2h of pretreatment, diff-THP-1 cells were stimulated with LPS (0.1 µg/mL) and continued to grow for 22 h. After the above mentioned time period, Total RNA was isolated from the diff.THP-1 cells using the Qiagen RNeasy RNA isolation Micro Kit and was used to synthesize cDNA. RNA (200 ng) was reverse-transcribed with Superscript IV VILO. Target genes were amplified from this cDNA using specific primers (Eurofins). Four transcripts (TNF, IL-6, IL-8 and IL-10) were designed using Primer-BLAST software to make target-specific primers (Table 1).



Primer Name	Sequence 5'-->3'	Amplicon Length	Tm	CG content (%)	Exon junction
CXCL8 Fw (1)	GCTCTGTGTGAAGGTGCAGTT	203	61.08	52.38	154/155
CXCL8 Rev (1)	ACCCAGTTTTTCCTTGGGGTC	203	59.81	55.00	
IL10 Fw (1)	AAGACCCAGACATCAAGGCG	94	60.59	55.00	437/438
IL10 Rev (1)	CAGGGAAGAAATCGATGACAGC	94	59.39	50.00	
TNF-a Fw(2)	TAGCCCATGTTGTAGCAAACCC	244	60.88	50.00	455/456
TNF-a rev(2)	AGGAGGTTGACCTTGGTCTG	244	58.94	55.00	
IL6 Fw (2)	AGAGGCACTGGCAGAAAACA	95	59.82	50.00	387/388
IL6 Rev (2)	TCACCAGGCAAGTCTCCTCA	95	60.47	55.00	

**Table 1:** List of the primers

RT-qPCR was performed on Mic qPCR cycler (Magnetic Induction Cycler by Bio Molecular System) with SYBR™ Green PCR Master Mix (ThermoFisher, Kat. 4309155): GAPDH was used as reference gene for normalization. The run protocol consists of 40 cycles of alterned denaturing phase (95°C for 3s) and amplification/quantification phase (60°C for 30s). The process ends with a melt program: 72°C to 95°C (0.3°C/s).

The cycle threshold value (Ct) corresponds to the cycle number when the PCR product fluorescent can be detected above the background signal and is given by the PCR machine for each sample.  $2^{-\Delta\Delta Ct}$  method of relative quantification was used to calculate the relative fold change expression of the different samples. Firstly, the difference between Ct from the gene of interest with the reference gene ( $\Delta Ct$ ) was calculated and, secondly, the difference of delta Ct between the treated sample and the untreated control sample ( $\Delta\Delta Ct$ ) was calculated like below:

$$\Delta Ct = Ct (\text{gene of interest}) - Ct (\text{reference gene})$$

$$\Delta\Delta Ct \text{ control} = \Delta Ct (\text{control sample}) - \text{average } \Delta Ct (\text{reference gene})$$

$$\Delta\Delta Ct \text{ treated} = \text{average } \Delta Ct (\text{control sample}) - \Delta Ct (\text{treated sample})$$

This approach was inspired by K. Livak and T.Schmittgen in 2001<sup>38</sup>.

Ct values were normalized to the control: Fold change (FC) control = 1.

Error bars on plots represent  $\pm$  SEM, unless otherwise noted. All primers were designed with NCBI primer blast tool and purchased from Eurofins MWG Operon.

### Cytokine Cytometric Bead Array (CBA)

BD™ Cytokine Cytometric Bead Array (CBA) kit (Human Soluble Protein Master Buffer Kit Cat# 558264) and cytokine-specific capture beads (BD CBA Soluble Protein Flex Set assays) were used to quantitatively measure IL-6 (Human IL-6 Flex Set (RUO) Cat. No. 558276), TNF- $\alpha$  (Human TNF Flex Set (RUO) Cat. No. 560112), and IL-10 (Human IL-10 Flex set (RUO) Cat. No. 558264), after 24 h of treatments (BDNVs B1/B2/B3 5, 22 and 45  $\mu\text{g}/\text{mL}$ ) and LPS stimulation (0.1  $\mu\text{g}/\text{mL}$ ) according to the manufacturer's protocol at DDEL, HIPS.

Multiplexed Bead-Based Immunoassays were analyzed with BD LSRFortessa FACS™ cell analyser. Outputs were computationally analyzed with the FCAP Array™ Analysis Software. BD CBA Soluble Protein Flex Set assays are used for the detection of cytokines, chemokines, and growth factors in the supernatant sample. The protein flex set having a distinct fluorescence is coated with a capture antibody specific for a soluble protein. The detection reagent containing a mixture of phycoerythrin (PE)-conjugated antibodies which provides a fluorescent signal in proportion to the amount of bound analyte. After the incubation of capture beads and detection reagent with standards or unknown samples containing recognized analytes, sandwich complexes (capture bead + analyte + detection reagent) are formed. The sandwich complexes formed can be measured quantitatively using flow cytometry to identify particles with fluorescence characteristics of both the bead and the detector. The outputs are generated in tables, which are then represented graphically using the BD™ CBA Analysis Software<sup>39</sup>. For representational purposes, only one analyte is displayed in Figure 3.

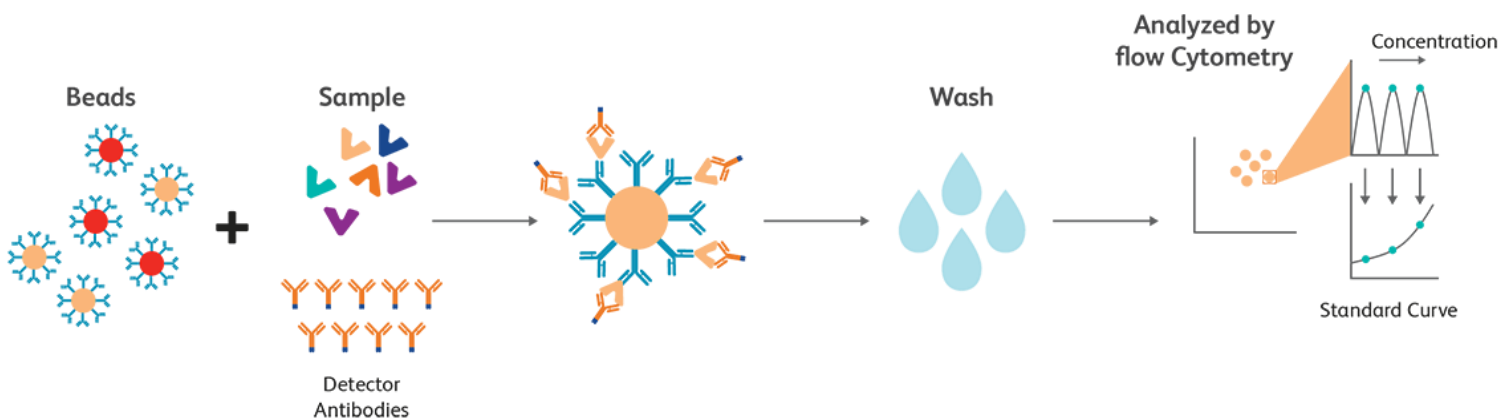


**Figure 3:** Overview of BD™ CBA assay protocol. Reproduced from Ref. 40

## **Results**

### **Isolation and physico-chemical characterization of BDNVs**

*Brassica oleracea* L. vesicles were isolated from the flower heads juice using ultracentrifugation method and purification on a discontinuous sucrose gradient. BDNVs mainly accumulated at the 8/30% (Band 1) and 30/45% (Band 2) interfaces of the sucrose gradient while a smaller band was also detected at the 45/60% interface (Band 3) (Figure 4a).

TEM analysis showed the morphology, integrity and size of isolated vesicles (Figure 4a). Analysis of the size distribution of the nanoparticles showed that BDNVs are nanosized and exhibit a fair degree of polydispersity. The BDNVs isolated from the various bands are not very dissimilar to each other in size, although an increasing trend can be observed from Band 1 to Band 3 (Figure 4b).

The average size measured by statistical analysis was about 52 nm (Band 1), 70 nm (Band 2), and 82 nm (Band 3), while the Zeta potential measurements established that all BDNVs were almost neutral (Table 2).

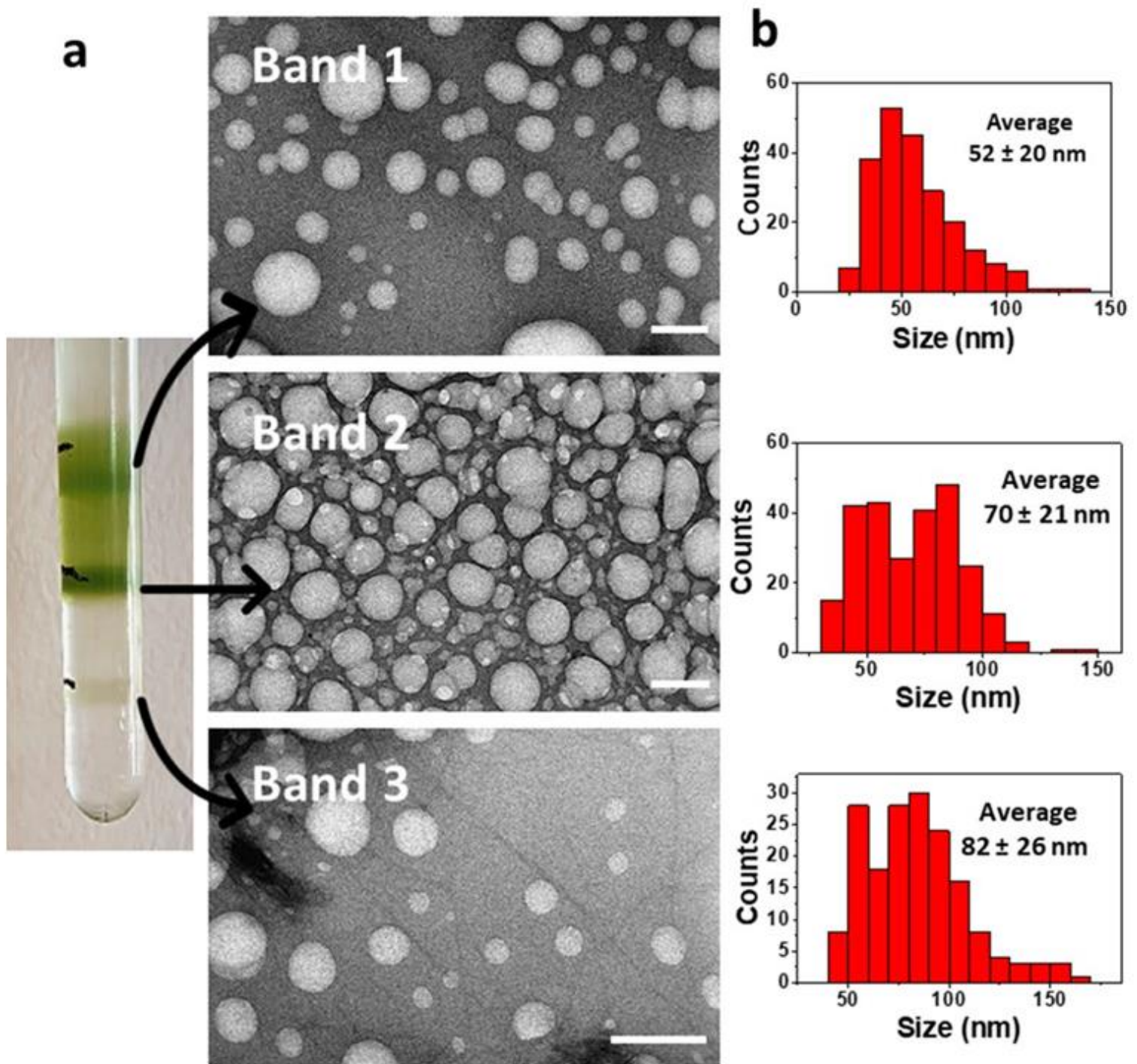


**Figure 4:** Characterization of BDNVs. (a) Broccoli-derived vesicles were collected as three bands after discontinuous sucrose gradient ultracentrifugation and analyzed at TEM. Representative TEM images of three BDNVs bands are shown in the three panels on the right. The scale bars indicate 100 nm.

(b) TEM-based size distribution measured on 200 BDNVs for each band.

Sample	Size (nm)	Zeta potential (mV)
Band 1	52 ± 20	0.00
Band 2	70 ± 21	2.70 ± 0.06
Band 3	82 ± 26	2.8 ± 0.3

**Table 2:** Size and zeta potential of isolated BDNVs. Data are shown as mean ± SD (n = 3).

### **Isolation and physico-chemical characterization of BDNVs isolated at DDEL, HIPS**

BDNVs were also isolated from Broccoli juice at DDEL, HIPS and purified using a sucrose gradient ultracentrifugation method as mentioned before. The majority of the BDNVs accumulated at the 8%/30% interface (Band 1, B1) and at the 30%/45% interface (Band 2, B2) and a small portion in 45%/60% interface (Band 3, B3) of the sucrose gradient (Figure 5a) as like the first year BDNVs isolation experiment.

#### **Cryo-Transmission Electron Microscopy (Cryo-TEM)**

BDNVs morphology isolated at DDEL, HIPS was examined by Cryo-TEM. The observations are shown in (Figure 5a). Cryo-TEM confirmed that all the samples contained intact, cup-shaped, membrane-bound vesicles. Size statistical analysis (BDNVs average size and size distribution) of Cryo-TEM images of each sample (B1, B2 and B3) was performed on 85 nanostructures by means of a freeware Image J analysis program (National Institutes of Health, USA) (Figure 5b). The average size of B1, B2 and B3 were 100 ±SD41 nm, 101±SD57nm and 113±SD55nm.

BDNVs isolated at DDEL, HIPS showed negative zeta potential irrespective of the Bands (B1/B2/B3) which indicates mutual repulsion and no tendency toward aggregated states (Table 3). The average zeta potential value of B1, B2 and B3 are respectively -26.0±SD0.8 mV, -24.0±SD4.0 mV and - 27.4±SD 1.2 mV.

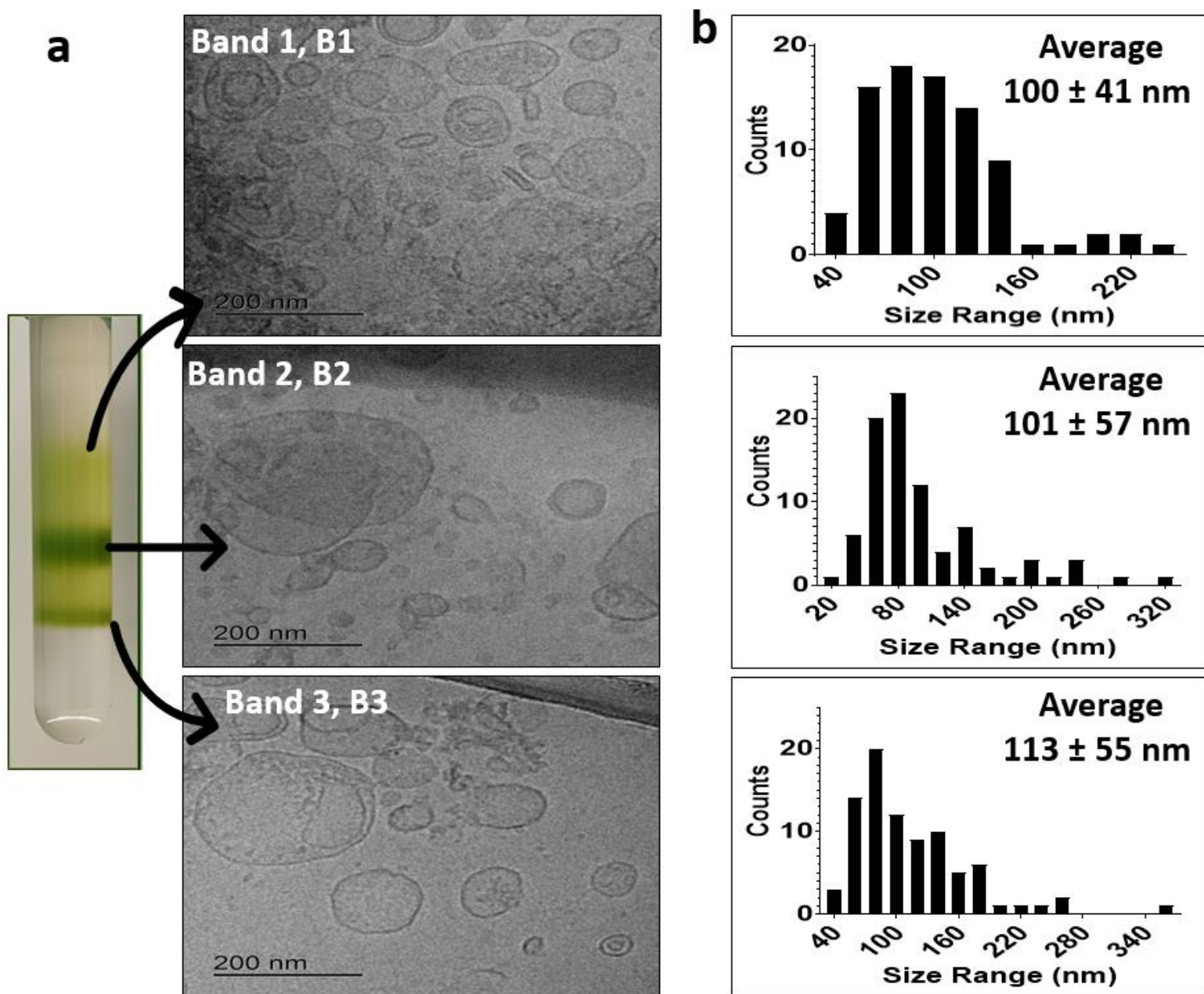


**Figure 5:** Characterization of BDNVs. (a) Broccoli-derived vesicles were collected as three bands after discontinuous sucrose gradient ultracentrifugation and analyzed at Cryo-TEM. Representative Cryo-TEM images of three BDNVs bands are shown in the three panels on the right. The scale bars indicate 200 nm.

(b) Cryo-TEM -based size distribution measured on 85 BDNVs for each band.

Sample	Size (nm)	Zeta Potential (mV)
Band 1, B1	100 ± 41	-26.0±0.8
Band 1, B2	101 ± 57	-24.0±4.0
Band 1, B3	113 ± 55	-27.4±1.2

**Table 3:** Size and zeta potential of isolated BDNVs. Data are shown as mean ± SD (n = 3).

#### Nanoparticle Tracking Analysis (NTA)

NTA measures Brownian motion related to hydrodynamic diameter of the particle by image analysis, tracking the motion of each particle which is related to particle size. The method is more suitable for polydisperse samples like BDNVs as it analyzes each particle separately. The size distribution and concentration of isolated BDNVs were measured by using NTA (Figure 6). As shown in Figure, average particle size of B1, B2 and B3 were 170±SD14 nm, 173±SD7 nm and 179±SD13 nm respectively. Moreover, B1 contained the highest number of particles (1.1e+013 particles/ml) compared to the other fractions (7.8e+012 for B2 and 5.6e+012 for B3) (Figure 6).

It is possible to note that NTA size is bigger for all band samples than Cryo-TEM size. This is due to the fact that Cryo-TEM measures the actual size, whereas NTA gives you hydrodynamic size which is the size of the nanoparticle plus the liquid layer around the particles.



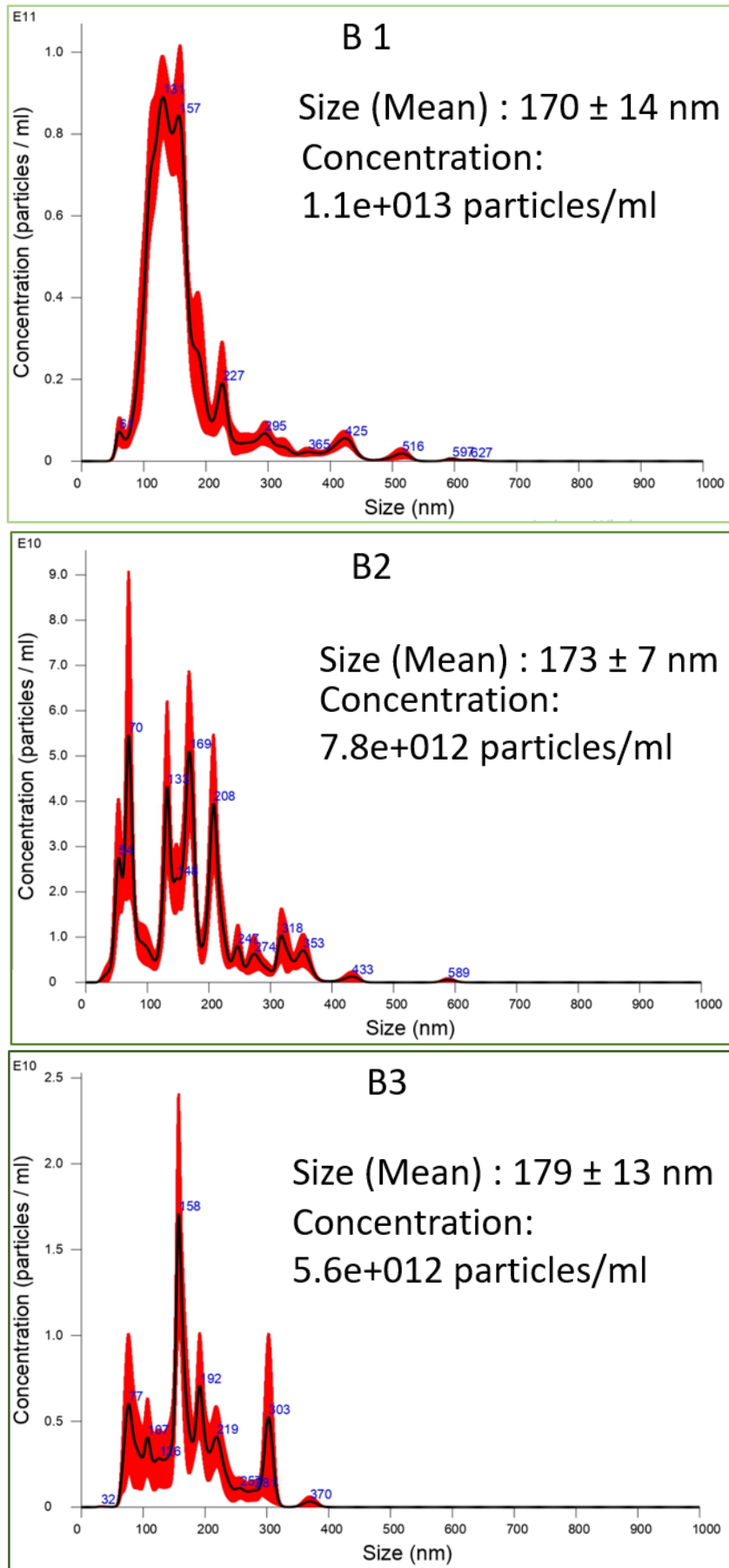


**Figure 6:** Size distribution and concentration of isolated BDNVs measured by NTA, N=3



### Determination of Protein Concentration

The protein content, as analysed by the Bradford method, was found to be  $1692 \pm 182 \mu\text{g/mL}$  (Band 1),  $1201 \pm 152 \mu\text{g/mL}$  (Band 2), and  $223 \pm 234 \mu\text{g/mL}$  (Band 3) ( $n = 2$ ). To see whether proteins were distributed among the outside and inside of vesicles, BDNVs were treated with RIPA buffer and compared with untreated vesicles by SDS-PAGE. Figure 7 shows that there were not differences in protein species between RIPA-treated and untreated BDNVs. Moreover, the densitometric analysis for each lane determined that RIPA extraction increased only 9%, 3% and 1% the overall intensity of Band 1, Band 2, and Band 3 respectively. Overall, these data indicate that the major proteins were expressed on the vesicle surface of all three Bands.

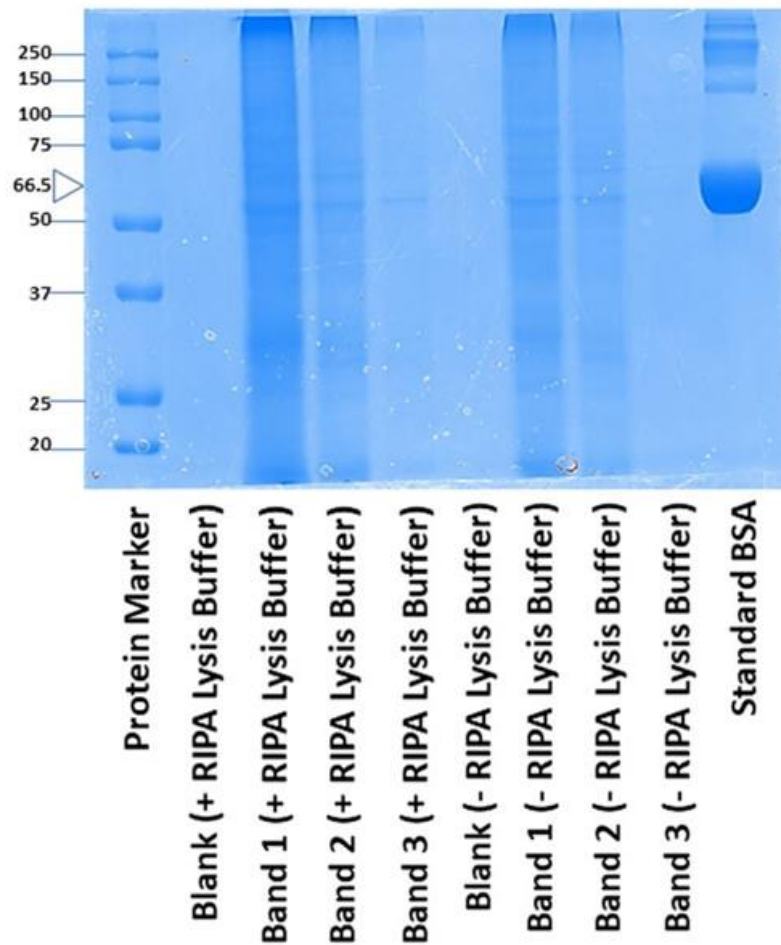


**Figure 7:** SDS-PAGE of protein extracted from BDNVs. Molecular weight of standards is shown on the left as kDa. BSA bovine serum albumin, whose MW is indicated as 66.5 kDa by an arrowhead.

The protein concentration of the BDNVs samples isolated at DDEL, HIPS was also determined according to the protocol mentioned above. The results are summarized in the Figure 8. As a summary of duplicate experiments, the protein concentration was higher when treated with RIPA lysis buffer in comparison with the non treated samples.

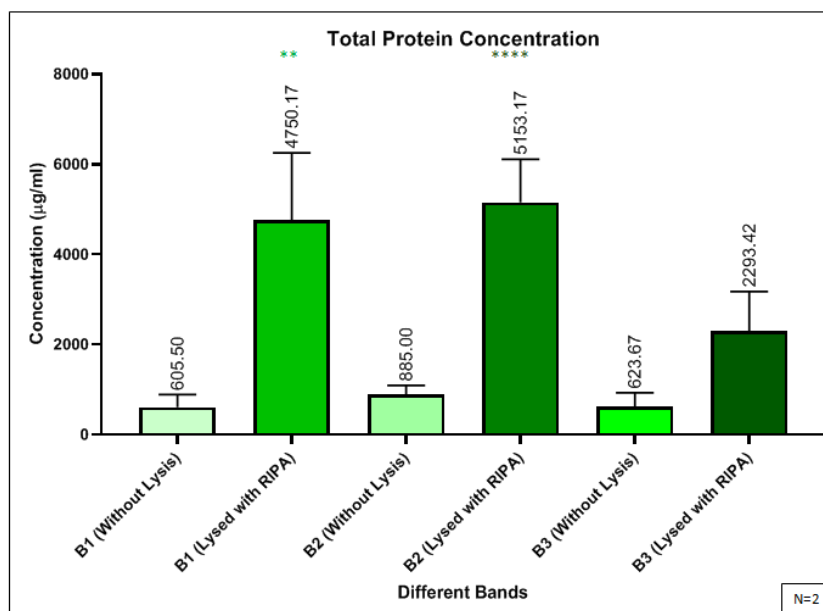


**Figure 8:** Determination of Protein concentration, N=2

### Viability Assay (MTT assay)

In order to test the ability of *Brassica oleracea* L. vesicles to influence the growth of human tumor cells, NCI-H441 (lung adenocarcinoma), Caco-2 (colorectal adenocarcinoma), and SHSY5Y (neuroblastoma) were treated for 24 h with a concentration range of vesicles (5–5000 µg/mL). The MTT assay showed that BDNVs inhibited tumor cell metabolic activity in a dose dependent manner compared with untreated cells (Figure 9). Overall Bands 2 and 3 were found to be more toxic than Band 1 irrespective of the cell lines.

The Cytocompatibility effects of BDNVs under in vitro conditions against A549 cells, diff.THP-1 cells and hAELVi cells were also examined during the research activities carried out at DDEL, HIPS. In terms of MTT results, considering A549 cells, 45 µg/ml, 100 µg/ml, 500 µg/ml and 5000 µg/ml of BDNVs B1 gave a significant reduction of cell viability, while this result was observed from all the concentration of B3 except 22 µg/ml (Figure 10). For diff.THP-1 cells, only higher two concentrations 500 µg/ml and 5000 µg/ml were significantly cytotoxic irrespective of the Bands B1, B2 and B3 (Figure 10). For hAELVi cells, 100 µg/ml, 500 µg/ml and 5000 µg/ml were significantly cytotoxic for both B1 and B3, while only the higher two

concentrations 500  $\mu\text{g/ml}$  and 5000  $\mu\text{g/ml}$  were found significantly cytotoxic for B2 (Figure 10). In general, The MTT assay showed that BDNVs inhibited cell viability in a dose dependent manner compared with untreated cells. In case of cancer cell line A549, the inhibition was associated with lower concentrations such as 45  $\mu\text{g/ml}$  for B1 and B2 and 5  $\mu\text{g/ml}$  for B3. Whereas in case of non cancerous cell lines (diff. THP-1 and hAELVi), the inhibition was related to higher treatment conditions such as 500  $\mu\text{g/ml}$  and 5000  $\mu\text{g/ml}$  for diff. THP-1 and 100  $\mu\text{g/ml}$ , 500  $\mu\text{g/ml}$  and 5000  $\mu\text{g/ml}$  of BDNVs B1 and B3 in case of hAELVi cells.

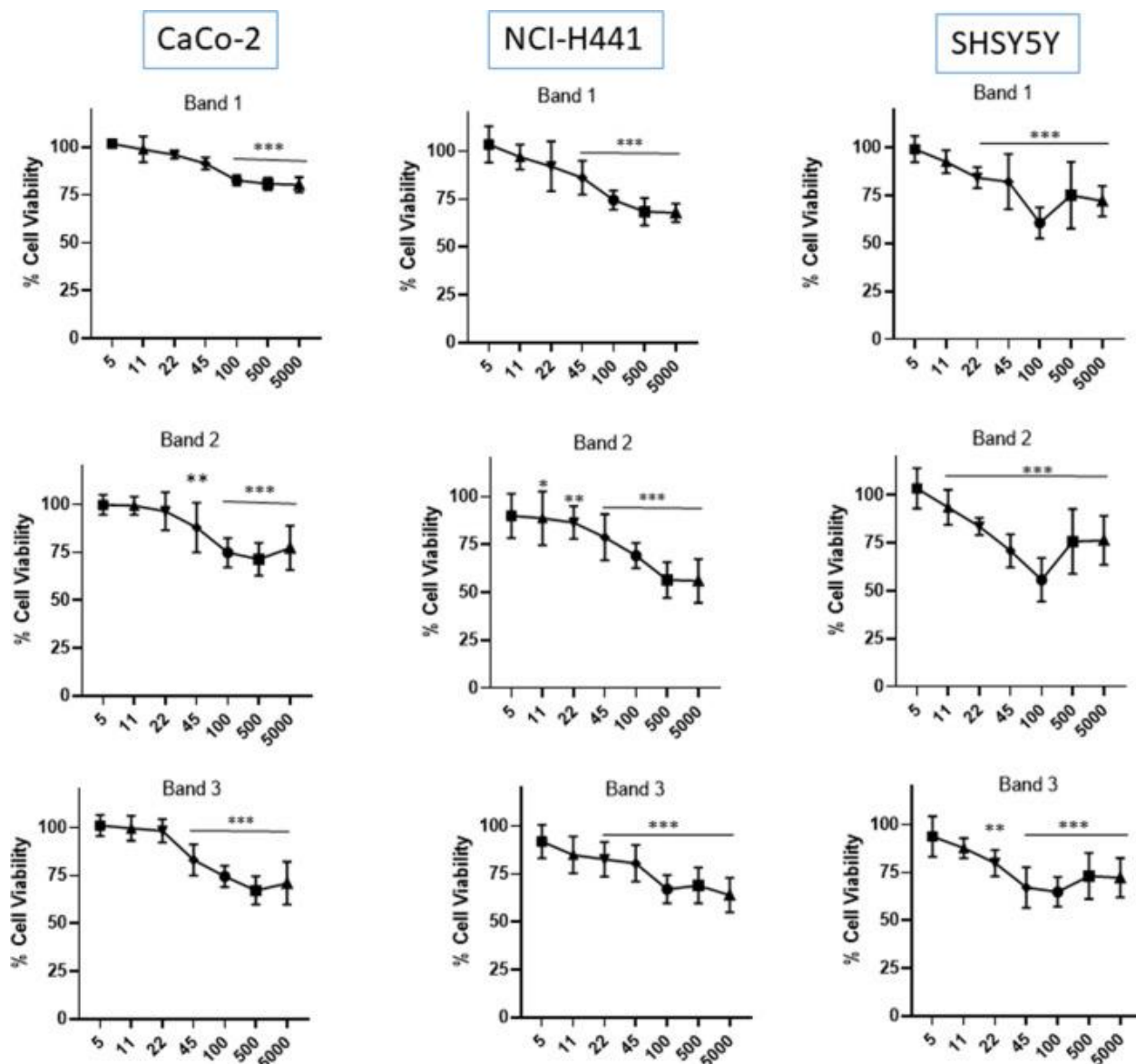
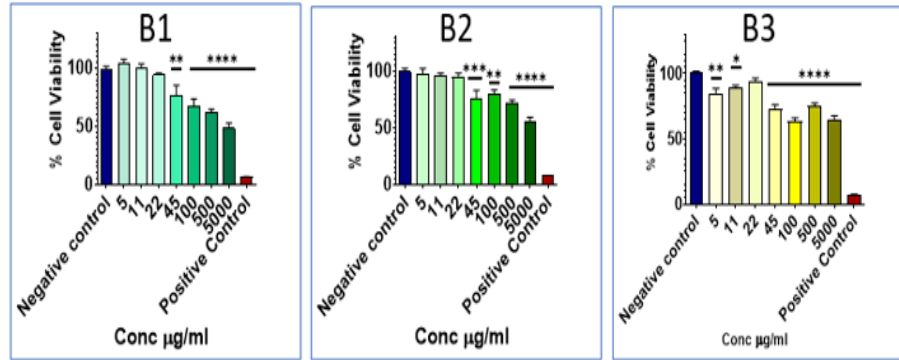
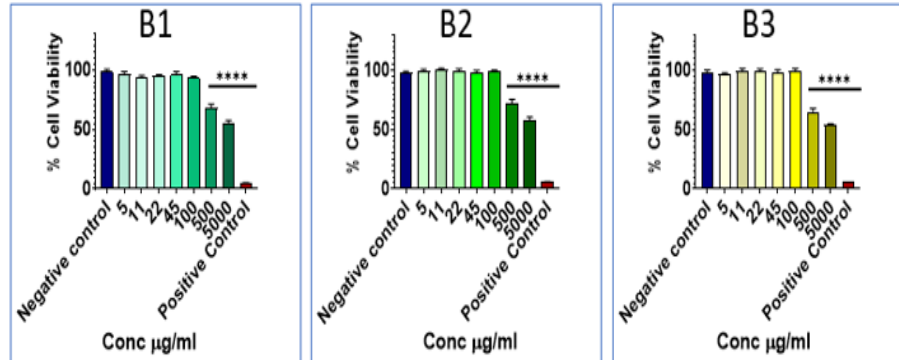


**Figure 9:** BDNVs inhibit the metabolism of tumor cell lines. Cell metabolism was measured by MTT assay after 24 h of treatment with different concentrations of BDNVs (indicated as  $\mu\text{g/mL}$ ). Negative controls are untreated cells (100% of vitality), whereas 10% Triton X-100 was used as positive control. Each bar represents the mean  $\pm$  SD of three independent experiments.

A549 cells



diff. THP-1 cells



hAELVi cells

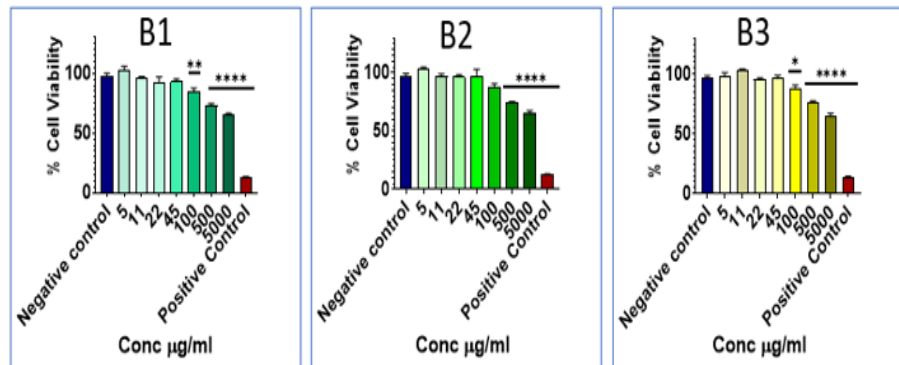


**Figure 10:** Cellular viability study. Cell metabolism was measured by MTT assay after 24 h of treatment with different concentrations of BDNVs (indicated as µg/mL). Negative controls are untreated cells (100% of vitality), whereas 10% Triton X-100 was used as positive control. Each bar represents the mean ± SD of two independent experiments.

## Cell uptake of BDNVs

In order to see whether these effects were due to the cell uptake of BDNVs, we obtained PKH26 fluorescently labelled BDNVs, incubated them for 2 and 24 h with Caco-2, NCI-H441 and SHSY5Y cells, and analysed by epifluorescence and confocal microscopy. Two concentrations that were responsible for not more of 20% of cytotoxicity were chosen, i.e. 5 and 22  $\mu\text{g}/\text{mL}$ . A fluorescent background signal was not detected when cells were incubated with medium only (Figure 11).

The application of fluorescent BDNVs to Caco-2 cells resulted in no or negligible uptake with 5  $\mu\text{g}/\text{mL}$  at both time points with all three Band preparations (Figure 12a–c,g–i,m–o). By using 22  $\mu\text{g}/\text{mL}$ , while no uptake was observed at 2 h with all three Bands (Figure 12d,j,p; just a single cell with Band 2, yellow arrowhead), some cells resulted positive at 24 h as judged by small dots (white arrows) or large dots (yellow arrowheads) around or close to nuclei (Figure 12e,f,k–l,q–r). Interestingly, while in most cases the punctuate fluorescent signals were located peripherally to the cell islands, we could catch an accumulation of dots in the central part of an island (Figure 12f).

NCI-H441 cells took up BDNVs more easily than Caco-2 cells, and at higher extent when challenged for 24 h with vesicles at the concentration of 22  $\mu\text{g}/\text{mL}$  (Figure 13). Interestingly, some cells were associated with two or more dots (yellow arrows) and others with more diffuse perinuclear staining (white arrowheads).

On the other hand, BDNVs were taken up by SHSY5Y cells already with 5  $\mu\text{g}/\text{mL}$  (Figure 14c,i,o). Band 1 and Band 3 at 22  $\mu\text{g}/\text{mL}$  were associated with more cells than at 5  $\mu\text{g}/\text{mL}$  (Figure 14, compare f with c, and r with o). Larger dots associated with cells were also observed (yellow arrowheads).

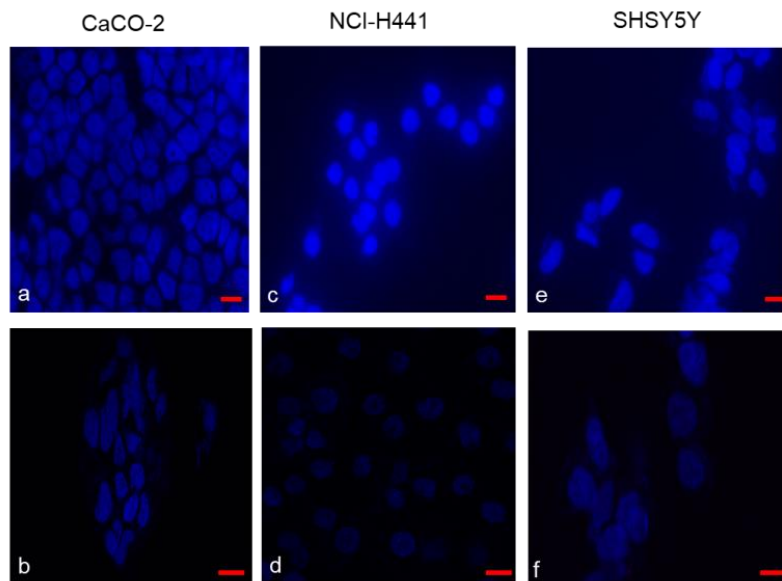


**Figure 11:** Controls, i.e. cells incubated with medium only, are shown for all cell types. Cells were incubated with medium only and stained with DAPI. a, c, and e represents the negative control from epifluorescence microscopic observation. Bar = 10  $\mu\text{m}$ . b, d, and f represent the negative control from confocal microscopic observation. Bar= 25  $\mu\text{m}$ .

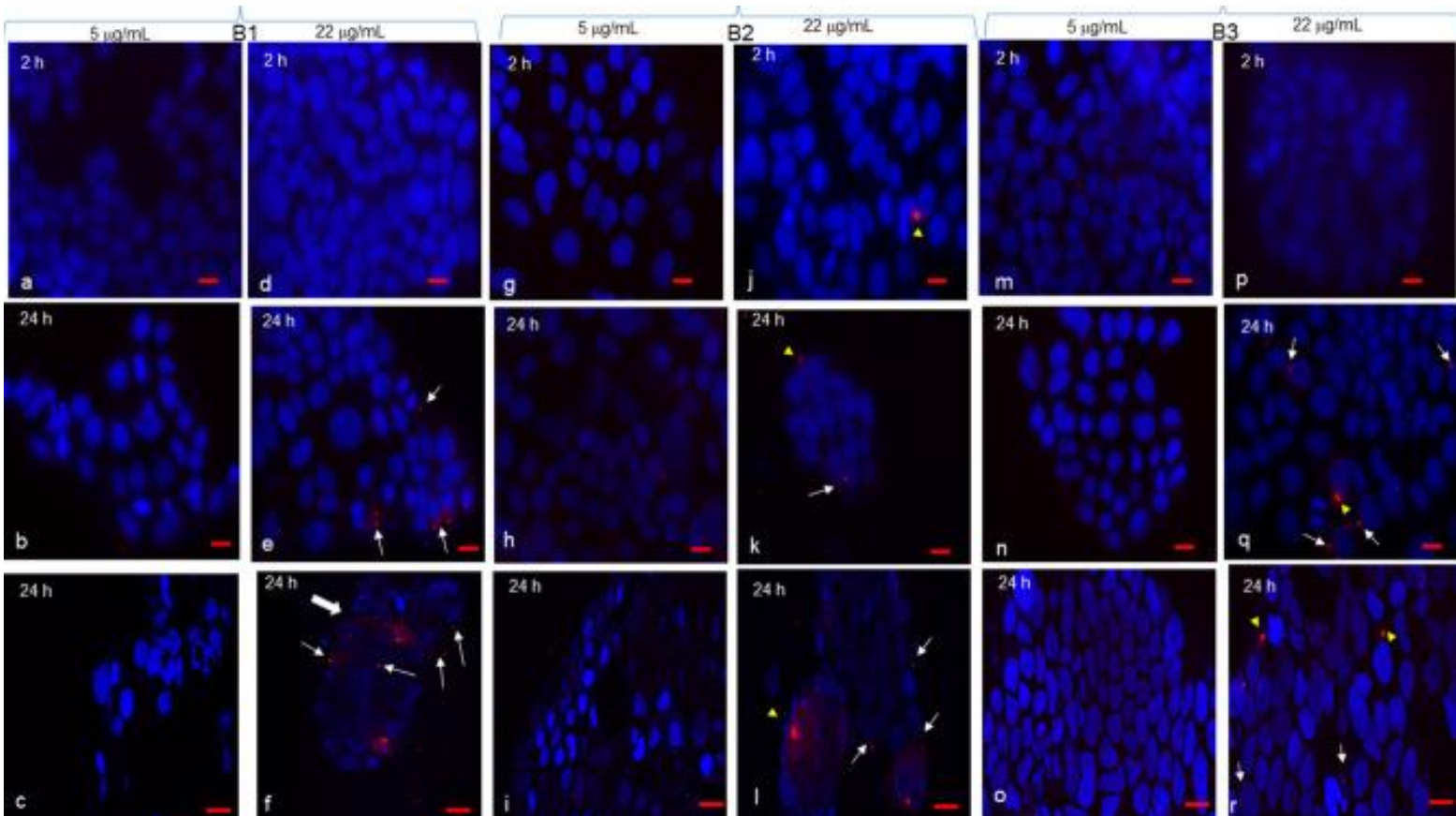


**Figure 12:** Caco-2 uptake of BDNVs. Caco-2 cells were grown on 8-chamber glass tissue culture slides, coverslips mounted, and incubated with Band 1 (a–f), Band 2 (g–l), or Band 3



(m–r) at 5 and 22  $\mu\text{g}/\text{mL}$  for 2 or 24 h. After each time point, cells were observed by confocal microscopy (c,f,i,l,o,r) or by epifluorescence (all the remaining panels). White arrows and yellow arrowheads indicate single small and large dots around nuclei respectively. A thick arrow in (f) indicates a point of entrance into an island of numerous BDNVs. Bar in (a,b,d,e,g,h,j,m,n,p,q) = 10  $\mu\text{m}$ ; bar in (c,f,i,l,o,r) = 25  $\mu\text{m}$

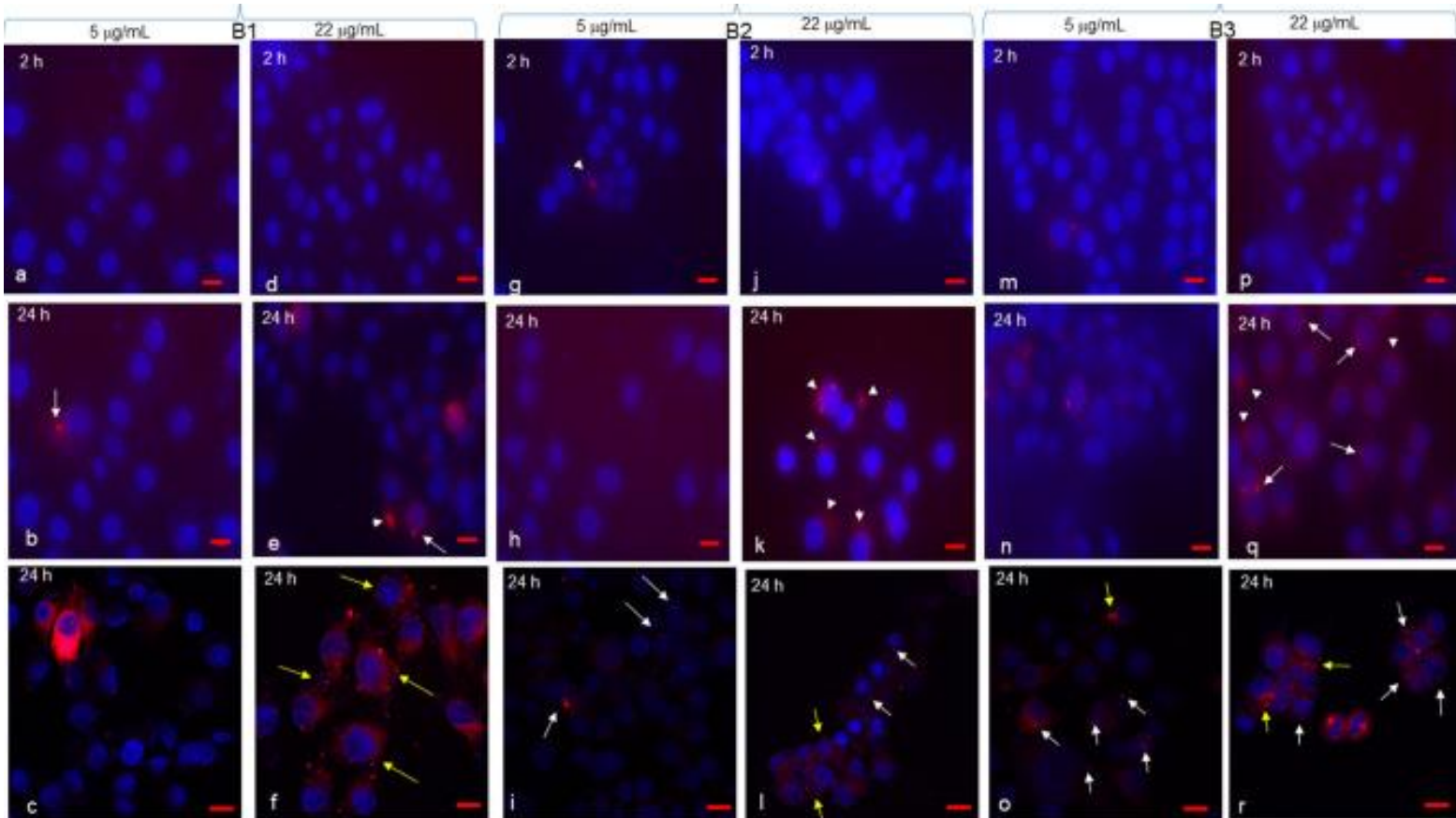


**Figure 13:** NCI-H441 uptake of BDNVs. NCI-H441 cells were grown on 8-chamber glass tissue culture slides, coverslips mounted, and incubated with Band 1 (a–f), Band 2 (g–l), or Band 3 (m–r) at 5 and 22  $\mu\text{g}/\text{mL}$  for 2 or 24 h. After each time point, cells were observed by confocal microscopy (c,f,i,l,o,r) or by epifluorescence (all the remaining panels). White arrows indicate single dots around nuclei. Yellow arrows point to a single cell with two or more dots around its nucleus. White arrowheads indicate diffuse perinuclear staining. Bar in (a,b,d,e,g,h,j,m,n,p,q) = 10  $\mu\text{m}$ ; bar in (c,f,i,l,o,r) = 25  $\mu\text{m}$ .

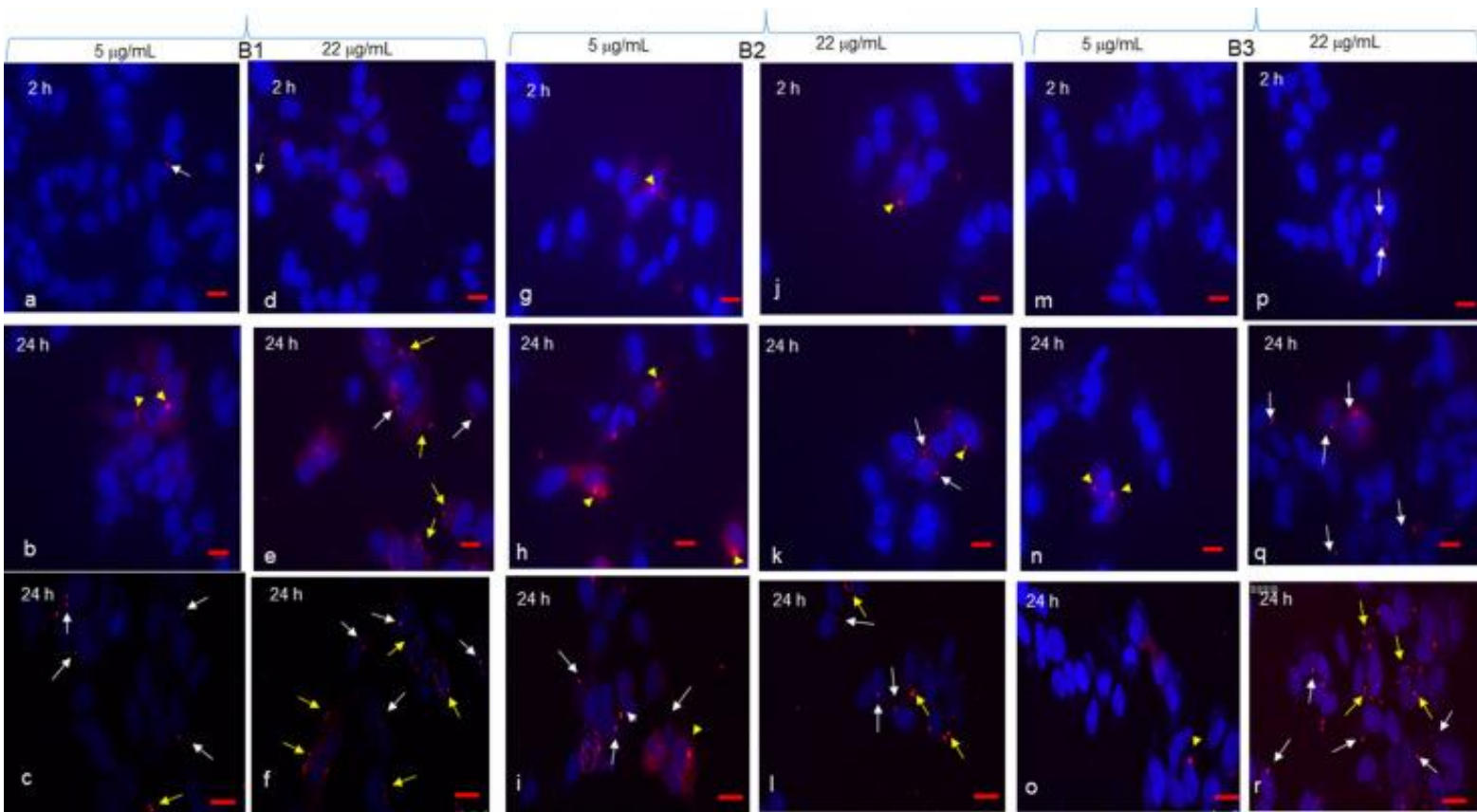


**Figure 14:** SHSY5Y uptake of BDVs. SHSY5Y cells were grown on 8-chamber glass tissue culture slides, coverslips mounted, and incubated with Band 1 (a–f), Band 2 (g–l), or Band 3 (m–r) at 5 and 22  $\mu\text{g}/\text{mL}$  for 2 or 24 h. After each time point, cells were observed by confocal microscopy (c,f,i,l,o,r) or by epifluorescence (all the remaining panels). White arrows indicate single dots around nuclei. Yellow arrowheads indicate larger dots. Yellow arrows point to a single cell with two or more dots around its nucleus. Bar in (a,b,d,e,g,h,j,m,n,p,q) = 10  $\mu\text{m}$ ; bar in (c,f,i,l,o,r) = 25  $\mu\text{m}$



The concentrations that was responsible for not more than 20% of cytotoxicity was chosen, i.e. 22  $\mu\text{g}/\text{mL}$  for cellular uptake studies considering diff. THP-1 cells and hAELVI cells at DDEL, HIPS.

diff.TH-1 cells were grown on 8-chamber glass tissue culture slides, cover slips mounted, and incubated with B1, B2, or B3 at 22  $\mu\text{g}/\text{mL}$  for 6h. The cells were stimulated with LPS after 2h of BDNVs pretreatment and continued for incubation. After 6h, cells were observed by confocal microscopy. A fluorescent background signal was not detected when cells were incubated with medium only (Figure 15, upper panel). In general, cells resulted positive at 6 h as judged by small dots or large dots around or close to nuclei (Figure 15, lower panel).

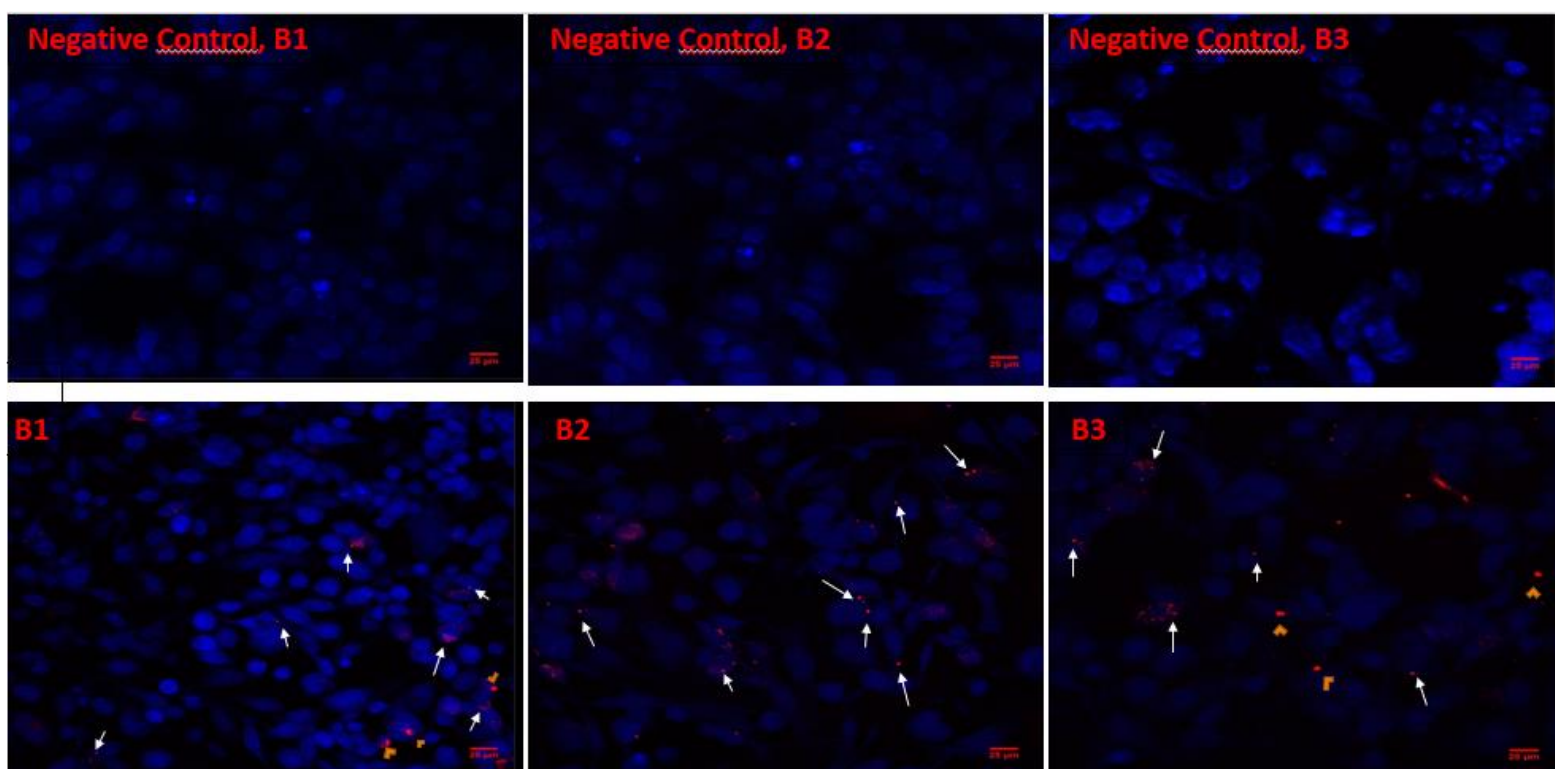


**Figure 15:** Stimulated diff. THP-1 uptake of BDNVs. Upper panel represents negative controls, i.e. cells incubated with medium only. Lower panel represents cellular uptake of BDNVs (B1, B2 and B3). White arrows indicate single dots around nuclei. Yellow arrowheads indicate larger dots. Bar = 25  $\mu\text{m}$ .

Like diff.TH-1, hAELVi cells were grown on 8-chamber glass tissue culture slides, cover slips mounted, and incubated with B1, B2, or B3 at 22  $\mu\text{g}/\text{mL}$ . After 6h, cells were observed by confocal microscopy. In general, no positive signals were observed in either negative controls or cells incubated with labelled BDNVs (B1, B2 or B3) (Figure 16).

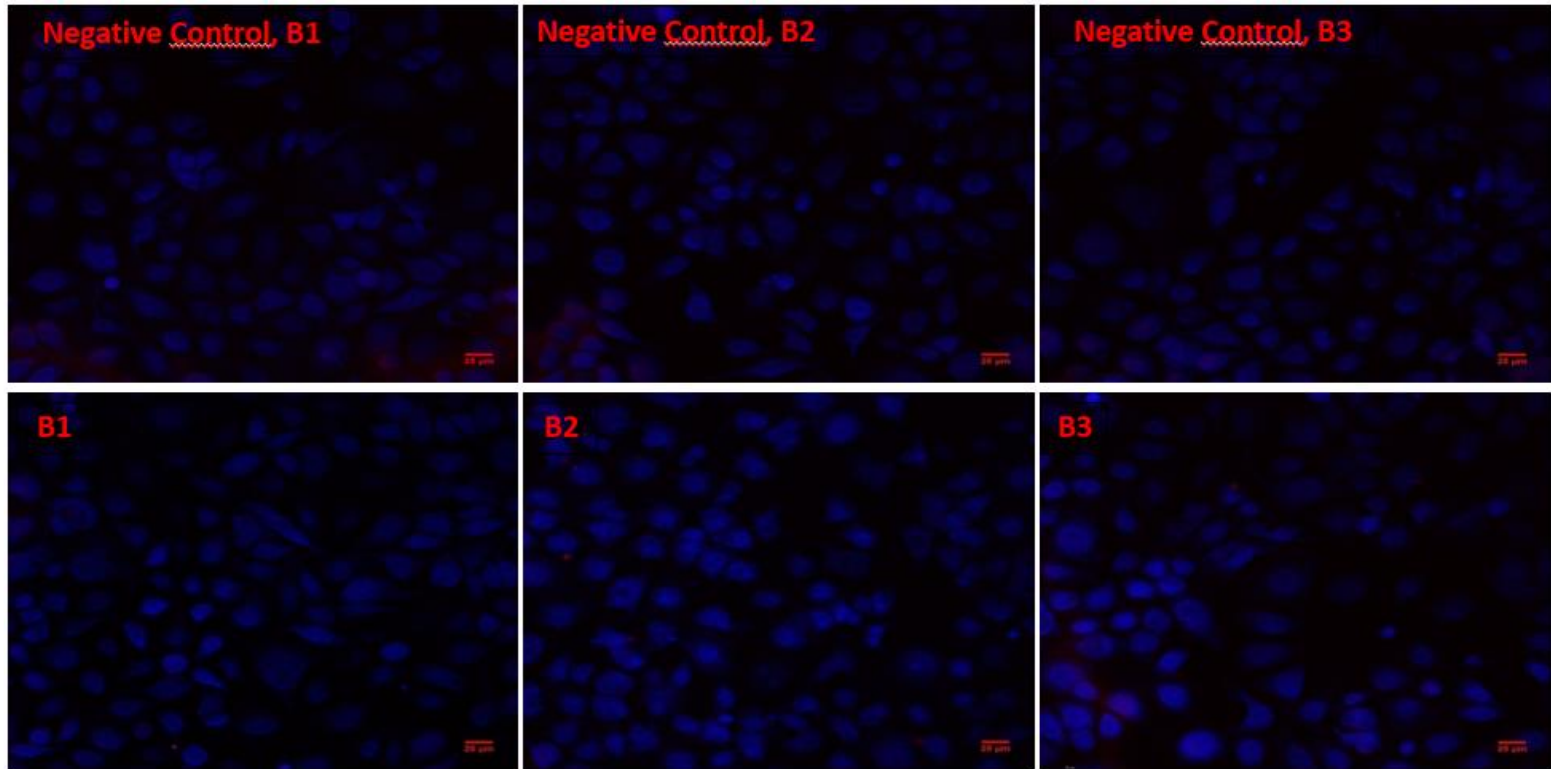


**Figure 16:** hAELVi uptake of BDNVs. Upper panel represents negative controls, i.e. cells incubated with medium only. Lower panel represents cells incubated with labelled BDNVs (B1, B2 and B3). Bar = 25 µm.

### **Uptake Mechanism**

diff.THP-1 cells were incubated with inhibitors to block cellular uptake of labelled BDNVs. As shown in Figure 17, the uptake of BDNVs in stimulated differentiated THP-1 cells markedly inhibited by filipin III in case of B1 and B2 whereas by cytochalasin D and filipin III in case of B3. Filipin III is the inhibitor of Caveolin dependent Endocytosis and Cytochalasin D is the inhibitor of Macropinocytosis. So the internalization of B1 and B2 in stimulated diff.THP-1 cells is mostly via Caveolin dependent Endocytosis whereas B3 mostly internalized by Macropinocytosis and Caveolin dependent Endocytosis (Figure 17).

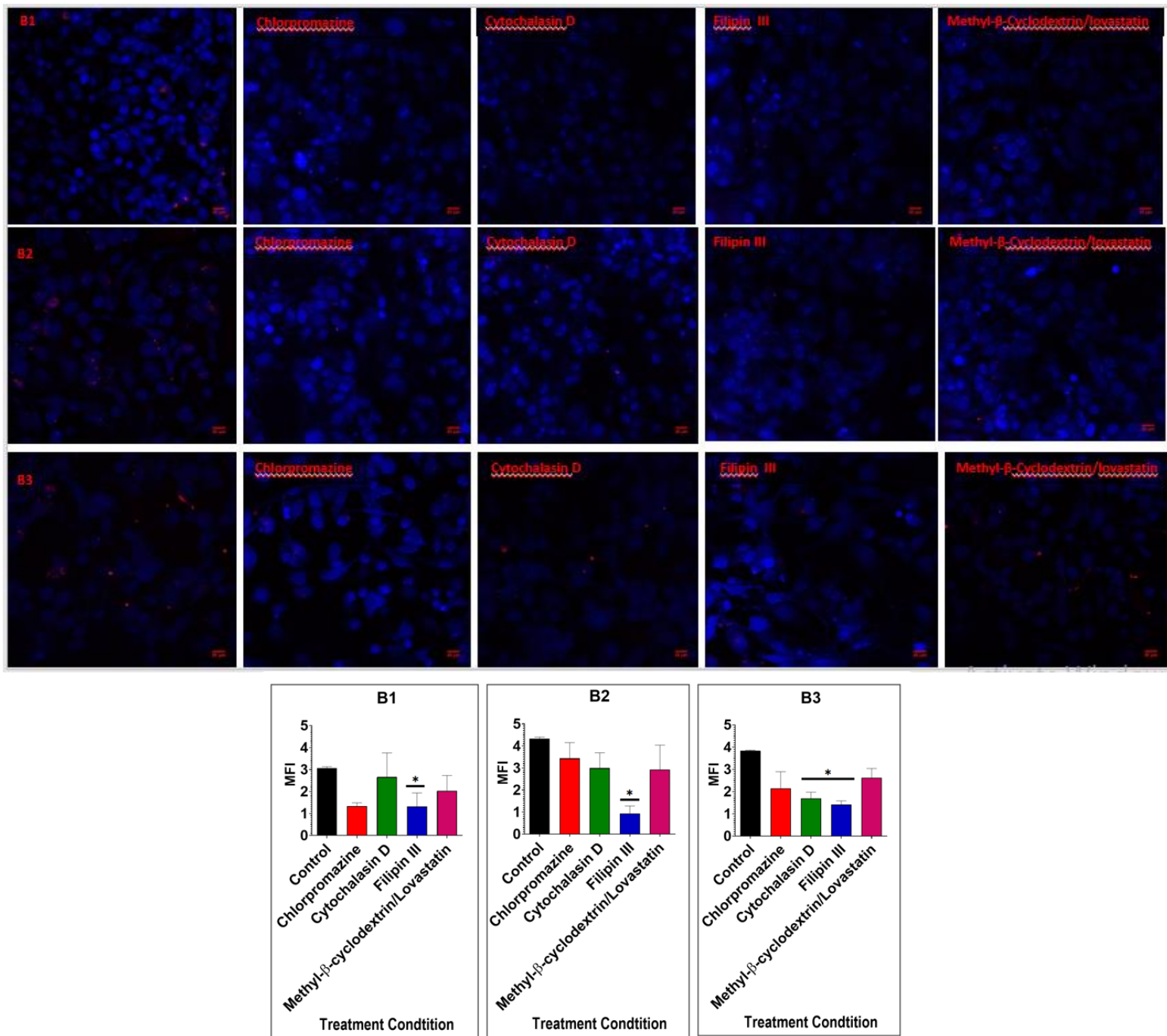


**Figure 17:** The inhibition of BDNVs internalization in stimulated diff.THP-1 cells. diff.THP-1 cells were pretreated with Chlorpromazine, Cytochalasin D, Filipin III and Methyl-β-cyclodextrin/lovastatin for 1 h and then incubated with PKH26-label BDNVs (red) for 2h, stimulated with LPS 0.1 μg/ml and incubated for an additional 4 h in the presence of the inhibitors. Cells were then fixed and stained with DAPI (blue). The red fluorescence intensity of BDNVs was determined by ImageJ software. Bar graphs show the Mean Fluorescence Intensity of BDNVs. Scale bar = 25 μm.

## Anti-oxidant activity of BDNVs

To understand whether BDNVs could operate as antioxidants, the three tumoral cell lines (Caco-2, NCI-H441 and SHSY5Y) were considered. Caco-2 and NCI-H441 cells are responsive to oxidative stress elicited by  $H_2O_2$ <sup>27,28</sup> while SHSY5Y are reactive to the neurotoxin 6-OHDA<sup>29</sup>. Using a ROS-sensitive fluorescent probe ( $H_2DCFDA$ ), we observed that the intracellular levels of ROS were higher in Caco-2 and NCI-H441 cells treated with  $H_2O_2$  and SHSY5Y cells treated with 6-OHDA as compared with unstimulated cells (Figure 18). Pre-treatment with either 5 or 22  $\mu\text{g/mL}$  BDNVs determined a reduction of ROS levels when cells were challenged with either  $H_2O_2$  or 6-OHDA and brought them to those of control unstimulated cells. All Bands were capable to reduce significantly the ROS production.

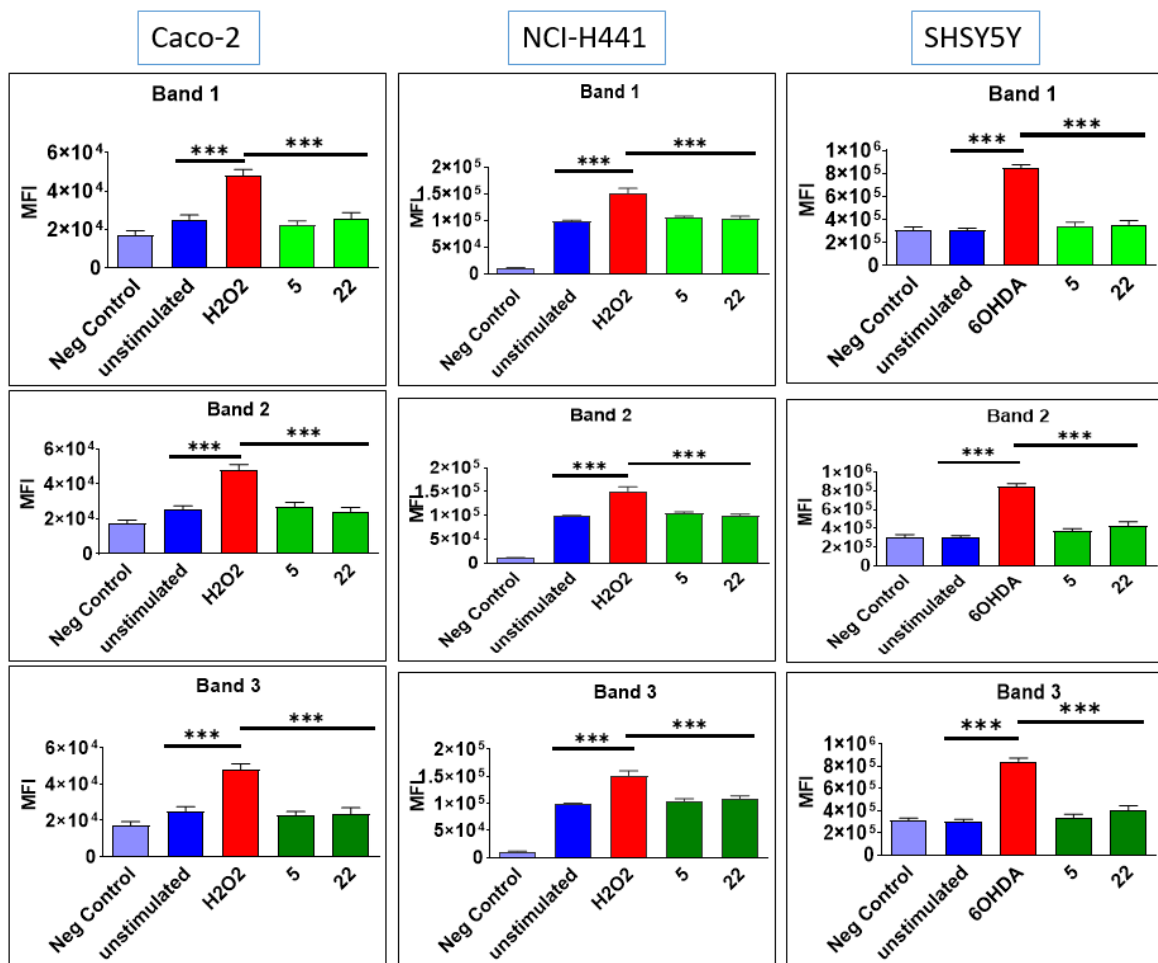


**Figure 18:** Efficacy of BDNVs on oxidative stress. Cells were incubated with 5 or 22  $\mu\text{g/mL}$  BDNVs for 24 h before treatment with 100  $\mu\text{M}$   $H_2O_2$  (Caco-2 and NCI-H441) or 100  $\mu\text{M}$  6-OHDA (SHSY5Y) for further 24 h. The mean fluorescence intensity (MFI) was measured by multiwell spectrofluorimeter after incubation with  $H_2DCFDA$ . Data are shown as mean  $\pm$  SD of two experiments conducted each in quadruplicate. \*\*\* $p < 0.001$ . BDNVs at 5 and 22  $\mu\text{g/mL}$  were significantly different as compared with  $H_2O_2$ - or 6-OHDA-stimulated cells, but not towards unstimulated cells.



### Extraction and identification of GSLs in BDNVs

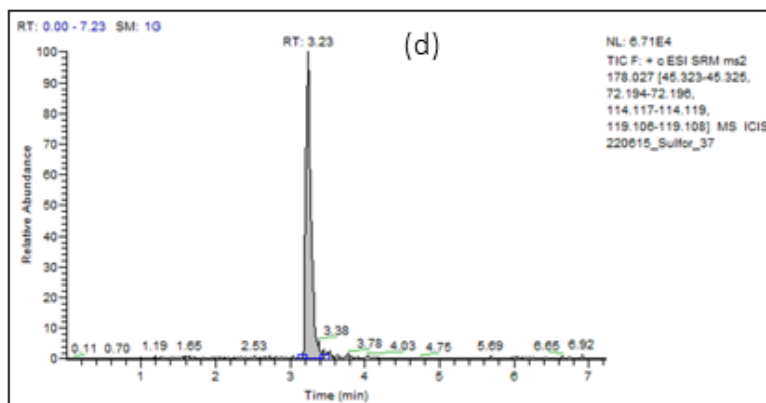
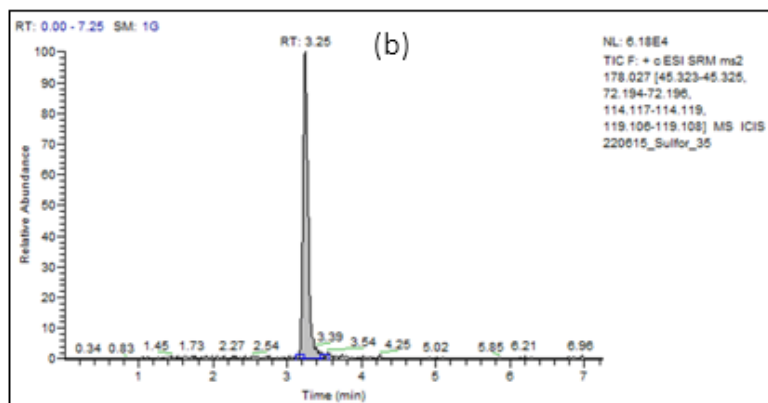
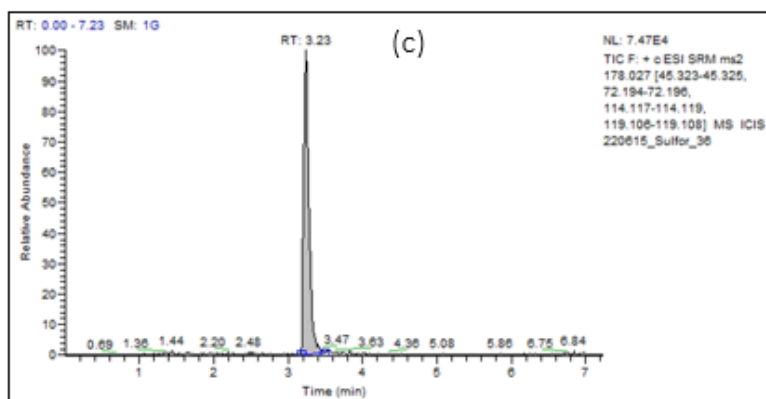
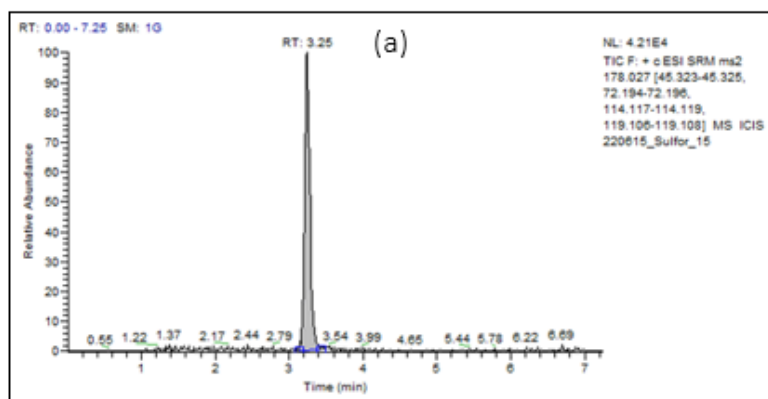
The occurrence of GSLs in methanol/aqueous extracts obtained from BDNVs suspensions was verified by a careful elaboration of the corresponding RPLC-ESI-FTMS and -FTMS/MS (AIF) data. Specifically, ion currents were systematically extracted for a set of exact  $m/z$  values corresponding to the deprotonated forms of GSLs typical of Brassicaceae vegetables, in accordance with the comprehensive study (involving 25 different species) recently published by Dong et al. and based on the same MS instrumentation used during this work<sup>41</sup>. When chromatographic peaks emerged from the ion current extraction, the occurrence of specific glucosinolate fragments was assessed in the AIF FTMS/MS data acquired in the same retention time intervals of those peaks. If positive, this elaboration provided the final confirmation of the identification of glucosinolates. As a result, the occurrence of glucobrassicin, glucoraphanin and neoglucobrassicin was confirmed in most samples. The corresponding chromatographic peak areas were then compared with the one related to the internal standard glucocamelinin and an estimate of their concentrations, expressed as glucocamelinin equivalents, was obtained. Considering dilution and pre-concentration steps included in the sample preparation procedure and assuming a quantitative extraction, the concentrations in the original aqueous suspensions of BDNVs were calculated and are reported in Table 4. As apparent, all the three GSLs were found in the extract related to Band 1, with concentrations much higher than those observed for the other bands. Actually, as shown in the table, glucobrassicin and neoglucobrassicin could not be detected in extracts related to Bands 2 and 3.

Compound	Band 1	Band 2	Band 3
Glucobrassicin	8.9 ± 1.3	ND	ND
Glucoraphanin	8.7 ± 1.1	0.80 ± 0.08	0.30 ± 0.04
Neoglucobrassicin (N-methoxy-glucobrassicin)	2.6 ± 0.3	ND	ND

**Table 4:** Concentrations, expressed as glucocamelinin equivalents and in nanomole/L units, estimated for glucosinolates in the aqueous suspensions corresponding to Bands 1, 2 and 3. Data are shown as mean ± SD (n = 3). ND not detected.

## Determination of SFN content

Cruciferous vegetable like Broccoli is already known to be rich in GSLs. Among the glucosinolates, Glucoraphanin and glucobrassicin are those particular type which produces sulforaphane when undergo a myrosinase-catalyzed hydrolysis<sup>42</sup>. SFN which is an isothiocyanate, has attracted much attention in recent years since it was discovered as one of the most potent naturally occurring inducer of phase-II detoxification enzymes as well as has been reported to inhibit the growth of a variety of cancers, such as cervical<sup>43</sup>, breast<sup>44</sup>, and bladder cancer<sup>45</sup>; renal cell carcinoma<sup>46</sup>; non-small-cell lung cancer<sup>47</sup>; and colon and prostate cancers<sup>48</sup>. The SFN content was determined by LC-MS/MS. The highest SFN content was found in B1 followed by B2 and B3. The differences caused by various solvent system (M, R and MF) were not significant. The results are shown in Figure 19, 20 and Table 5.



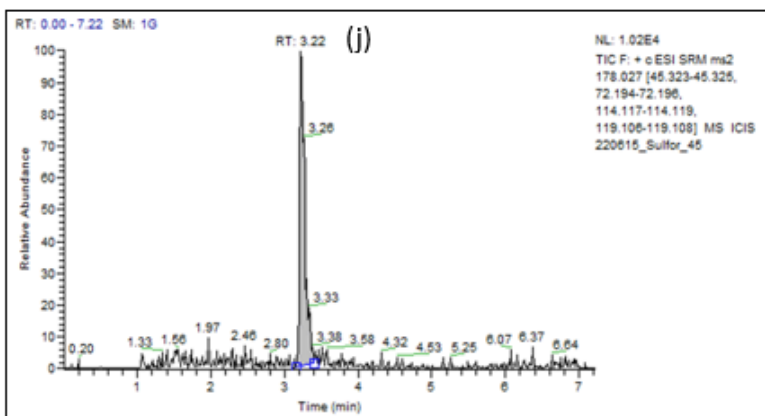
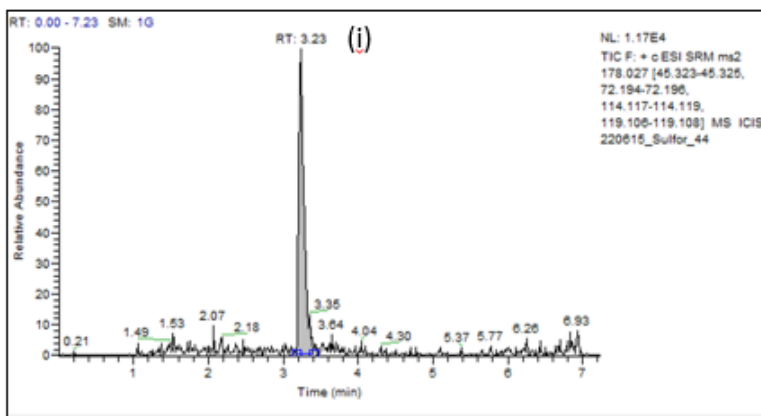
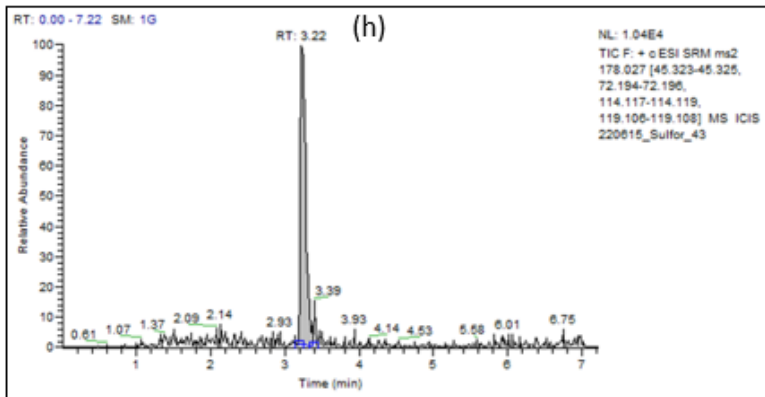
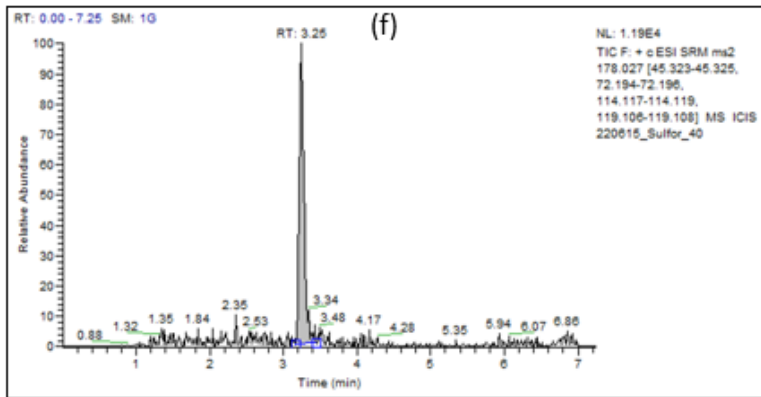
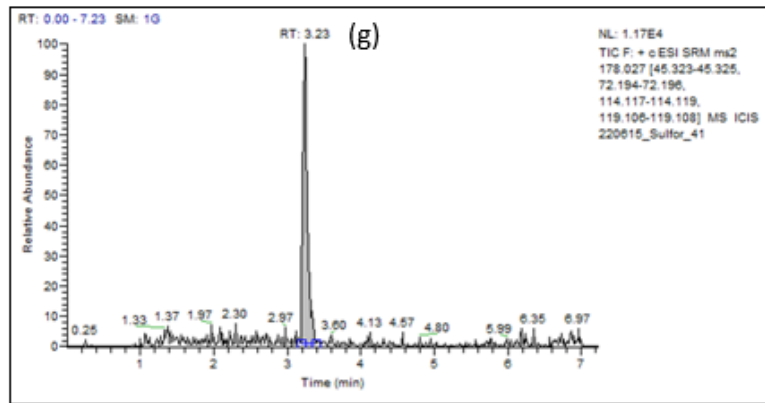
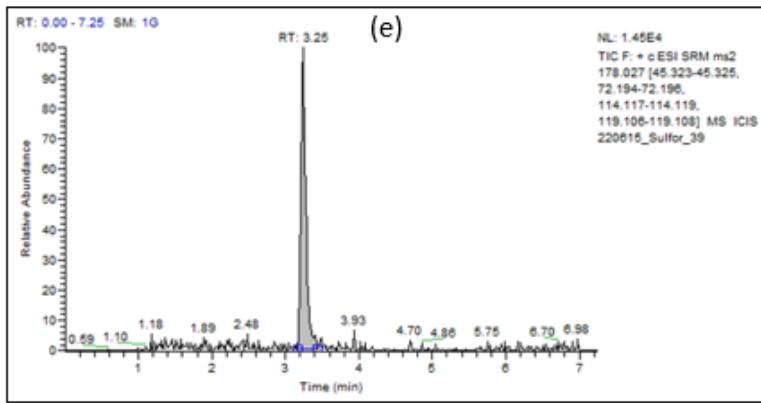


**Figure 19:** Chromatograms of (a) Standard, 10 ng (b) B1 in M (c) B1 in R (d) B1 in MF (e) B2 in M (f) B2 in R (g) B2 in MF (h) B3 in M (i) B3 in R (j) B3 in MF, N=2



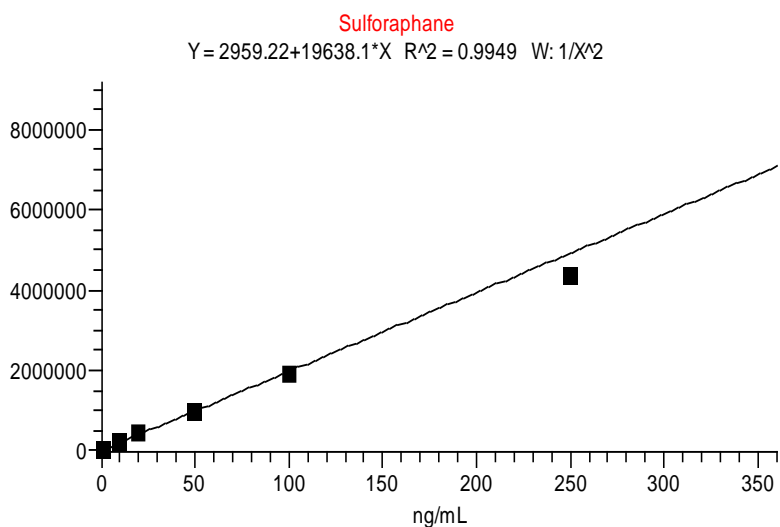


**Figure 20:** Linearity Curve of SFN Standard

Sample Name	Concentration of SFN (ng/mL)
B1M	1683.37
B1R	1837.24
B1MF	1653.53
B2M	357.23
B2R	283.53
B2MF	248.66
B3M	247.06
B3R	266.07
B3MF	219.88

**Table 5:** Content of SFN in different Bands

## Identification of Bioactive Natural Compounds with GNPS

Recently, Global Natural Products Social Molecular Networking (GNPS) has been reported as an open-access web-based mass spectrometry database platform which is known for the storage, analysis, and sharing of raw, processed or identified tandem mass (MS/MS) spectrometry data. GNPS can enable molecular networking (MN) by comparing all MS/MS spectra, visualizing spectral correlations, and detecting sets of spectra from related molecules, even if the spectra are not matched to any known compounds<sup>33</sup>. GNPS database can also be used to identify known compounds by using high throughput dereplication<sup>33</sup>. GNPS library searching was performed with the top 6 matched peaks and cosine score above 0.7 as mentioned before. The GNPS database indicated the presence of 4 pharmaceutically potent compounds in different bands as presented in Table 6. GNPS lists the name of the Compounds as they are mentioned in the library from which the compounds were tagged. This means the name of the compounds vary based on the source of the library. There were some compounds presented specifically in a particular band like Arbutin presented in B2 where as some compounds were presented in more than one band like 13-docosenamide presented in all of the three bands (B1, B2 and B3). Compounds which didn't have therapeutic activities like membrane protein were not mentioned in the corresponding tables but are available in the related links mentioned here (B1 <https://gnps.ucsd.edu/ProteoSAFe/status.jsp?task=94056aca63364935aef2aea8ed745fb9>; B2 <https://gnps.ucsd.edu/ProteoSAFe/status.jsp?task=1e4363b4007a4ebbbbed845664313ce3>; B3 <https://gnps.ucsd.edu/ProteoSAFe/status.jsp?task=6b7c10ccfe4d4e2c91d69d349e8be939>). The structures of the identified compounds are presented in Figure 21.

Compound Name	Cosine	Exact Mass	Source	Function/Activity	Ref.
Pheophorbide A	0.93	592.268	B1, B2	Antiviral activity	49,50
				Anti proliferative Activity in several cancer cell lines (Burkitt Lymphoma, Hepatocellular carcinoma Hep3B, Uterine sarcoma MES-SA, Resistant Human Hepatoma cell R-HepG2, Human breast adenocarcinoma MDA-MB-231, Human Breast tumor MCF-7, Human oral squamous cell carcinoma YD10B, Murine oral squamous cell carcinoma AT-84, Glioblastoma cells U87MG)	51,52, 53,54, 55,56, 57,58, 59
				Anti-inflammatory activity	60
				Anti-oxidant activity	61
				Immunostimulatory activity	62
13-Docosenamide	0.85	337.335	B1, B2, B3	Anti-parasitic activity	63
				Antiviral Activity	64
				Antifungal Activity	65,66 67
				Antibacterial Activity	66,67
9-Octadecenamide	0.90	281.272	B1, B2, B3	Antinociceptive and anti-inflammatory activity	68
				Antibacterial Activity	69,67
				Antifungal Activity	67
Arbutin	0.92	272.09	B2	hypolipidemic effect	70
				Anti-inflammatory activity	71
				Anti-Melanogenic Effect	72
				Antioxidant activity	73

**Table 6:** Identification of potent compounds with therapeutic activities through GNPS library searching.

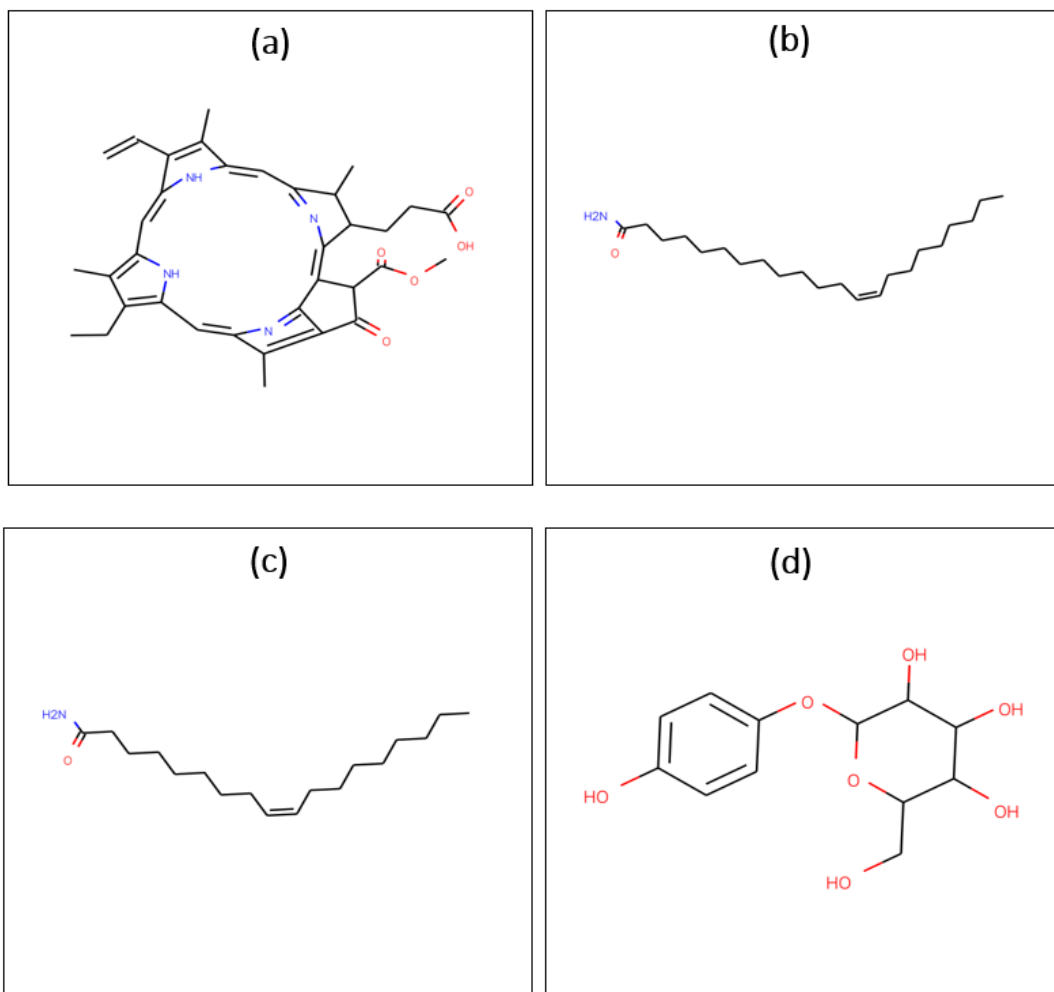


**Figure 21:** Structures of the identified compounds. (a) Pheophorbide A (b) 13-Docosenamide (c) 9-Octadecenamide (d) Arbutin

### Filter Compatibility Study (Terminal Sterilization)

In the filter compatibility study done at DDEL, HIPS, both the particle size and concentrations were measured before and after filtration to determine the filtration effects on BDNVs. As shown in the Figure 22 and Figure 23 below, neither the filtration process, nor the selected filter membrane materials affected particle size as well as particles concentration except one condition (B3 filtration with 0.2  $\mu\text{m}$  filter). In case of B3 filtration with 0.2  $\mu\text{m}$  filter, there is a significant reduction of size (mean) in comparison with the unfiltered condition.

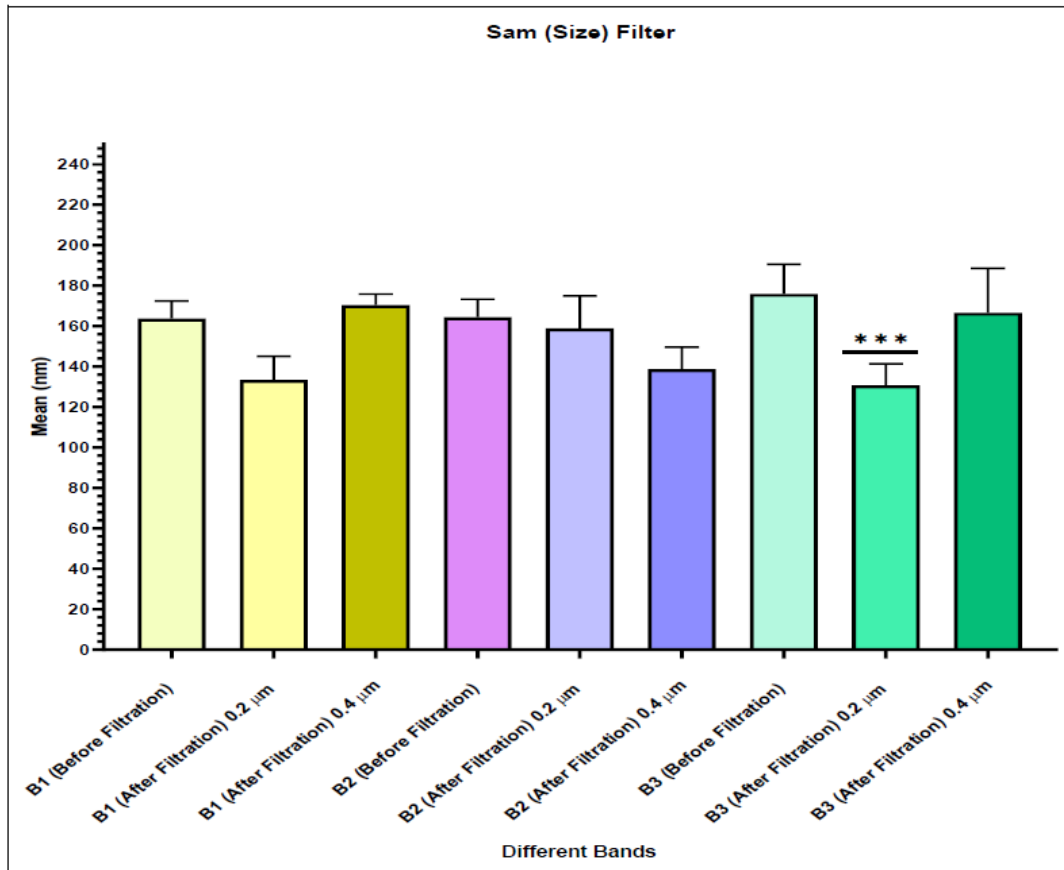
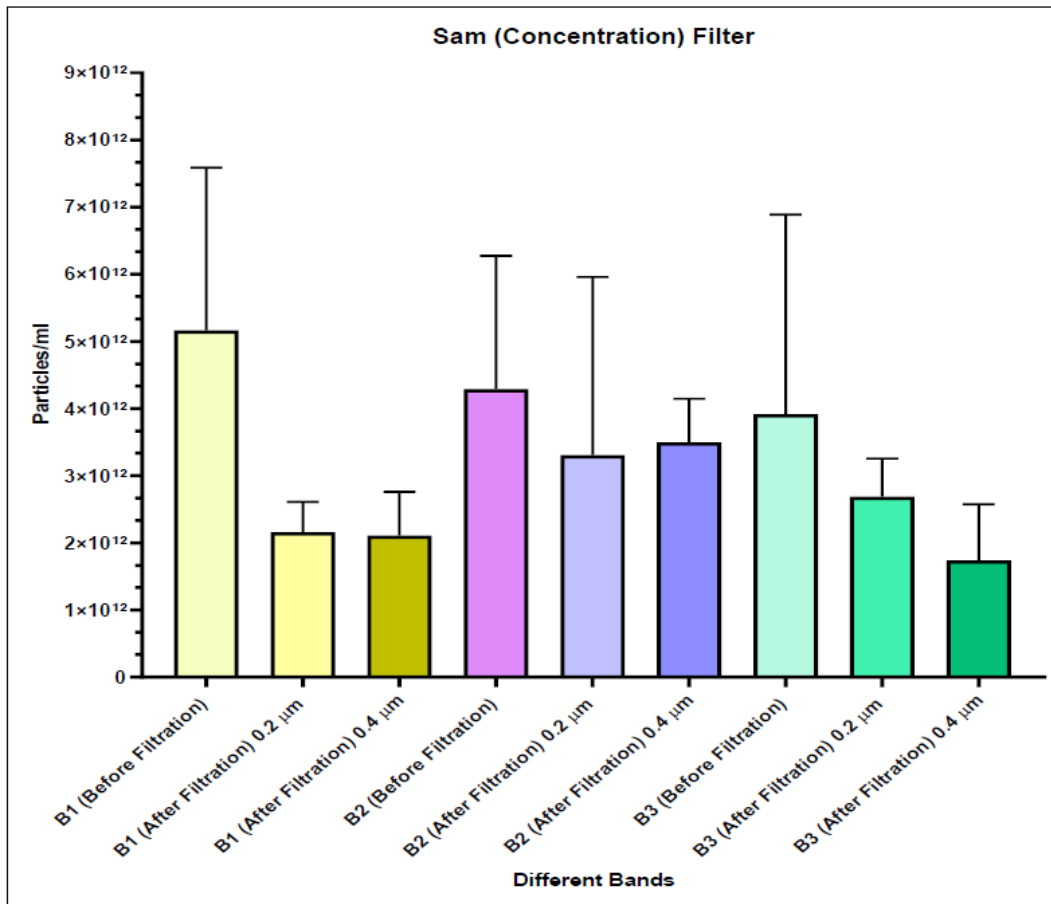


Figure 22: Particle size (Mean), Before & After-filtration, N=2



**Figure 23:** Particle Concentration, Before & After-filtration, N=2

## Long-Term Stability Study

The physical stability of the BDNVs was analyzed by measuring their size, concentration and zeta potential.

The size of the BDNVs was not significantly changed until after 8 weeks of storage except for the storage condition at 4°C. In case of 4°C, there was a significant change of size of B3 after 4 weeks of storage (Figure 24).

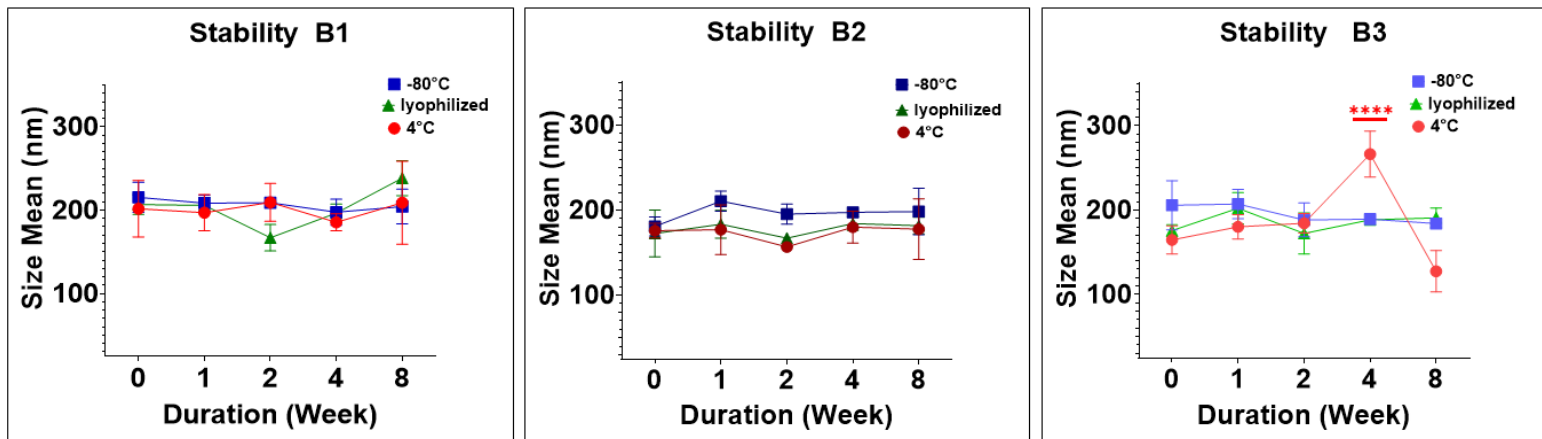


**Figure 24:** Long-Term Stability Study of BDNPs (Size). n=3

In case of concentration, there was a significant change mostly at 4°C. In case of B1, the concentration was significantly decreased after 2 weeks and 8 weeks whereas in case of B2, there was a significant concentrations drop at last time points (4 weeks and 8 weeks). Except 4°C condition, there were other two significant changes of the concentrations at the intermediate time points (Lyophilized condition of B2 and -80°C of B3 after 4 weeks) followed by no significant difference at the end time point (after 8 weeks) (Figure 25).

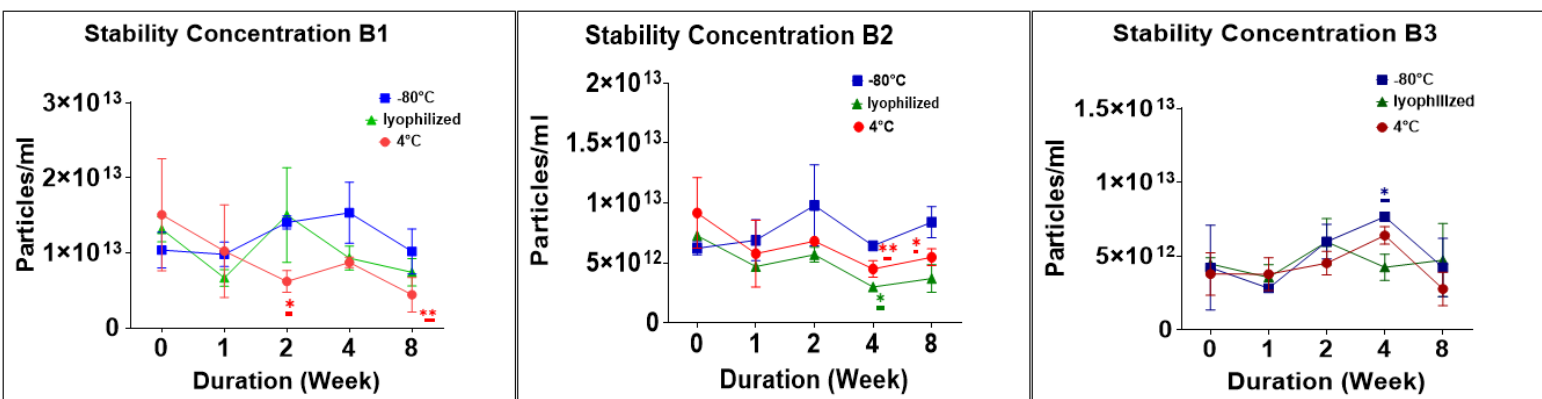


**Figure 25:** Long-Term Stability Study of BDNVs (Concentration). n=3

The stability study of zeta potential revealed that irrespective of the conditions, the zeta potential value of all Bands (B1, B2 and B3) were stable at -80°C even after 8 weeks. In case of lyophilized condition, there was a significant change after 8 weeks in case of B2. For the 4°C condition, significant change observed both in B2 and B3 after 8 weeks of stability (Figure 26).

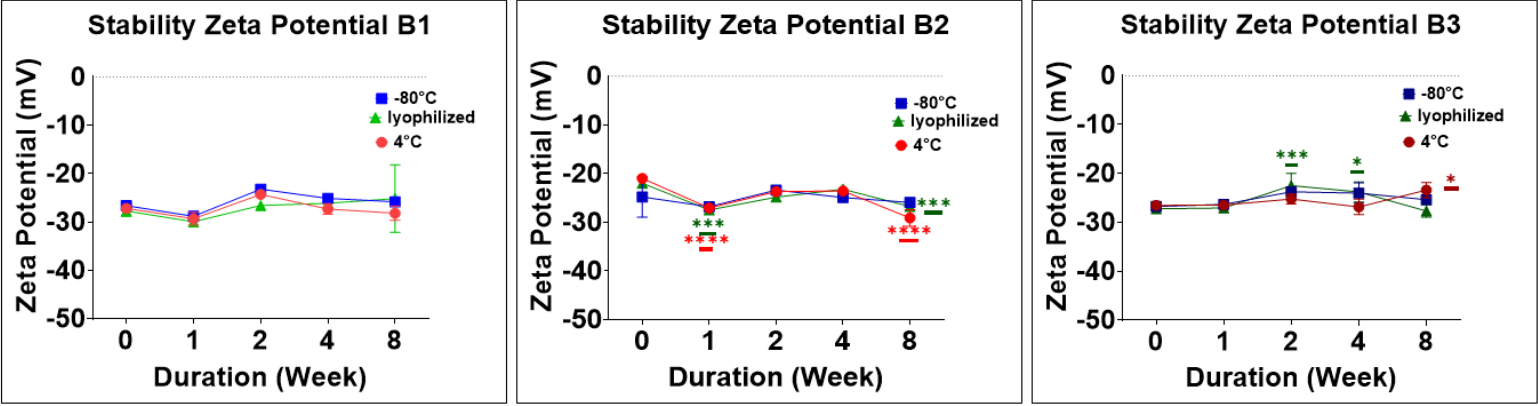
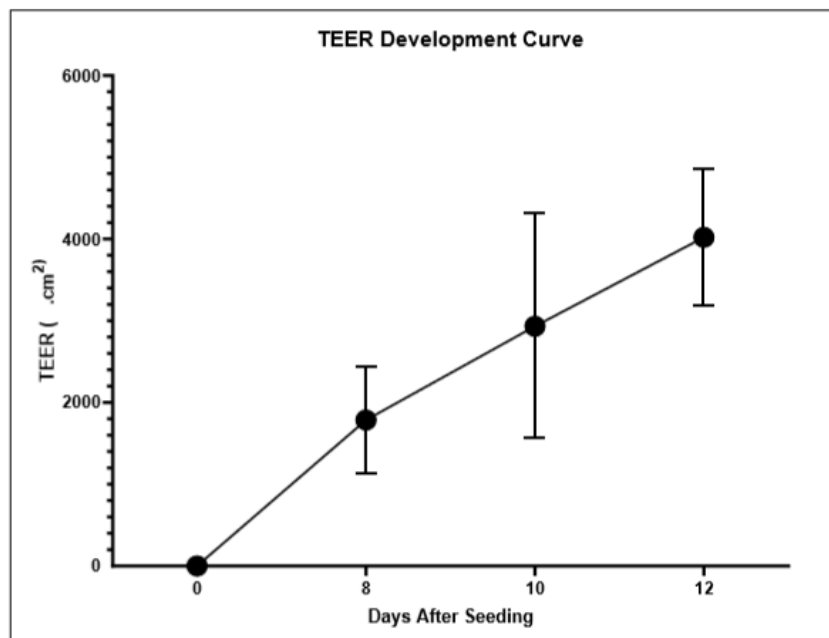


Figure 26: Long-Term Stability Study of BDNVs (Zeta Potential). n=3



### Trans-Epithelial Electrical Resistance (TEER)

A three-dimensional model of epithelial ATI like cells (hAELVi) co-cultured with surrogates for alveolar macrophages occurs to be a relevant model for either designing new pharmaceuticals for respiratory medicine or assessing the toxicity of nanomaterials, such as nanoparticles like BDNVs and drug carriers. In Transwell inserts, hAELVi cells formed a monolayer which corresponds to the thin epithelial layer observed in alveoli<sup>22</sup>. This observation was confirmed by TEER measurements, that reached around 3000  $\Omega \cdot \text{cm}^2$  after 10 days of seeding (Figure 27) and increased continuously (around 4000  $\Omega \cdot \text{cm}^2$ ) even after treatment (LPS stimulation and BDNVs treatment) at 12 days. Comparison between TEER measurements before (at 10<sup>th</sup> day) and after treatment (at 12<sup>th</sup> day) revealed no significant differences (Figure 28). Anyhow, the TEER values in both before and after treatment are higher than 1000  $\Omega \cdot \text{cm}^2$ , indicating an electrical tight barrier<sup>22</sup>.



**Figure 27:** TEER development curve of hAELVi cells seeded on Transwell.

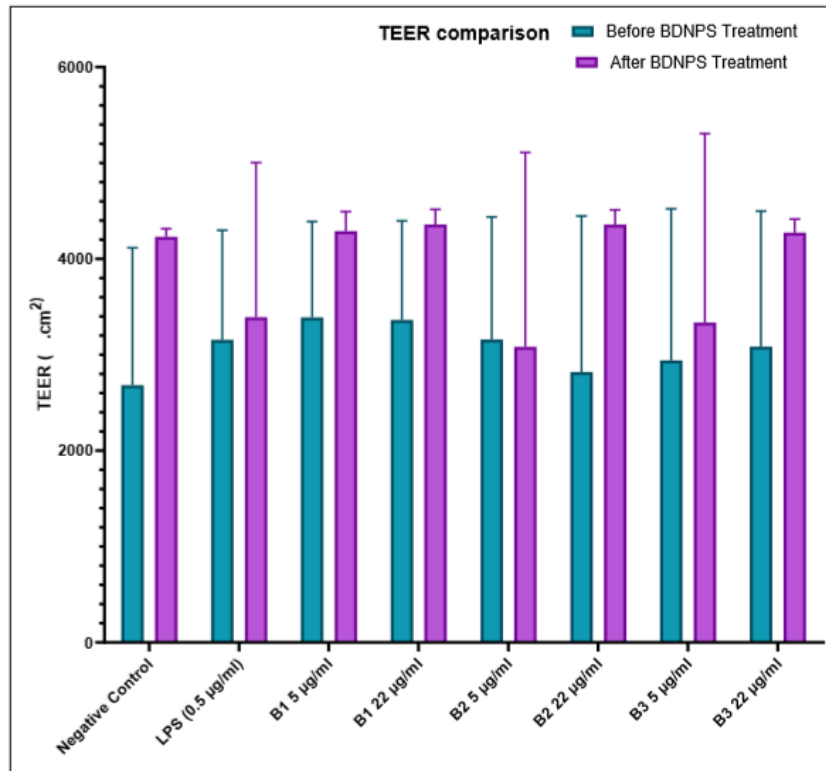


**Figure 28:** TEER comparison of hAELVi cells co-cultured with dTHP-1 in Transwell before and after LPS inflammatory stimulus followed by BDNVs treatment

## Cytokine Gene Expression

LPS stimulation markedly increased TNF, IL-6 and IL-8 expression which was reduced by BDNVs pre-treatment at different concentrations in case of TNF (Figure 29). In case of IL-6 and IL-8, there were reduction of expression but were not significant. LPS determined a decrease in the anti-inflammatory cytokine IL-10. The pretreatment of BDNVs also caused a non significant increase of IL-10 expression in comparison to LPS treatment.

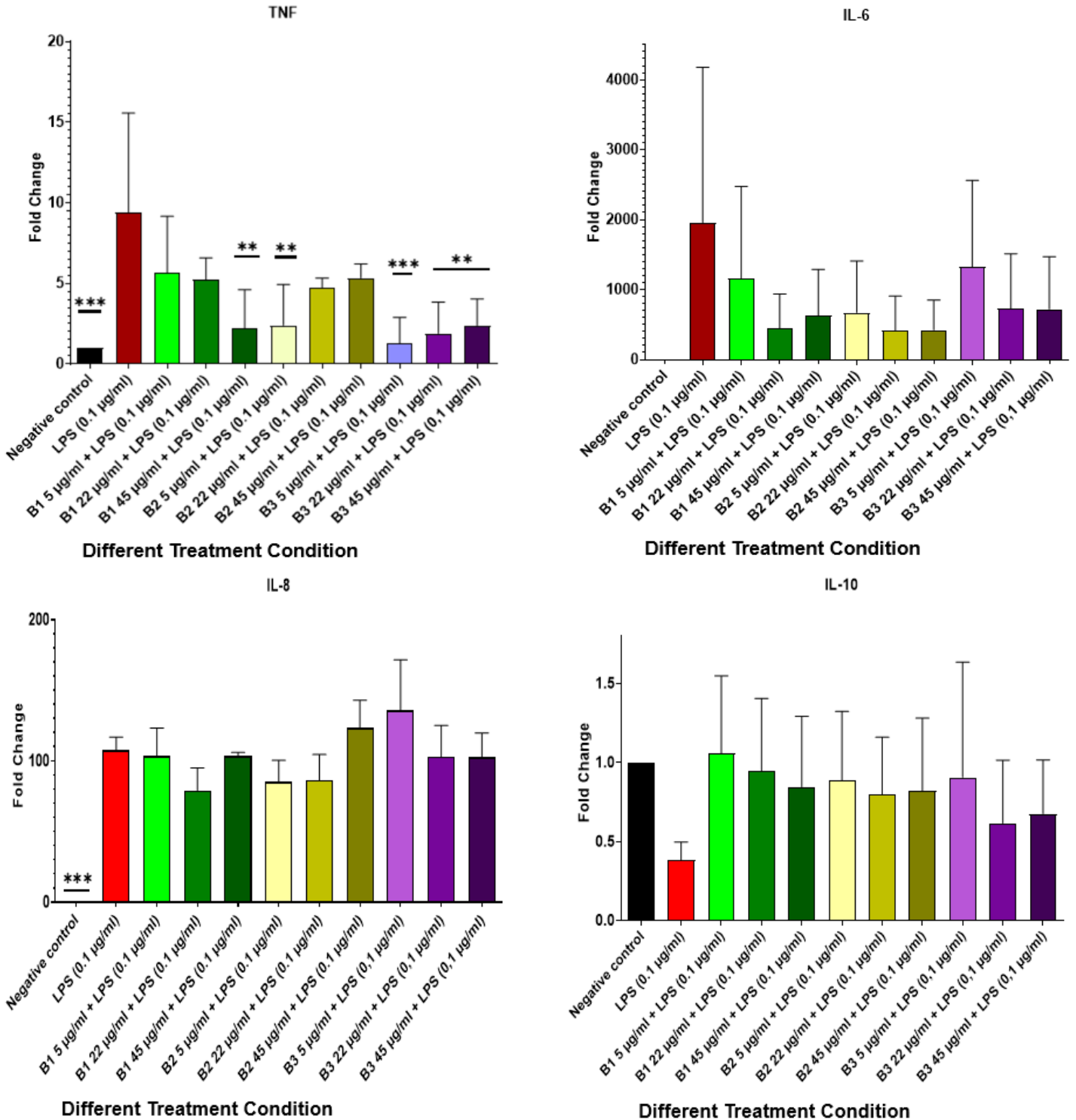
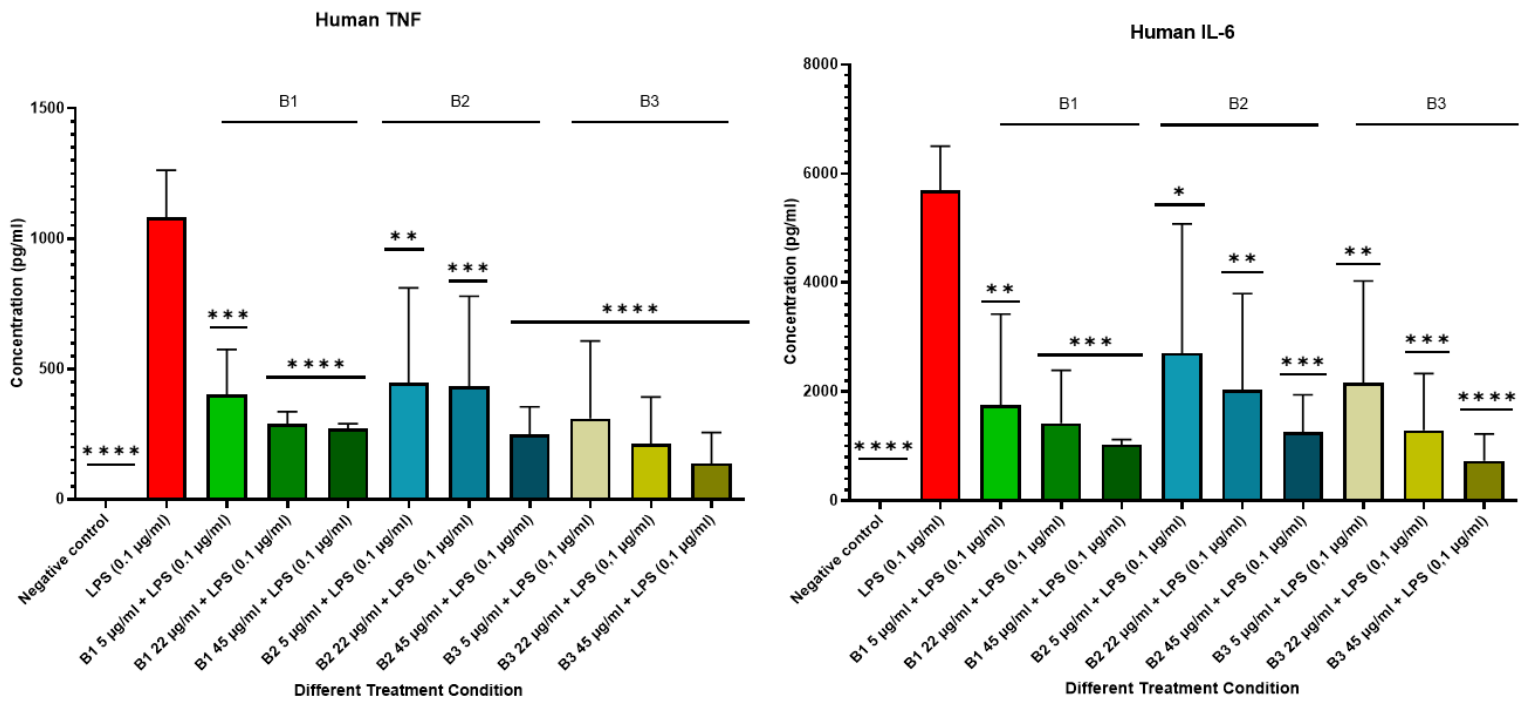
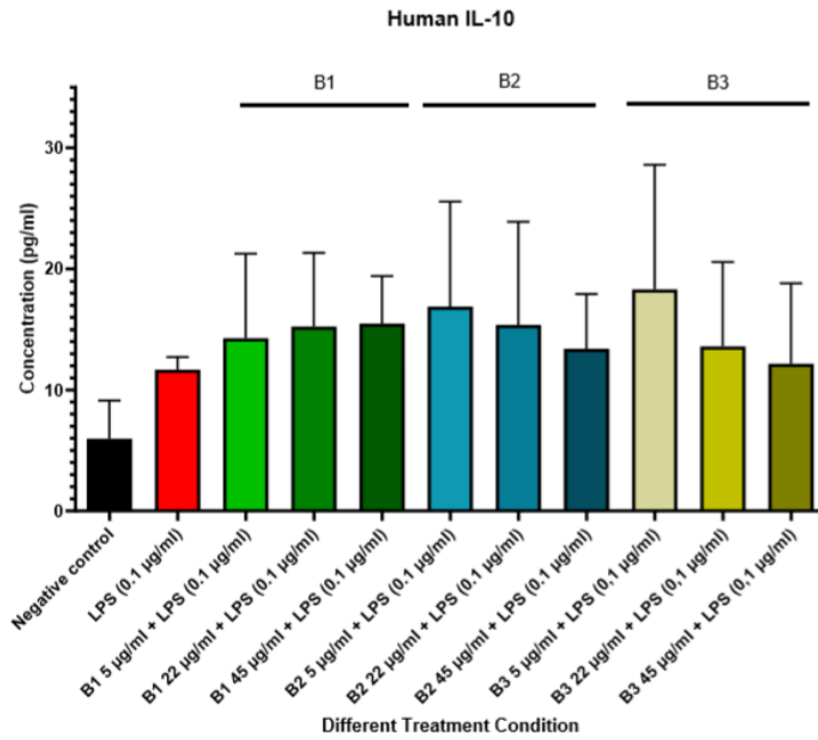


Figure 29: RT-qPCR analysis Considering diff.TH1 cells with BDNVs Treatment. N=2

## Cytokine Cytometric Bead Array (CBA)

To investigate the effects of BDNVs on cytokine protein expression, we quantitatively measured the pro-inflammatory cytokines TNF, IL-6 and anti-inflammatory cytokine IL-10 by CBA method. LPS stimulation markedly increased the release of the pro-inflammatory cytokines which were reduced by BDNVs pre-treatment at different concentrations in a dose dependent manner (Figure 30). The pretreatment of BDNVs was also caused a non significant increase of IL-10 release in comparison to LPS treatment.

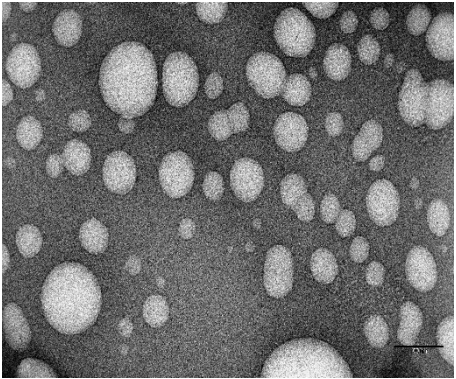
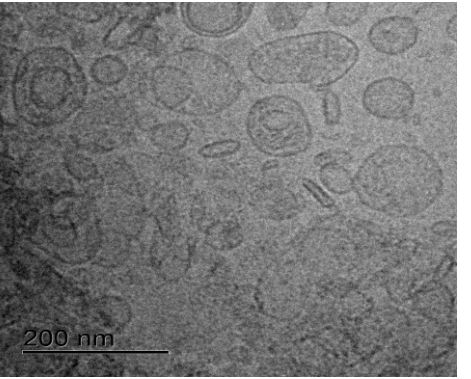
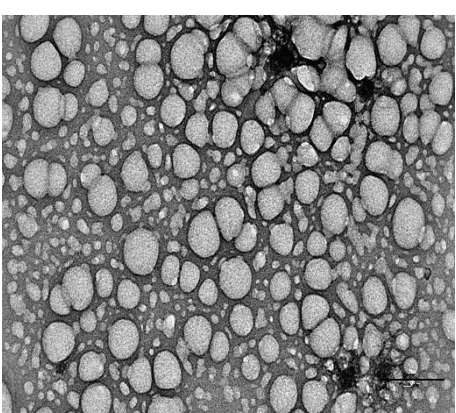
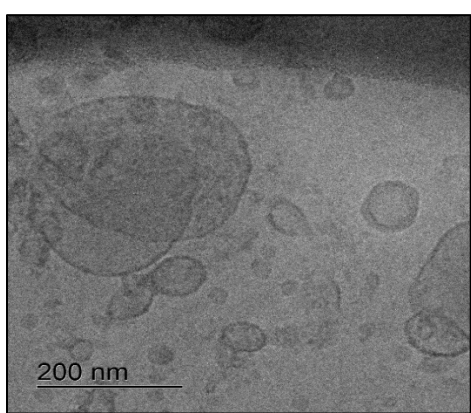
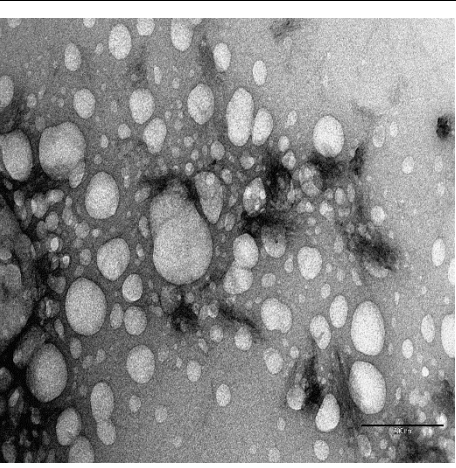
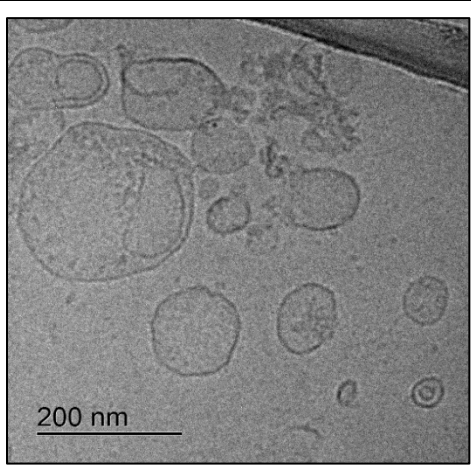




**Figure 30:** Cytokine release profile of diff. THP-1 cells considering BDNVs treatment. N=2

### Comparison of Isolation of BDNVs from Two different countries (Italy and Germany):

		University of Foggia, Italy (UniFg)				DDEL, HIPS, Germany				
Source		Local Grocery Store			Organic Supermarket					
Isolation Method		Sucrose gradient Ultracentrifugation (8%, 30%, 45% and 60%)			Sucrose gradient Ultracentrifugation (8%, 30%, 45% and 60%)					
Physicochemical Characterization	Number of Bands	8/30% (Band 1), 30/45% (Band 2), 45/60% (Band 3)			8/30% (Band 1), 30/45% (Band 2), 45/60% (Band 3)					
	Morphology	TEM			Cryo-TEM					
	Size (Mean)	52 nm, 70 nm and 82 nm			100 nm, 101 nm and 113 nm					
	Zeta Potential	0.0 (mV), 2.7 (mV), 2.8 (mV)			-26.0 (mV), -24.0 (mV), -27.4 (mV)					
	Protein Concentration	Band 1= 1692 µg/mL Band 2= 1201 µg/mL Band 3= 223 µg/mL			Band 1= 4750 µg/mL Band 2= 5153 µg/mL Band 3= 2293 µg/mL					
Isolation of Compounds										
		Compound	Band 1	Band 2	Band 3	Compound	Band 1	Band 2	Band 3	
		Glucobrassicin (nanomole/L)	8.9 ± 1.3	ND	ND	Sulforaphane (ng/ml)	Solvent Methanol	1683,4	357,2	247,1
		Glucoraphanin (nanomole/L)	8.7 ± 1.1	0.80 ± 0.08	0.30 ± 0.04		Solvent RIPA Lysis Buffer+Methanol	1837,2	283,5	266,1
		Neoglucobrassicin (N-methoxy-glucobrassicin) (nanomole/L)	2.6 ± 0.3	ND	ND		Solvent 1% Formic acid in Methanol	1653,5	248,7	219,9

Microscopic Observation	University of Foggia, Italy (UniFg)	DDEL, HIPS, Germany
Band 1		
Band 2		
Band 3		

**Table 7:** Comparison of Isolation of BDNVs from Two different countries (Italy and Germany)

## Discussion

Plant-derived vesicles (PDVs) are comprised of nano and micro vesicles and have been shown to have powerful anti-inflammatory, anti-oxidant and anti-neoplastic activities<sup>74-78</sup>. These effects are likely dependent on their cargoes, i.e. lipids, proteins, nucleic acids, and metabolites, although detailed analyses of PDVs biomolecules have been reported only for a few plant species<sup>74</sup>. In vitro and in vivo animal models have therefore shown that PDVs can exert a wealth of therapeutic actions, especially at the level of gastrointestinal tract. Within the number of plants investigated in these studies, broccoli have been used for their production of PDVs only in a single previous work<sup>79</sup>. They isolated nanoparticles by a sequential centrifugation method followed by column filtration method, obtaining a vesicle population with mean size and Zeta potential of about 32 nm and – 17 mV respectively. Conversely, we obtained three bands from the sucrose gradient ranging from about 50–80 nm in size by TEM during isolation at university of Foggia, Italy as well as about 100-115 nm in size by Cryo-TEM during isolation at DDEL,HIPS. At DDEL,HIPS, hydrodynamic size was also determined by NTA within the range of 170-180 nm. During first isolation, the measured Zeta potential value was nearly zero where as during isolation at DDEL, HIPS the zeta potential value was mostly negative (about -25 mV). Thus, the purification step makes a difference as well as the vegetative stage of the starting matrix, highlighting that a unified protocol would assure to have comparable and reproducible results in the field. The size difference between different methods used is because of the principles of the measurement system as well as the difference in sample preparation techniques. Such as for the measurement by TEM, the samples need to be dehydrated and fixed before testing which can cause the shrinkage or size reduction. Different from TEM, Cryo-TEM analyzed the sample at very low temperature without fixation and staining so that representing more actual size<sup>80</sup>. On the other hand NTA measured the hydrodynamic size of a polydispersed sample<sup>81</sup>. So the size measured by NTA will be bigger than the TEM or Cryo-TEM measurement which representing vesicle size plus the liquid layer around it.

In any case, the isolated BDNVs have nanometric dimensions which make them very interesting as potential anticancer agents. Nanosized dimensions allows them to penetrate deeply into tumor tissues thanks to the ‘enhanced permeability and retention effect’ (EPR effect), which is dependent on the hyperpermeable tumor vasculature, resulting in an important intratumoral drug accumulation<sup>82</sup>. Moreover, nanoformulations can be incorporated with dyes, contrast agents, drug payloads or inorganic nanoclusters, serving as imaging-guided combinatorial cancer therapeutics<sup>83</sup>.



The MTT assay performed on four different cancer cell lines, belonging to the respiratory tract, colon and central nervous system, shows that BDNVs inhibited the metabolic activity of all of them, identifying BDNVs as a broad anti-cancer agent. PDVs have been shown to block tumoral cell proliferation by different mechanisms, such as causing cell cycle arrest at G2/M checkpoint<sup>84</sup>, or inciting apoptosis<sup>23</sup>. Whether BDNVs block metabolic activity of tumoral cell lines due to the arrest of cell cycle or to apoptosis is something that will be the focus of future studies. The MTT results also gives an idea about which concentration sets can be considered for cellular uptake/internalization study, at the end suggesting which dose should be used for the evaluation of biological activities (antioxidant, anti-inflammatory) to treat different chronic inflammatory diseases, including respiratory, intestinal and neurological ones. The assay performed on diff. THP-1 to select the concentrations for anti-inflammatory activity determination as well as cell uptake experiments. The results of the assay performed on non cancerous cell lines i.e. diff. THP-1 cells and hAELVi cells representing that the application of BDNVs is less toxic than cancer cell lines (significant reduction of mortality only with higher concentrations like 100 µg/ml, 500 µg/ml and 5000 µg/ml).

However, BDNVs were endowed also with anti-oxidant effects and it is known that ROS promote tumor development and progression<sup>85</sup>. Thus, it is likely that BDNVs act as anti-tumoral because they are natural anti-oxidants. Sulforaphane (SFN) is a phytochemical belonging to the isothiocyanate family commonly found in many cruciferous vegetables, such as broccoli, brussels sprouts, kale, and cabbages. It has the ability to induce phase II anti-oxidant enzymes and is endowed with anti-inflammatory<sup>86-88</sup> and anti-proliferative<sup>89-91</sup> activities. Interestingly it was reported that SFN was enriched in nanoparticles compared to that in microparticles isolated from broccoli-derived lipid extracts<sup>79</sup>. In accordance with this evidence we found that all three nanostructured bands were endowed with anti-oxidant, anti-proliferative and anti-inflammatory activities. Glucoraphanin (precursor of SFN), glucobrassicin and neoglucobrassicin had been successfully detected in the BDNVs isolated at UniFg whereas it was confirmed that BDNVs isolated at DDEL, HIPS contains Sulforaphane. The fact that all three bands either isolated at UniFg or DDEL, HIPS, had relevant biological activities, make other biological constituents relevant in this context. It must be said that as to the analytical determination of anti-oxidant molecules, this study is the first in which BDNVs are used as source for the determination of GSLs and SFN. So far, the huge body of scientific literature concerning the determination of bioactive compounds from broccoli was produced using crude tissues. For instance, levels of

GSLs can fluctuate dramatically even between cultivars and different growing conditions<sup>92,93</sup>. Also, the stability of these bioactive compounds can be influenced both by different processes used during their extraction and by their storage. Recently, it has been demonstrated how the cutting styles affect the stability and accumulation of bioactive compounds in broccoli<sup>94</sup>. Band 1 also contains appreciable quantities of glucobrassicin and neoglucobrassicin, which were not detected in Band 2 and Band 3. Probably, in our experimental procedures, the mechanical procedure of extraction has caused a massive reduction of glucobrassicin and neoglucobrassicin in Band 2 and Band 3. Moreover, the effect of storage should be taken in account since in an another study it has been observed that the freezing process can decrease glucoraphanin levels<sup>95</sup>. This decrease is likely due to the inhibition of hydrolysis of glucoraphanin by myrosinase.

Except the protein content, we could not determine lipid and RNA molecules, thus we have to further investigate BDNV payload to fully correlate with biological activities. As to the proteins expressed by PDVs, interestingly, it has been observed that garlic-derived vesicles are uptaken by HepG2 hepatocellular carcinoma cells through the interaction of cellular CD98 and lectin-type proteins located on the vesicle surface<sup>96</sup>. The exact protein profile of BDVs will unveil how they interact with cancer as well as non cancer cells and allow to better comprehend their full therapeutic potential.

Anti-metabolic and anti-oxidant activities of BDNVs are mediated by their cell uptake. In our experiment, it was observed that BDNVs were internalized by different cancer cell lines (CaCO<sub>2</sub>, NCI-H441 and SHSY5Y cells) as well as by stimulated diff. THP-1 cells whereas no observation was detected in case of non cancerous cell line such as hAELVi. The uptake of nano- and micro-sized vesicles differ, ranging from phagocytosis of ~ 188 nm ginger vesicles by colon cancer cells<sup>97</sup> to garlic EVs of < 150 nm that are internalized by macropinocytosis in hepatocytes<sup>96</sup>. Thus, during our uptake mechanism study with stimulated diff. THP-1 cells, we found that BDNVs B1 and B2 were internalized mostly via Caveolin dependent Endocytosis whereas BDNVs B3 mostly internalized by Macropinocytosis and Caveolin dependent Endocytosis.

In case of anti inflammatory activity determination experiment, results are more significant in cytokine release (CBA assay) than in mRNA expression (RT-qPCR). CBA measure the accumulation of released cytokine over time, while RT-qPCR focus on a specific time point. This major difference between those techniques can explain the high contrast in standard

deviation values. It may be possible that RNA expression is faster and more sensitively regulated than cytokine release. In our experiment, CBA seemed to be a more robust technique to investigate cytokine regulation. The results are more significant in case of CBA assay considering TNF and IL-6 cytokines. In case of IL-10 there was an upregulation of the release in both experiments but not statistically significant.

Four biologically active compounds were identified in BDNVs with the help of GNPS database searching. Alongside presence of Sulforaphane in BDNVs was confirmed by LC-MS/MS. The anti inflammatory activity of sulforaphane is related to the reduction of the level of pro-inflammatory cytokines (TNF, IL-6)<sup>98,99</sup> as well as the induction of the anti-inflammatory cytokine (IL-10)<sup>99,100</sup>. These evidences are consistent with our anti inflammatory experiments. So the anti inflammatory activity of the BDNVs may be handled by the Sulforaphane presents inside BDNVs which is an inhibitor of the nuclear factor kappa B (NFκB) pathway as well as an inducer of the nuclear factor erythroid 2-related factor 2 (Nrf2) pathway<sup>101-103</sup>.

Freeze drying or lyophilization is a suitable method for the preservation of heat-sensitive materials like BDNVs. So the suitability of the freeze drying method was analyzed along with the traditional -80°C storage conditions in a 8 weeks stability experimental model. The results revealed that the freeze drying system can be a suitable alternative of the -80°C storage condition though there was a significant change in one of the physical parameter i.e. zeta potential value.

The comparison between two isolation (UniFg and DDEL, HIPS) revealed that there were differences in the physicochemical characteristics which is obvious as factors including farming and harvesting conditions such as climate, region, and degree of maturation can affects the content of such vesicles. In case of UniFg, the source is local grocery market and in case of DDEL, HIPS the source is organic supermarket which can be a major source of differentiation as Logozzi et al. revealed that there were significant difference of physical as well as biological properties depending on the cultivation method (Organic Vs Conventional)<sup>104</sup>.

## **Conclusion**

These results will open up the authenticity of considering BDNVs for the treatment of chronic diseases including Cancer. Plant-derived vesicles PDVs that carry chemicals, proteins, and nucleic acids from vegetables and fruits may provide far more treatment options than synthetic drugs and protein medicine<sup>105</sup>. Plants represent green, sustainable and renewable sources of nanovesicles, and this can ensure a constant and never-ending production, in turn providing bioproducts that are immediately available at low dosages, stable and more effective than the current products, and therefore more suitable for clinical use and the market<sup>106</sup>.

Here we showed that BDNVs were endowed with anti-proliferative, anti-oxidant and anti-inflammatory activities dependent on cell uptake. We also confirmed the presence of different bioactive compounds inside the BDNVs. However, the clinical translation of BDNVs into therapy application is still a long way to go. As a kind of biological medicine, production standard, shelf-life, and quality control remain to be determined. In vivo pre-clinical animal models of cancer need to be investigated. BDV nanovesicles are apt to be further exploited for the theranostics of cancer as well as other chronic diseases such as chronic respiratory diseases, although bioactives should be identified yet.

## Bibliography

1. Beasley, R., A. Semprini, *et al.* "Risk factors for asthma: is prevention possible?" *Lancet*. 2015; 386(9998): 1075-1085.
2. Rycroft, C. E., A. Heyes, *et al.* "Epidemiology of chronic obstructive pulmonary disease: a literature review." *Int J Chron Obstruct Pulmon Dis*. 2012; 7: 457-494.
3. Cohen-Cymerknoh, M., D. Shoseyov, *et al.* "Managing cystic fibrosis: strategies that increase life expectancy and improve quality of life." *Am J Respir Crit Care Med*. 2011; 183(11): 1463-1471.
4. Barnes, P. J. "Pathophysiology of allergic inflammation." *Immunol Rev*. 2011; 242(1): 31-50.
5. Fischer, B. M., E. Pavlisko, *et al.* "Pathogenic triad in COPD: oxidative stress, protease-antiprotease imbalance, and inflammation." *Int J Chron Obstruct Pulmon Dis*. 2011; 6: 413-421.
6. Nichols, D. P. and Chmiel, J. F. "Inflammation and its genesis in cystic fibrosis." *Pediatr Pulmonol* 50 Suppl. 2015; 40: S39-56.
7. Rogers, D. F. "Physiology of airway mucus secretion and pathophysiology of hypersecretion." *Respir Care*. 2007; 52(9): 1134-1146; discussion 1146-1139.
8. Yang, C., Zhang, M., and Merlin, D. Advances in plant-derived edible nanoparticle-based lipid nano-drug delivery systems as therapeutic nanomedicines. *J. Mater. Chem. B* 6, 2018; 1312–1321.
9. Teng Y, Ren Y, Sayed M, et al. Plant-derived exosomal microRNAs shape the gut microbiota. *Cell Host Microbe*. 2018; 24(5):637–652.e8.
10. Wang Q, Zhuang X, Mu J, et al. Delivery of therapeutic agents by nanoparticles made of grapefruit-derived lipids. *Nat Commun*. 2013;4:1867. doi: 10.1038/ncomms2886
11. You JY, Kang SJ, Rhee WJ. Isolation of cabbage exosome-like nanovesicles and investigation of their biological activities in human cells. *Bioact Mater*. 2021;6(12):4321–4332.
12. Xia Y, Chen T, Chen W, et al. A dual-modal aptasensor based on a multifunctional acridone derivate for exosomes detection. *Anal Chim Acta*. 2022;1191:339279.
13. Li, X., Liang, Z., Du, J., Wang, Z., Mei, S., Li, Z., et al. Herbal decoctosome is a novel form of medicine. *Sci. China Life Sci*. 2019; 62, 333–348.
14. Alfieri M, Leone A, Ambrosone A. Plant-Derived Nano and Microvesicles for Human Health and Therapeutic Potential in Nanomedicine. *Pharmaceutics*. 2021; 6;13(4):498.
15. Starrett W. and Blake J. D. "Sulforaphane inhibits de novo synthesis of IL-8 and MCP-I in human epithelial cells generated by cigarette smoke extract." *Journal of Immunotoxicology*. 2011; 8:2, 150-158.
16. Lee Y.-J. and Lee S.-H. "Sulforaphane induces antioxidant and antiproliferative responses by generating reactive oxygen species in human bronchial epithelial BEAS-2B cells." *JKMS*. 2011; 26:1474-1482.

17. Bassan, P. *et al.* Extraction, profiling and bioactivity analysis of volatile glucosinolates present in oil extract of *Brassica juncea* var. *raya*. *Physiol. Mol. Biol. Plants*. 2018; 24, 399–409.
18. Chung, I. M., Rekha, K., Rajakumar, G. & Thiruvengadam, M. Production of glucosinolates, phenolic compounds and associated gene expression profiles of hairy root cultures in turnip (*Brassica rapa* ssp. *rapa*). *3 Biotech*. 2016; 6, 175.
19. De Leo V, Maurelli AM, Ingrosso C, Lupone F, Catucci L. Easy preparation of Liposome@PDA microspheres for fast and highly efficient removal of methylene blue from water. *Int. J. Mol. Sci*. 2021; **22**:11916.
20. Trapani A, et al. Glutathione-loaded solid lipid nanoparticles based on Gelucire® 50/13: Spectroscopic characterization and interactions with fish cells. *J. Drug Deliv. Sci. Tech*. 2018; 47:359–366.
21. Schwende, H.; Fitzke, E.; Ambs, P.; Dieter, P. Differences in the State of Differentiation of THP-1 Cells Induced by Phorbol Ester and 1,25-Dihydroxyvitamin D3. *J. Leukoc. Biol*. 1996, 59 (4), 555–561.
22. Kuehn, A.; Kletting, S.; Carvalho-Wodarz, C. de S.; Repnik, U.; Griffiths, G.; Fischer, U.; Meese, E. U.; Huwer, H.; Wirth, D.; May, T.; Schneider-Daum, N.; Lehr, C. M. Human Alveolar Epithelial Cells Expressing Tight Junctions to Model the Air-Blood Barrier. *ALTEX* 2016, 33 3, 251–260
23. Raimondo S, et al. Citrus limon-derived nanovesicles inhibit cancer cell proliferation and suppress CML xenograft growth by inducing TRAIL-mediated cell death. *Oncotarget*. 2015;**6**:19514–19527.
24. Puzar Dominkus P, et al. PKH26 labeling of extracellular vesicles: Characterization and cellular internalization of contaminating PKH26 nanoparticles. *Biochim. Biophys. Acta Biomembr*. 2018;**1860**:1350–1361.
25. L. M. Alexander, S. Pernagallo, A. Livigni, R. M. Sánchez-Martín, J. M. Brickman, M. Bradley, *Mol. BioSyst*. 2010, 6, 399.
26. J. Zhang, X. Zhu, Y. Jin, W. Shan, Y. Huang, *Mol. Pharmaceutics* 2014, 11, 1520
27. De Leo, V. et al. Eudragit S100 Entrapped Liposome for Curcumin Delivery: Anti- Oxidative Effect in Caco-2 Cells. *Coatings*. 2020; 10, 114.
28. Castellani, S. et al. Nanoparticle delivery of grape seed-derived proanthocyanidins to airway epithelial cells dampens oxidative stress and inflammation. *J Transl Med*. 2018; 16, 140.
29. Trapani, A. et al. Cyto/Biocompatibility of Dopamine Combined with the Antioxidant Grape Seed-Derived Polyphenol Compounds in Solid Lipid Nanoparticles. *Molecules*. 2021; 26, 916.
30. Yu, L., Deng, Z., Liu, L., Zhang, W. & Wang, C. Plant-derived nanovesicles: A novel form of nanomedicine. *Front. Bioeng. Biotechnol*. 2020; 8, 584391.

31. Cataldi, T. R., Rubino, A., Lelario, F. & Bufo, S. A. Naturally occurring glucosinolates in plant extracts of rocket salad (*Eruca sativa* L.) identified by liquid chromatography coupled with negative ion electrospray ionization and quadrupole ion-trap mass spectrometry. *Rapid Commun Mass Spectrom.* 2007; 21, 2374-2388.
32. Hauder J, Winkler S, Bub A, Rüfer CE, Pignitter M, Somoza V. LC-MS/MS quantification of sulforaphane and indole-3-carbinol metabolites in human plasma and urine after dietary intake of selenium-fortified broccoli. *J Agric Food Chem.* 2011; 59(15):8047-57.
33. Wang, Mingxun, *et al.* Sharing and community curation of mass spectrometry data with Global Natural Products Social Molecular Networking. *Nature Biotechnology.* 2016; 34.8, 828- 837.
34. Bernal-Chávez, S.A. *et al.* Insights into Terminal Sterilization Processes of Nanoparticles for Biomedical Applications. *Molecules.* 2021; 26, 2068.
35. Costa, A.; de Souza Carvalho-Wodarz, C.; Seabra, V.; Sarmiento, B.; Lehr, C.-M. Triple Co-Culture of Human Alveolar Epithelium, Endothelium and Macrophages for Studying the Interaction of Nanocarriers with the Air-Blood Barrier. *Acta Biomater.* 2019; 91, 235– 247.
36. Hittinger, M.; Mell, N. A.; Huwer, H.; Loretz, B.; Schneider-Daum, N.; Lehr, C.-M. Autologous Co-Culture of Primary Human Alveolar Macrophages and Epithelial Cells for Investigating Aerosol Medicines. Part II: Evaluation of IL-10-Loaded Microparticles for the Treatment of Lung Inflammation. *Altern. Lab. Anim.* 2016; 44 (4), 349–360.
37. Elbert, K. J.; Schäfer, U. F.; Schäfers, H.-J.; Kim, K.-J.; Lee, V. H. L.; Lehr, C.-M. Monolayers of Human Alveolar Epithelial Cells in Primary Culture for Pulmonary Absorption and Transport Studies. *Pharm. Res.* 1999; 16 (5), 601–608
38. Livak KJ, Schmittgen TD. Analysis of relative gene expression data using real-time quantitative PCR and the 2<sup>-</sup>(-Delta Delta C(T)) Method. *Methods.* 2001; 25(4):402-8.
39. [www.bdbiosciences.com/content/dam/bdb/marketing-documents/Human-Soluble-Protein-Master-Buffer-Kit-User-Manual](http://www.bdbiosciences.com/content/dam/bdb/marketing-documents/Human-Soluble-Protein-Master-Buffer-Kit-User-Manual)
40. [www.bdbiosciences.com/en-it/products/reagents/immunoassays/cba](http://www.bdbiosciences.com/en-it/products/reagents/immunoassays/cba)
41. Dong, M. *et al.* Rapid screening and characterization of glucosinolates in 25 Brassicaceae tissues by UHPLC-Q-exactive orbitrapMS. *Food Chem.* 2021; 365, 130493.
42. Shapiro, T.; Fahey, J.; Wade, K.; Stephenson, K.; Talalay, P. Chemoprotective glucosinolates and isothiocyanates of broccoli sprouts: Metabolism and excretion in humans. *Cancer Epidemiol., Biomarkers Prev.* 2001; 10, 501–508.

43. Cheng Y. M., Tsai C. C., Hsu Y. C. Sulforaphane, a dietary isothiocyanate, induces G2/M arrest in cervical cancer cells through cyclinB1 downregulation and GADD45 $\beta$ /CDC2 association. *International Journal of Molecular Sciences*. 2016; 17(9).
44. Peng X., Zhou Y., Tian H., et al. Sulforaphane inhibits invasion by phosphorylating ERK1/2 to regulate E-cadherin and CD44v6 in human prostate cancer DU145 cells. *Oncology Reports*. 2015; 34(3):1565–1572.
45. Leone A., Diorio G., Sexton W., et al. Sulforaphane for the chemoprevention of bladder cancer: molecular mechanism targeted approach. *Oncotarget*. 2017; 8(21):35412–35424.
46. Juengel E., Maxeiner S., Rutz J., et al. Sulforaphane inhibits proliferation and invasive activity of everolimus-resistant kidney cancer cells *in vitro*. *Oncotarget*. 2016; 7(51):85208–85219.
47. Wang D. X., Zou Y. J., Zhuang X. B., et al. Sulforaphane suppresses EMT and metastasis in human lung cancer through miR-616-5p-mediated GSK3 $\beta$ / $\beta$ -catenin signaling pathways. *Acta Pharmacologica Sinica*. 2017; 38(2):241–251
48. Clarke J. D., Dashwood R. H., Ho E. Multi-targeted prevention of cancer by sulforaphane. *Cancer Letters*. 2008; 269(2):291–304.
49. Ohta, S.; Ono, F.; Shiomi, Y.; Nakao, T.; Aozasa, O.; Nagate, T.; Kitamura, K.; Yamaguchi, S.; Nishi, M.; Miyata, H. Anti-herpes simplex virus substances produced by the marine alga, *Dunaliella primolecta*. *J. Appl. Phycol.* 1998, 10, 349–355
50. Ratnoglik, S.L.; Aoki, C.; Sudarmono, P.; Komoto, M.; Deng, L.; Shoji, I.; Fuchino, H.; Kawahara, N.; Hotta, H. Antiviral activity of extracts from *Morinda citrifolia* leaves and chlorophyll catabolites, pheophorbide a and pyropheophorbide a, against hepatitis c virus. *Microbiol. Immunol.* 2014, 58, 188–194
51. Nakamura, Y.; Murakami, A.; Koshimizu, K.; Ohigashi, H. Identification of pheophorbide a and its related compounds as possible anti-tumor promoters in the leaves of *Neptunia oleracea*. *Biosci. Biotechnol. Biochem.* 1996, 60, 1028–1030
52. Tang, P.M.; Chan, J.Y.; Au, S.W.; Kong, S.K.; Tsui, S.K.; Waye, M.M.; Mak, T.C.; Fong, W.P.; Fung, K.P. Pheophorbide a, an active compound isolated from *Scutellaria barbata*, possesses photodynamic activities by inducing apoptosis in human hepatocellular carcinoma. *Cancer Biol. Ther.* 2006, 5, 1111–1116
53. Tang, P.M.; Liu, X.Z.; Zhang, D.M.; Fong, W.P.; Fung, K.P. Pheophorbide a based photodynamic therapy induces apoptosis via mitochondrial-mediated pathway in human uterine carcinosarcoma. *Cancer Biol. Ther.* 2009, 8, 533–539



54. Tang, P.M.; Zhang, D.M.; Xuan, N.H.; Tsui, S.K.; Waye, M.M.; Kong, S.K.; Fong, W.P.; Fung, K.P. Photodynamic therapy inhibits P-glycoprotein mediated multidrug resistance via JNK activation in human hepatocellular carcinoma using the photosensitizer pheophorbide a. *Mol. Cancer* 2009, 8, 56
55. Bui-Xuan, N.H.; Tang, P.M.; Wong, C.K.; Fung, K.P. Photo-activated pheophorbide-a, an active component of *Scutellaria barbata*, enhances apoptosis via the suppression of ERK- mediated autophagy in the estrogen receptor-negative human breast adenocarcinoma cells MDA-MB-231. *J. Ethnopharmacol.* 2010, 131, 95–103
56. Hoi, S.W.; Wong, H.M.; Chan, J.Y.; Yue, G.G.; Tse, G.M.; Law, B.K.; Fong, W.P.; Fung, K.P. Photodynamic therapy of pheophorbide a inhibits the proliferation of human breast tumour via both caspase-dependent and -independent apoptotic pathways in in vitro and in vivo models. *Phytother. Res.* 2012, 26, 734–742
57. Ahn, M.Y.; Yoon, H.E.; Kwon, S.M.; Lee, J.; Min, S.K.; Kim, Y.C.; Ahn, S.G.; Yoon, J.H. Synthesized pheophorbide a-mediated photodynamic therapy induced apoptosis and autophagy in human oral squamous carcinoma cells. *J. Oral Pathol. Med.* 2013, 42, 17–25
58. Ahn, M.Y.; Yoon, H.E.; Moon, S.Y.; Kim, Y.C.; Yoon, J.H. Intratumoral photodynamic therapy with newly synthesized pheophorbide a in murine oral cancer. *Oncol. Res.* 2017, 25, 295–304
59. Cho, M.; Park, G.M.; Kim, S.N.; Amna, T.; Lee, S.; Shin, W.S. Glioblastoma-specific anticancer activity of pheophorbide a from the edible red seaweed *Grateloupia elliptica*. *J. Microbiol. Biotechnol.* 2014, 24, 346–353
60. Lauritano, C.; Helland, K.; Riccio, G.; Andersen, J.H.; Ianora, A.; Hansen, E.H. Lysophosphatidylcholines and chlorophyll-derived molecules from the diatom *Cylindrotheca closterium* with anti-inflammatory activity. *Mar. Drugs* 2020, 18, 166
61. Lanfer-Marquez, U.M.; Barros, R.M.C.; Sinnecker, P. Antioxidant activity of chlorophylls and their derivatives. *Food Res. Int.* 2005, 38, 885–891
62. Bui-Xuan, N.H.; Tang, P.M.; Wong, C.K.; Chan, J.Y.; Cheung, K.K.; Jiang, J.L.; Fung, K.P. Pheophorbide a: A photosensitizer with immunostimulating activities on mouse macrophage raw 264.7 cells in the absence of irradiation. *Cell. Immunol.* 2011, 269, 60–67
63. Miranda, N.; Volpato, H.; da Silva Rodrigues, J.H.; Caetano, W.; Ueda-Nakamura, T.; de Oliveira Silva, S.; Nakamura, C.V. The photodynamic action of pheophorbide a induces cell death through oxidative stress in *Leishmania amazonensis*. *J. Photochem. Photobiol. B* 2017, 174, 342–354
64. Donio M., Ronica S., Viji V. T., Velmurugan S., Jenifer J. A., Michaelbabu M., et al. Isolation and characterization of halophilic *Bacillus* sp. BS3 able to produce pharmacologically important biosurfactants. *Asian Pac. J. Trop. Med.* 2013; 6, 876–883.

65. Zhang, S., Xu, B., Zhang, J., Gan, Y., 2018. Identification of the antifungal activity of *Trichoderma longibrachiatum* T6 and assessment of bioactive substances in controlling phytopathogens. *Pestic. Biochem. Physiol.* 147, 59–66
66. Pradheesh, G., Suresh, J., Suresh, S., Alexramani, V., 2017. Antimicrobial activity and identification of potential ethanolic antimicrobial compounds from the medicinal plant *Pisonia Grandis* R.Br. *World J. Pharm. Pharm. Sci.* 6, 1686–170
67. Dos Reis CM, da Rosa BV, da Rosa GP, do Carmo G, Morandini LMB, Ugalde GA, Kuhn KR, Morel AF, Jahn SL, Kuhn RC. Antifungal and antibacterial activity of extracts produced from *Diaporthe schini*. *J Biotechnol.* 2019 Mar 20;294:30-37.
68. H.K. Shareef, H.J. Muhammed, H.M. Hussein, I.H. Hameed. Antibacterial effect of ginger (*Zingiber officinale*) roscoe and bioactive chemical analysis using gas chromatography mass spectrum *Orient. J. Chem.*, 32 (2) (2016), pp. 20-40
69. Premjanu, N., Jaynthy, C., 2014. Identification and characterization of antimicrobial metabolite from an endophytic fungus, *Colletotrichum gloeosporioides* isolated from *Lanea corammendalica*. *Int. J. ChemTech. Res.* 7, 369–374.
70. Cheng MC, Ker YB, Yu TH, Lin LY, Peng RY, Peng CH. Chemical synthesis of 9(Z)-octadecenamide and its hypolipidemic effect: a bioactive agent found in the essential oil of mountain celery seeds. *J Agric Food Chem.* 2010 Feb 10;58(3):1502-8
71. Lee HJ, Kim KW. Anti-inflammatory effects of arbutin in lipopolysaccharide-stimulated BV2 microglial cells. *Inflamm Res.* 2012 Aug;61(8):817-25
72. Lim Y.J., Lee E.H., Kang T.H., Ha S.K., Oh M.S., Kim S.M., Yoon T.J., Kang C., Park J.H., Kim S.Y. Inhibitory effects of arbutin on melanin biosynthesis of alpha-melanocyte stimulating hormone-induced hyperpigmentation in cultured brownish guinea pig skin tissues. *Arch. Pharm. Res.* 2009;32:367–373.
73. Wu L.H., Li P., Zhao Q.L., Piao J.L., Jiao Y.F., Kadowaki M., Kondo T. Arbutin, an intracellular hydroxyl radical scavenger, protects radiation-induced apoptosis in human lymphoma U937 cells. *Apoptosis.* 2014;19:1654–1663
74. Alfieri M, Leone A, Ambrosone A. Plant-derived nano and microvesicles for human health and therapeutic potential in nanomedicine. *Pharmaceutics.* 2021;13:348.
75. Yu L, Deng Z, Liu L, Zhang W, Wang C. Plant-derived nanovesicles: A novel form of nanomedicine. *Front. Bioeng. Biotechnol.* 2020;8:584391.
76. Rome S. Biological properties of plant-derived extracellular vesicles. *Food Funct.* 2019;10:529–538.

77. Di Gioia S, Hossain MN, Conese M. Biological properties and therapeutic effects of plant-derived nanovesicles. *Open Med. (Wars)* 2020;**15**:1096–1122. doi: 10.1515/med-2020-0160.
78. Dad HA, Gu TW, Zhu AQ, Huang LQ, Peng LH. Plant exosome-like nanovesicles: Emerging therapeutics and drug delivery nanoplatforms. *Mol. Ther.* 2021;**29**:13–31.
79. Deng Z, et al. Broccoli-derived nanoparticle inhibits mouse colitis by activating dendritic cell AMP-activated protein kinase. *Mol. Ther.* 2017;**25**:1641–1654. doi: 10.1016/j.ymthe.2017.01.025.
80. I. Tatischeff, E. Larquet, J.M. Falcón-Pérez, P.Y. Turpin, S.G. Kruglik, Fast characterisation of cell-derived extracellular vesicles by nanoparticles tracking analysis, cryo-electron microscopy, and Raman tweezers microspectroscopy, *J. Extracell Vesicles* 2012; 1.
81. Wilson DR, Green JJ. Nanoparticle Tracking Analysis for Determination of Hydrodynamic Diameter, Concentration, and Zeta-Potential of Polyplex Nanoparticles. *Methods Mol Biol.* 2017;**1570**:31-46.
82. Brigger I, Dubernet C, Couvreur P. Nanoparticles in cancer therapy and diagnosis. *Adv. Drug. Deliv. Rev.* 2002; **54**:631–651.
83. Gou Y, et al. Bio-inspired protein-based nanoformulations for cancer theranostics. *Front. Pharmacol.* 2018; **9**:421.
84. Stanly C, et al. Grapefruit-derived micro and nanovesicles show distinct metabolome profiles and anticancer activities in the A375 human melanoma cell line. *Cells.* 2020; **9**:2722
85. Arfin, S. *et al.* Oxidative stress in cancer cell metabolism. *Antioxidants.* 2021; **10**, 642. 10.3390/antiox10050642.
86. Sun CC, et al. Sulforaphane attenuates muscle inflammation in dystrophin-deficient mdx mice via NF-E2-related factor 2 (Nrf2)-mediated inhibition of NF-kappaB signaling pathway. *J. Biol. Chem.* 2015;**290**:17784–17795.
87. Pennisi M, et al. Inflammasomes, hormesis, and antioxidants in neuroinflammation: Role of NRLP3 in Alzheimer disease. *J. Neurosci. Res.* 2017;**95**:1360–1372.
88. Fuentes F, Paredes-Gonzalez X, Kong AN. Dietary glucosinolates sulforaphane, phenethyl isothiocyanate, indole-3-carbinol/3,3'-diindolylmethane: Anti-oxidative stress/inflammation, Nrf2, epigenetics/epigenomics and in vivo cancer chemopreventive efficacy. *Curr. Pharmacol. Rep.* 2015;**1**:179–196.
89. Singh SV, et al. Sulforaphane-induced G2/M phase cell cycle arrest involves checkpoint kinase 2-mediated phosphorylation of cell division cycle 25C. *J. Biol. Chem.* 2004;**279**:25813–25822.
90. Lewinska A, Adamczyk-Grochala J, Deregowska A, Wnuk M. Sulforaphane-induced cell cycle arrest and senescence are accompanied by DNA hypomethylation and changes in microRNA profile in breast cancer cells. *Theranostics.* 2017;**7**:3461–3477.

91. Suppipat K, Park CS, Shen Y, Zhu X, Lacorazza HD. Sulforaphane induces cell cycle arrest and apoptosis in acute lymphoblastic leukemia cells. *PLoS ONE*. 2012;**7**:e51251.
92. Wang, J. *et al.* Genotypic variation of glucosinolates in broccoli (*Brassica oleracea* var. *italica*) florets from China. *Food Chem*. 2012; 133, 735–741.
93. Bhandari, S. R., Jo, J. S. & Lee, J. G. Comparison of glucosinolate profiles in different tissues of nine brassica crops. *Molecules* 2015; 20, 15827–15841.
94. Torres-Contreras, A. M., Nair, V., Cisneros-Zevallos, L. & Jacobo-Velazquez, D. A. Stability of bioactive compounds in broccoli as affected by cutting styles and storage time. *Molecules* 2017; 22, 1.
95. Shams R, Abu-Khudir R, Ali EM. Freezing reduces healthy benefits of broccoli grown in Egypt. *J. Food Nutr. Popul. Health*. 2017; 1:22.
96. Song H, et al. Internalization of garlic-derived nanovesicles on liver cells is triggered by interaction with CD98. *ACS Omega*. 2020;**5**:23118–23128.
97. Zhang, M. *et al.* Edible ginger-derived nanoparticles: A novel therapeutic approach for the prevention and treatment of inflammatory bowel disease and colitis-associated cancer. *Biomaterials*. 2016; 101, 321–340.
98. Liu, Y.; Zhang, Z.; Lu, X.; Meng, J.; Qin, X.; Jiang, J. Anti-nociceptive and anti-inflammatory effects of sulforaphane on sciatic endometriosis in a rat model. *Neurosci. Lett*. 2020, 723, 134858.
99. Ali, M.; Bonay, M.; Vanhee, V.; Vinit, S.; Deramaudt, T.B. Comparative effectiveness of 4 natural and chemical activators of Nrf2 on inflammation, oxidative stress, macrophage polarization, and bactericidal activity in an in vitro macrophage infection model. *PLoS ONE* 2020, 15, e0234484
100. Subedi, L.; Lee, J.; Yumnam, S.; Ji, E.; Kim, S. Anti-Inflammatory Effect of Sulforaphane on LPS-Activated Microglia Potentially through JNK/AP-1/NF- $\kappa$ B Inhibition and Nrf2/HO-1 Activation. *Cells* 2019, 8, 194
101. Mokhtari, R.B.; Baluch, N.; Homayouni, T.S.; Morgatskaya, E.; Kumar, S.; Kazemi, P.; Yeger, H. The role of Sulforaphane in cancer chemoprevention and health benefits: A mini-review. *J. Cell Commun. Signal*. 2017, 12, 91–101.
102. Eren, E.; Tufekci, K.U.; Isci, K.B.; Tastan, B.; Genc, K.; Genc, S. Sulforaphane Inhibits Lipopolysaccharide-Induced Inflammation, Cytotoxicity, Oxidative Stress, and MiR-155 Expression and Switches to Mox Phenotype through Activating Extracellular Signal Regulated Kinase 1/2-Nuclear Factor Erythroid 2-Related Factor 2/Antioxidant Response Element Pathway in Murine Microglial Cells. *Front. Immunol*. 2018, 9, 36.

103. Su, X.; Jiang, X.; Meng, L.; Dong, X.; Shen, Y.; Xin, Y. Anticancer Activity of Sulforaphane: The Epigenetic Mechanisms and the Nrf2 Signaling Pathway. *Oxidative Med. Cell. Longev.* 2018, 2018, 5438179.
104. Logozzi, M.; Di Raimo, R.; Mizzoni, D.; Fais, S. Nanovesicles from Organic Agriculture Derived Fruits and Vegetables: Characterization and Functional Antioxidant Content. *Int. J. Mol. Sci.* 2021, 22, 8170
105. Yu, L., Deng, Z., Liu, L., Zhang, W. & Wang, C. Plant-derived nanovesicles: A novel form of nanomedicine. *Front. Bioeng. Biotechnol.* 2020; **8**, 584391.
106. Logozzi, M., Di Raimo, R., Mizzoni, D. & Fais, S. Nanovesicles from organic agriculture derived fruits and vegetables: Characterization and functional antioxidant content. *Int. J. Mol. Sci.* 2021; 22, 8170.